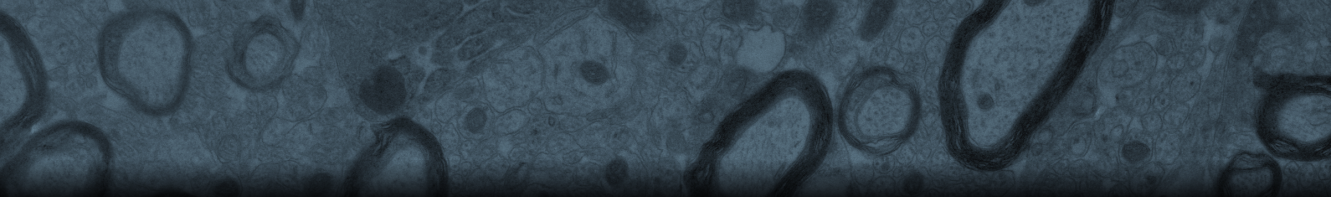

LIÈGE université

MULTIPARAMETER MRI QUANTIFICATION OF MICROSTRUCTURAL BRAIN ALTERATIONS IN MULTIPLE SCLEROSIS

Emilie LOMMERS, M.D.

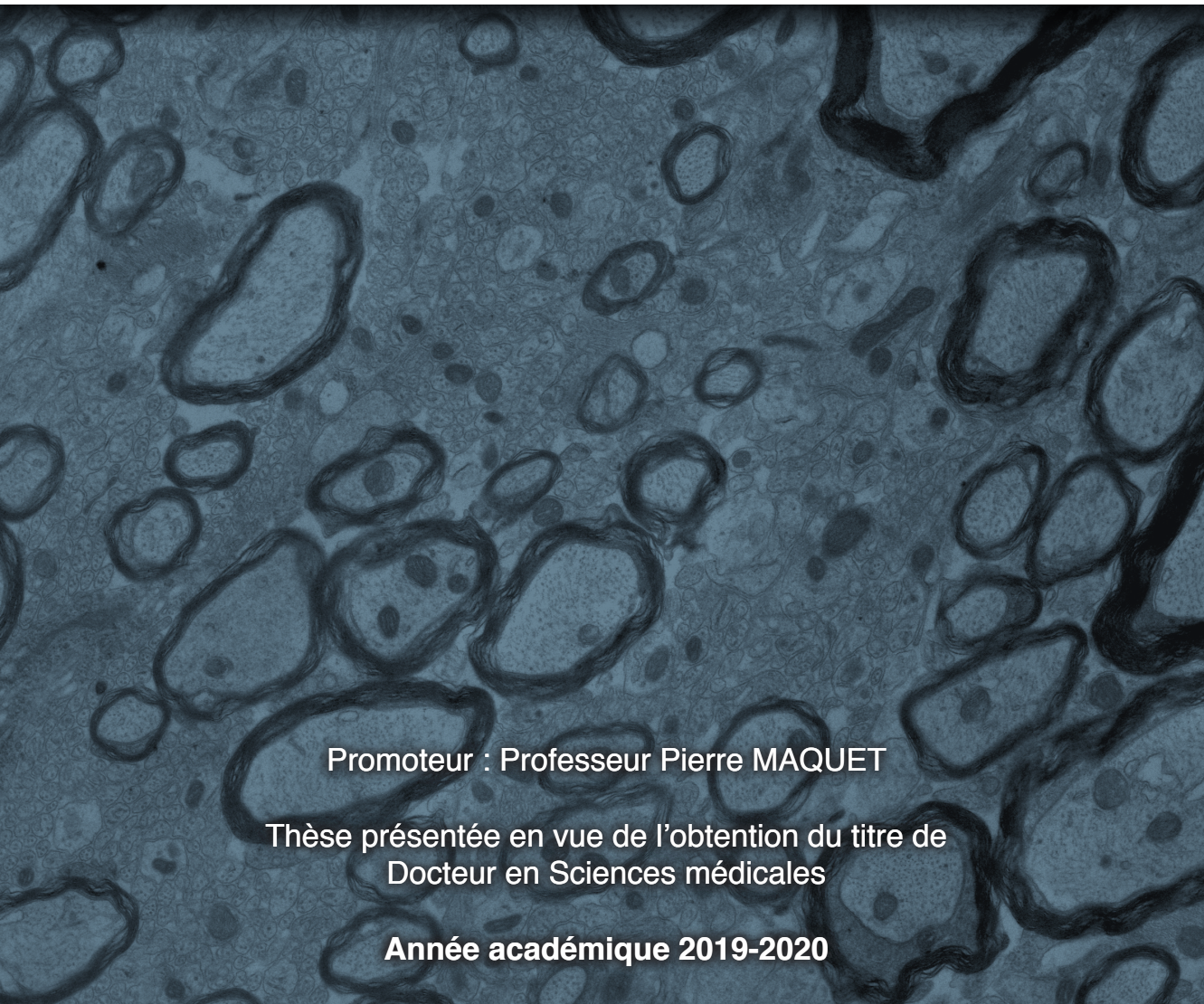

Promoteur : Professeur Pierre MAQUET

Thèse présentée en vue de l'obtention du titre de
Docteur en Sciences médicales

Année académique 2019-2020

Université de Liège
GIGA-CRC in vivo imaging
Faculté de Médecine
Service de Neurologie, CHU de Liège

Multiparameter MRI quantification of microstructural brain alterations in multiple sclerosis

Emilie LOMMERS, M.D.

Thèse présentée en vue de l'obtention du titre de
Docteur en Sciences médicales

Année académique 2019-2020

Cover picture: Transmission electron microscopy cross-section of a 28 days old wild-type mouse spinal cord, illustrating myelinated axons within white matter. Photo reproduced by kind permission of Rachelle FRANZEN, GIGA-Neurosciences/Nervous System Disorders and Therapy Unit.

Promoteur

Professeur Pierre MAQUET
Université de Liège

Composition du Jury

Professeur Christophe PHILLIPS, Président du Jury
Université de Liège

Madame Evelyne BALTEAU
Université de Liège

Professeur Dominique DIVE
Université de Liège

Professeur Gaëtan GARRAUX
Université de Liège

Professeur Céline LOUAPRE
Institut du Cerveau et de la Moelle épinière, Paris

Professeur Vincent VAN PESCH
Université Catholique de Louvain

Ce travail a été réalisé grâce au soutien financier du Fonds National de la Recherche Scientifique (FRS-FNRS), du Fonds Léon Fredericq et de la Ligue Belge de la Sclérose en Plaques.

« Ne jamais rien faire qui n'ait pour buts et moyens l'émotion, la poésie et le cœur »

Eugène Ysaÿe

« Ce qui est important, ce n'est pas de finir une œuvre, mais d'entrevoir qu'elle permette un jour de commencer quelque chose »

Joan Miró

MERCI…

Ce travail s'inscrit dans la durée. Il constitue le fil conducteur d'une tranche de vie à laquelle de nombreuses personnes se sont trouvées mêlées, de manière fortuite ou non, pour le pire ou le meilleur. Certaines de ces personnes ont joué un rôle fondamental dans la naissance, la consolidation et la trajectoire de ce fil. Ces remerciements leur sont tout particulièrement adressés.

Avant tout, je souhaite exprimer ma profonde reconnaissance envers le Professeur Pierre Maquet. Je le remercie d'avoir accepté la supervision de ce travail et de m'avoir guidée, patiemment, dans les dédales du monde scientifique. Je le remercie pour ses idées brillantes et ambitieuses, pour son enthousiasme permanent, pour son éternelle disponibilité,… Je le remercie également d'avoir permis un équilibre entre pratique clinique et recherche, lequel apporte une dimension supplémentaire à la prise en charge de nos patients.

Je tiens ensuite à remercier les membres du jury et particulièrement Christophe Phillips, Président du comité, pour son expertise inégalable dans le processing de l'image et le design statistique. Je remercie également Evelyne Balteau, sans qui le fonctionnement de l'IRM apparaîtrait sans doute toujours un peu nébuleux, ainsi que Dominique Dive et Gaëtan Garraux, pour leur partage de connaissances. Je témoigne enfin toute ma gratitude aux Professeurs Céline Louapre et Vincent van Pesch qui nous ont fait l'honneur de rejoindre ce jury et d'évaluer notre travail.

J'adresse également un remerciement chaleureux à tous les patients et sujets sains ayant participé à ce projet. Ils n'ont pas manqué d'enthousiasme ! Je remercie le Fonds National de la Recherche Scientifique, le Fonds Léon Fredericq et la Ligue Belge de la Sclérose en Plaques, pour leur soutien financier.

Je souhaite remercier les chercheurs du Centre de Recherches du Cyclotron. Je pense en particulier à Jessica Simon, dont l'aide précieuse m'a permis d'apprivoiser le logiciel statistique SAS, ainsi qu'aux personnes porteuses de nouveaux projets dans le domaine de la sclérose en plaques: Fabienne Collette, Solène Dauby, Camille Guillemin, Nora Vandeleene. Je me réjouis de nos futures collaborations !

Je remercie également mes collègues, qu'ils soient neurologues, neurochirurgiens, infirmiers, neuropsychologues, kinésithérapeutes… pour leurs nombreux encouragements. Je pense de façon émue à mon collègue et ami, Rémy Phan-Ba, dont le souvenir m'accompagne à tout moment.

Je profite de cette occasion pour remercier ma famille. Je remercie mes parents de nous avoir enseigné la valeur du savoir, de la patience, du courage, de l'empathie… et de nous inviter continuellement à penser plus loin. Je remercie mes sœurs – Anne, Céline, Thérèse – et mon frère Henri, pour leur présence et leur affection infinie.

Enfin, je remercie Julien… La musique, la peinture, le silence, la nature… sont autant de choses qui nous tirent vers le haut…

ABSTRACT

Multiple sclerosis (MS) is an inflammatory demyelinating and neurodegenerative disorder of the central nervous system (CNS), which stands as the most common cause of neurological disability in young adults. Traditionally, MS is primarily characterized by the accumulation of focal demyelinated plaques within the white matter (WM). With the advent of highly developed histopathological techniques in the second half of the 20th century, it became clear that focal lesions are also present in grey matter (GM), and that neurodegeneration diffusely affects macroscopically normal-appearing brain tissues (NABT). These observations are particularly evident in the progressive forms of the disease.

Nevertheless, in vivo evaluation of MS patients remains unsatisfactory, because conventional MRI is insensitive to many pathological mechanisms underpinning MS. In the present work, we precisely aimed at improving the impact of 3 Tesla MRI on the detection and characterization of these processes, using quantitative MRI (qMRI) parameters sensitive to iron and myelin contents: magnetization transfer (MT) saturation, effective transverse relaxation rate R2* (1/T2*) and longitudinal relaxation rate R1 (1/T1).

We designed a prospective cross-sectional study, contrasting 36 MS patients to 36 age-matched healthy controls. Processing and statistical analyses of MRI data were conducted on the basis of two distinct approaches: general analysis looked for differences in qMRI parameters summarized over three different NABT classes (normal appearing cortical and deep grey matters, normal appearing white matter), whereas voxel-based analyses assessed the spatial distribution of qMRI changes within normal appearing cortical and deep grey matters.

Consistent with histopathological findings, results suggest a widespread reduction in myelin and/or iron contents within NABT of MS patients, both at the global and loco-regional levels, and beyond the ability of atrophy measurements. Interestingly, these microstructural alterations tend to be more pronounced and diffuse in progressive MS population. Moreover, correlation analyses indicate that they might play a significant role in determining brain volume loss as well as irreversible disability in MS.

Our cross-sectional study proves that simultaneous quantification of multiple MRI parameters can sensitively assess NABT microstructure in MS. However, future large-scale studies should evaluate the reproducibility and predictive values of these results.

RESUME

La sclérose en plaques (SP) est une pathologie inflammatoire chronique du système nerveux central. Elle est une cause majeure de handicap neurologique chez l'adulte jeune. Depuis sa description initiale (Charcot, 1880), la SP a essentiellement été considérée comme une pathologie de la substance blanche, au sein de laquelle voyaient s'accumuler des lésions inflammatoires démyélinisantes focales (les plaques). Les importants progrès réalisés en histopathologie ont néanmoins permis de montrer que les plaques peuvent également toucher la substance grise, en particulier le ruban cortical. Il existe également des preuves de l'accumulation de lésions neurono-axonales au sein de la substance blanche et grise d'apparence normale. Ces caractéristiques sont des éléments pathophysiologiques dominants des phénotypes cliniques progressifs.

Dans la pratique de routine, les outils radiologiques utilisés dans l'évaluation de la SP demeurent imprécis, en raison de leur faible sensibilité vis à vis des processus pathologiques touchant la substance grise et blanche d'apparence normale. Ce travail a précisément pour objectif d'améliorer la détection et la caractérisation de ces altérations cérébrales diffuses, grâce à la quantification simultanée de trois paramètres remnographiques (3 Tesla) sensibles aux contenus en fer et myéline: le transfert de magnétisation, le taux de relaxation transverse effective (R2*) et le taux de relaxation longitudinale (R1).

Cette étude prospective transversale compare 36 patients SP à une population saine appareillée pour l'âge. L'analyse des données IRM a été réalisée selon deux approches. En premier lieu, pour chaque paramètre, les valeurs extraites de chaque voxel ont été moyennées au sein de chacune des classes tissulaires

d'apparence normale: substance grise corticale et profonde, substance blanche. Dans un second temps, des analyses "voxel-based" ont permis d'évaluer la distribution spatiale des différences entre patients et sujets contrôles, au sein de la substance grise uniquement.

De manière consistante avec la littérature existante, nos résultats suggèrent une réduction diffuse des contenus en fer et/ou myéline au sein des différents tissus d'apparence normale, et ce pour les deux types d'analyses. De façon intéressante, nous constatons que les anomalies observées sont plus prononcées et diffuses chez les patients présentant une phénotype clinique progressif. De plus, les études de corrélation indiquent que ces anomalies sont en lien avec la perte de volume cérébral et la progression du handicap.

Cette étude démontre l'intérêt de la quantification IRM multiparamétrique dans l'évaluation des processus pathologiques s'accumulant au sein des tissus cérébraux d'apparence normale. Des études longitudinales seront néanmoins indispensables pour évaluer la reproductibilité et la valeur prédictive de nos résultats.

CONTENTS

LIST OF FIGURES

LIST OF TABLES

LIST OF ABBREVIATIONS

BPF: Brain Parenchymal Fraction
CVLT: California Verbal Learning Test
EDSS: Expanded Disability Status Scale
GMF: Grey Matter Fraction
HC: Healthy Controls
LF: Lesion Fraction
MPM: Multiparameter mapping
MRI: Magnetic Resonance Imaging
MS: Multiple Sclerosis
MT: Magnetization Transfer
MTR: Magnetization Transfer Ratio
NABT: Normal Appearing Brain Tissue
NACGM: Normal Appearing Cortical Grey Matter
NADGM: Normal Appearing Deep Grey matter
NAGM: Normal Appearing Grey Matter
NAWM: Normal Appearing White Matter
qMRI: Quantitative MRI
RRMS: Relapsing-Remitting Multiple Sclerosis
PMS: Progressive Multiple Sclerosis
R1: Longitudinal Relaxation Rate R1 (1/T1)
R2*: Effective Transverse Relaxation Rate R2* (1/T2*)
SDMT: Symbol Digit Modalities test
TIV: Total Intracranial Volume
T25FW: Time 25-Foot Walk
VBM: Voxel-Based Morphometry
VBQ: Voxel-Based Quantification

PART A

GENERAL INTRODUCTION

Chapter I: CLINICAL ASPECTS OF MULTIPLE SCLEROSIS

Multiple sclerosis (MS) is a chronic immune-mediated disease of the central nervous system (CNS). It stands as the most common cause of neurological disability in young adults, affecting more than 2,3 million people worldwide *(Aarli et al., 2014)*. While both genetic and environmental risk factors have been implicated in the pathogenesis of MS *(Reich et al., 2018)*, its prevalence is variable across continents and even countries. The higher prevalence is observed in Northern America and Europe (> 100/ 100 000) *(Aarli et al., 2014)*.

1. DISEASE PHENOTYPES

MS shows different patterns of evolution and variable rates of disability accumulation. The course of the disease is believed to result from the expression of two clinical phenomena, relapses of acute neurological symptoms followed by partial or complete recovery (remission), and progression, which refers to the steady and irreversible worsening of the clinical status over months or years *(Compston and Coles, 2008; Reich et al., 2018)*. For 85% of the patients, relapses are the exclusive clinical expression of MS during the early years of the disease and this defines the relapsing–remitting MS (RRMS) phenotype. Females are twice as likely to have RRMS as males. In a proportion of patients, the course of MS converts to a secondary progressive phase (SPMS). Finally, 15% of the patients begin with a progressive course from onset, without any relapses, i.e. primary progressive MS (PPMS), which incidence is similar in males and females *(Lublin and Reingold, 1996; Miller and Leary, 2007)*.

Relapses are considered to be the clinical manifestations of focal, acute and recurrent inflammatory demyelinating lesions, i.e. the plaques, occurring throughout the central nervous system (CNS). Resolution of inflammation, remyelination and plasticity are likely to contribute to total or partial remission. Post-mortem and brain imaging studies unanimously indicate that focal lesions can outnumber relapses by as much as 10 to 1, supporting the concept that relapses are often a subjective readout of focal inflammatory activity because their severity depends on whether plaques occur in an articulate area of the brain *(Barkhof et al., 1992; Frischer et al., 2015)*.

On the other hand, neurodegeneration (mainly axonal and neuronal loss) is accepted as the major cause of progressive and irreversible neurological disability in MS patients. For several decades, neurodegeneration was exclusively linked to axonal transection within plaques, following repeated episodes of demyelination and failure of repair or compensatory mechanisms *(Dutta and Trapp, 2007; Trapp et al., 1998)*. However, this view has been challenged by a large body of data from clinical, radiological and neuropathological studies. It has been shown that relapse frequency beyond year 2 does not appear to predict the key outcome of secondary progression or time to significant irreversible disability *(Scalfari et al., 2010)* and that once this clinical threshold has been reached, the rate of progression seems to be homogeneous and independent of the preceding disease course *(Confavreux et al., 2000; Confavreux and Vukusic, 2006)*. By the same token, results from clinical trials evaluating the efficacy of first-line disease-modifying treatments failed to demonstrate a clear effect of relapse reduction on delaying progression *(IFNB Multiple Sclerosis Study Group, 1993; Johnson et al., 1995; PRISMS Study Group, 1998; Shirani et al., 2012)*. Moreover, while still representing the most common outcome measure for evaluating treatment efficacy in MS, the number of focal lesions depicted on magnetic resonance imaging (MRI) – hyperintense T2/FLAIR and T1 enhan-

cing lesions – modestly correlates with late disability *(Barkhof, 2002; Fisniku et al., 2008)*. Most important of all, advanced histopathological techniques have extensively demonstrated that besides focal lesions, MS brain tissue, which appears normal on clinical MR scans, nevertheless displays abnormalities. It consists of diffuse and chronic inflammatory processes within grey and white matters, that seem partly independent from focal pathology and occur since the earlier stage of the disease. They are responsible for a progressive and widespread neurono-axonal damage, leading ultimately to brain atrophy *(DeLuca et al., 2006; Haider et al., 2016; Kutzelnigg et al., 2005)*.

Consequently, this analysis brings to light the interplay between two biological processes – focal inflammation and diffuse neurodegeneration – occurring both in white and grey matters and driving the clinical phenotype of MS in the course of time. These processes are not uniformly expressed across patients, thus contributing to the heterogeneity in phenotypic expression of the disease (**Figure 1**). As proposed recently *(Lublin et al., 2014)*, it would therefore be more appropriate to differentiate MS phenotypes as relapsing-remitting MS with or without focal inflammatory activity and progressive MS (PMS – both SPMS and PPMS) with or without focal inflammatory activity and/or progression. In an individual patient, the transition from the relapsing-remitting to the progressive phase is likely to be the point at which neuronal injury exceeds brain compensatory capacity. Male gender, older age at disease onset, disease duration and higher early (first 2 years) relapse frequency are associated with a significantly shorter time to onset of progression *(Kremenchutzky et al., 2006; Scalfari et al., 2014)*.

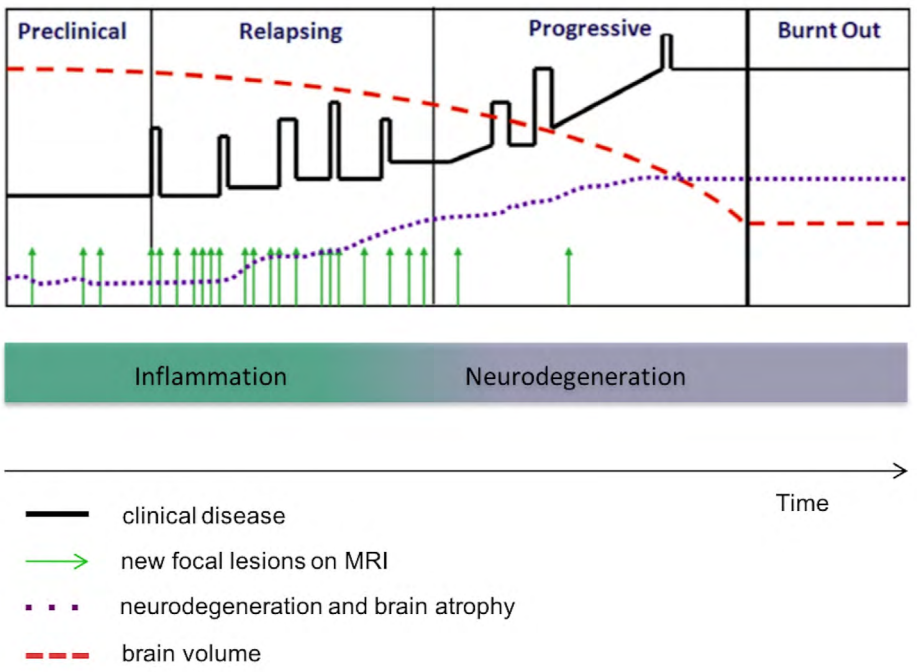

Figure 1: Time course of disease phenotype in relation with two different pathological processes, focal inflammation and diffuse neurodegeneration.

In the early phase of the disease, white matter lesions dominate. This is associated with clinical relapses (black line) and new lesions on MRI (green arrows). In the progressive stage, diffuse white and grey matters injury is seen in addition to focal white matter lesions. This results in neurodegeneration, brain atrophy (blue dotted line) and reduction of brain volume (red dashed line). At the "burn-out stage", inflammation and neurodegeneration decrease to level seen in age-matched controls, although the patients may become affected by concomitant age-related diseases such as stroke or Alzheimer's disease. Adapted from *(Lassmann and Van Horssen, 2011)*.

2. CLINICAL EVALUATION OF MS PATIENTS

At disease onset, the symptoms and signs of multiple sclerosis are notoriously variable. They depend on the focal inflammatory activity which can virtually occur anywhere in the CNS: sensory-motor deficits, gait disturbance, visual impairment reflecting demyelination in the optic nerve, oculomotor dysfunction, cerebellar or vestibular involvement, bowel or bladder dysfunction… With disease progression, the same manifestations can be observed but progressive cognitive and locomotor impairment dominates the clinical picture. Additionally, other non-specific symptoms may appear, such as fatigue (motor and cognitive), pain as well as mood disorders *(Compston and Confavreux, 2006)*.

While careful neurological examination still remains the gold standard, standardized measures/scales of disability are required to track clinical disease evolution over time. The Expanded Disability Status Scale (EDSS) is the most popular instrument to describe disease progression *(Kurtzke, 1983)*. It consists of an ordinal rating system ranging from 0 (normal neurological status) to 10 (death due to MS) by 0.5 intervals. Lower EDSS values measure impairments based on the neurological examination, while the upper range of the scale (> EDSS 6) estimates patient disability. The EDSS range from 4 to 6 heavily depends on walking ability **(see Appendix 1, Table S1.1)**. Despite its lack of sensitivity and intra- and inter-rater reliability, the EDSS is still the most widely accepted global measure of neurological impairment in MS *(Schwid et al., 2002)*.

Overcoming some limitations of EDSS, the Multiple Sclerosis Functional Composite (MSFC) integrates multidimensional metrics of overall MS clinical status: assessment walking speed on short distance ("Timed 25-Foot Walk", T25FT), assessment of upper arm dexterity ("9-Hole Peg Test", 9HPT) as well

as evaluation of attention ("Paced Auditory Serial Addition test", PASAT) *(Polman and Rudick, 2010)*.

The protocol for a Brief International Cognitive Assessment for Multiple Sclerosis (BICAMS) is also recommended. This protocol is not a substitute for full cognitive assessment or screening, but rather a monitoring instrument of some principal cognitive functions. BICAMS comprises the Symbol Digit Modalities Test (attention and working memory), the California Verbal Learning Test-II (verbal memory) and the Brief Visuospatial Memory Test-Revised (visual memory) *(Benedict et al., 2012; Langdon et al., 2012)*.

A wealth of other clinical measures referring to patient-reported outcomes (fatigue, mood alteration, quality of life,…) *(Nowinski et al., 2017)* as well as actigraphy methods *(Kos et al., 2009)* were proposed for MS patient follow up, but they still need to be validated for clinical study purpose.

Chapter II: IN DEPTH OF MULTIPLE SCLEROSIS PATHOLOGY

Since its first description *(Charcot, 1880)*, the view of MS pathology centered on focal demyelinated plaques in the white matter (WM). With the advent of advanced histopathological techniques in the second half of the 20th century, it became clear that focal lesions are also present in grey matter (GM) *(Brownell and Hughes, 1962; Rudick et al., 2009)*. Furthermore, a diffuse neurodegeneration globally affects macroscopically normal-appearing white and grey matters (respectively NAWM and NAGM).

Multiple sclerosis is currently considered as a complex disease, involving focal and diffuse pathological processes, both occurring in the entire CNS and responsible for inflammation, demyelination, remyelination as well as neurono-axonal loss *(DeLuca et al., 2006; Haider et al., 2016; Kutzelnigg et al., 2005)*. **Figure 2** illustrates the anatomical regions of WM and GM pathologies discussed in our work.

1. WHITE MATTER PATHOLOGY

1.1 FOCAL WHITE MATTER LESIONS

While WM plaques can occur anywhere throughout the neuraxis, their distribution is certainly not random with periventricular, centrum semi-ovale and corpus callosal WM involvement being common *(Brownell and Hughes, 1962)*. Different from any other CNS inflammatory diseases, MS plaques are characterized by a selective perivenous and confluent primary demyelination, with loss of oligodendrocytes *(Lassmann, 2013)*. Axons are preserved to a variable

extent and the amount of axonal destruction is variable between lesions *(Trapp et al., 1998)*.

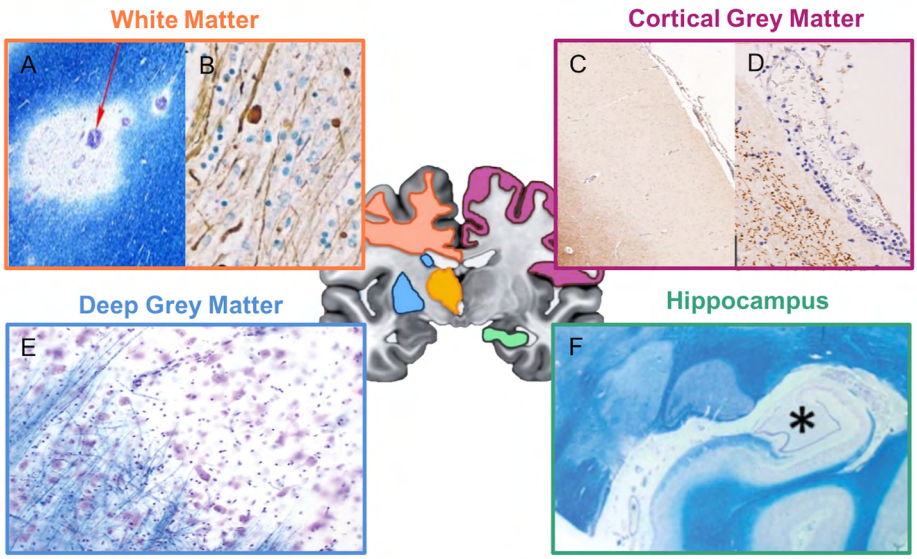

Figure 2: White and grey matters pathology in MS.

Schematic representation of pathology distribution in WM and GM discussed in this work (WM – orange box; cortical GM – burgundy red box; hippocampus – green box; deep GM – blue box), adapted from *(DeLuca et al., 2015)*. (A) Myelin stain (Luxol Fast Blue – LFB) in an acute active lesion. Lesion is centered around a small vessel surrounded by inflammatory cells *(Frohman et al., 2006)*; (B) Diffuse axonal injury, reflected by axonal swellings and end bulbs in the NAWM of PMS (immunocytochemistry for neurofilament) *(Kutzelnigg et al., 2005)*; (C) Subpial lesion overlaid by a perivascular meningeal inflammatory infiltrate (Myelin Proteolipid Protein – PLP – staining); (D) Higher magnification of the perivascular meningeal infiltrate (PLP staining) *(Popescu et al., 2012)*; (E) Border zone of a chronic thalamic lesion. The GM lesion (top right) is devoid of myelin (LFB staining) and hypocellular. Comparison with adjacent normal appearing grey matter (bottom left) reveals a reduction in the number of neurons and paucity of cells with oligodendrocytes morphology (LFB staining) *(Schoonheim et al., 2013)*; (F) Diffuse demyelination of the left hippocampus (asterisk, LFB staining) *(Schoonheim et al., 2013)*.

Inflammation initiated around veins is considered as the causal event of lesion formation. B and T lymphocytes as well as plasmocytes are recruited and cross the disrupted blood-brain barrier into the perivascular space, where ongoing immunological interactions take place. Early infiltration by phagocytic cells with a morphological phenotype of activated microglia or macrophages, gobble myelin debris. The extent of this reaction and the content of different myelin components in macrophages allow a temporal staging of lesions *(Brück et al., 1995; Frischer et al., 2015, 2009)*.

Acute active lesions are rich in macrophages at their core while microglial activation is most pronounced at their edge. Such active lesions are mainly seen in patients with RRMS **(Figure 3)**. They need to be differentiated from chronic active lesions – slowly expanding lesions – which are the most frequent in PMS. They show an inactive demyelinated center and a rim of activated microglia/macrophages at the edge. Only few of these macrophages contain early myelin degradation products suggesting a slow expansion of the pre-existing plaques. Chronic inactive lesions, most abundant in the MS brain, are sharply circumscribed areas of demyelination with profound reduction of activated microglia and fibrillary gliosis. In relation to the severity of inflammation, extensive and profound acute axonal injuries – axonal swelling and bulbs – take place in both acute active plaques and active edge of chronic active lesions. In inactive lesions, there is still a low degree of ongoing acute axonal injury, indicating the permanent deterioration of chronically demyelinated axons *(Dutta and Trapp, 2007; Frischer et al., 2015, 2009)*.

Remyelination by oligodendrocytes progenitor cells (OPCs) is highly variable within lesions and appears less efficient than in cortical GM. The extent of remyelination is determined by several factors, including the potential of progenitor cells to differentiate, the conservation of axons and the occurrence

of demyelination in remyelinated area. Completely remyelinated WM plaques are classified as shadow plaques *(Brück et al., 2003; Franklin et al., 2012; Frischer et al., 2015)*.

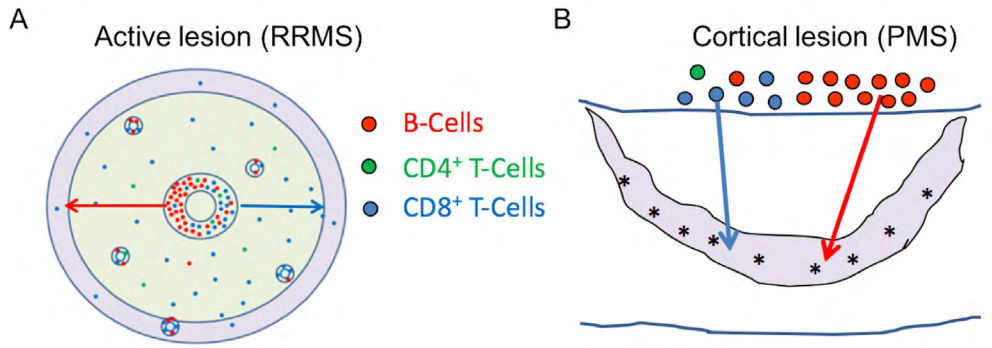

Figure 3: Relation between inflammation and tissue injury in MS lesions.

(A) Schematic of an active multiple sclerosis lesion with inflammation centered on a large vein surrounded by a demyelinated tissue area containing macrophages with different stages of myelin degradation (green zone), and a rim of initial tissue injury (grey zone) characterized by microglial activation, oligodendrocyte injury (loss of myelin associated glycoprotein) and oligodendrocyte apoptosis. The highest density of lymphocytes, mostly CD20+ B cells, is seen in the perivascular space of the central vein. CD8+ T cells also diffusely infiltrate the lesion parenchyma (green zone); (B) Schematic of a subpial lesion with meningeal inflammatory aggregates responsible for active demyelination and neurodegeneration in the underlying cortex, without parenchymal cellular infiltrations. This implies a soluble factor in the CSF, diffusing in the cortical parenchyma (asterisk). Adapted from *(Machado-Santos et al., 2018; Magliozzi et al., 2010)*.

1.2 DIFFUSE CHANGES IN NORMAL APPEARING WHITE MATTER

Diffuse alteration of NAWM is most pronounced in PMS. It consists of perivascular and diffuse inflammatory infiltrates of T and B cells as well as a diffuse activation of microglia and astrocytes. It is associated with diffuse axonal injury and loss throughout the NAWM. The reduction in the intensity of myelin staining which is generally observed, is due to decreased fiber density (axons and myelin) and not to primary demyelination. These changes are partly imputable to Wallerian degeneration in relation with axonal loss within focal WM lesions. However, the extent of global injury in the NAWM does not correlate with number, size or location of focal WM lesions *(Haider et al., 2016; Kutzelnigg et al., 2005)*. A moderate correlation is observed between NAWM and cortical demyelination, suggesting neuronal loss in cortex as a contributing factor. Nevertheless, it seems that diffuse damage in NAWM is at least in part mediated by the diffuse inflammatory reaction itself *(Frischer et al., 2009; Haider et al., 2016; Kutzelnigg et al., 2005)*.

2. GREY MATTER PATHOLOGY

2.1 NEOCORTICAL LESIONS

Like in WM lesions, primary demyelination and oligodendrocyte destruction are the pathological hallmark of GM focal lesions. However, the degree of inflammation, microglial activation and macrophages recruitment are much less pronounced. Demyelination is associated with fewer axonal and neurons loss but is accompanied by an even greater loss of synapses. Remyelination is more extensive in cortex compared to WM *(Haider et al., 2016; Kutzelnigg et al., 2005; Popescu et al., 2012)*.

Different types of cortical lesions are found in the MS brain, which are more frequently reported in PMS. Type 1, or leukocortical lesions, are present at the cortico-subcortical border and affect both WM and GM. Type 2 lesions are small perivenous intracortical lesions. Type 3 lesions are located in the subpial layers, expanding from the pial surface into the deeper cortical layers. They are associated with inflammatory aggregates in leptomeninges and become extensive in the later stage of the disease *(Haider et al., 2016; Kutzelnigg et al., 2005; Popescu et al., 2012)*. Subpial cortical demyelination is a highly specific feature of MS pathology **(Figure 3)**.

Neurono-axonal loss is also detected in NAGM distant from lesions *(Klaver et al., 2015)*. Compelling evidence suggests that diffuse intraparenchymal inflammatory reaction and/or diffusible cytotoxic factors are able to induce profound synaptic dysfunction and secondary disruption of the neurono-axonal unit, without any demyelination *(Centonze et al., 2010; Jürgens et al., 2016; Mandolesi et al., 2015)*. Deafferentation after axonal transection in connected WM tracts should also be considered as a mechanism of diffuse cortical neurodegeneration *(DeLuca et al., 2015, 2006)*.

2.2 NON-NEOCORTICAL GREY MATTER DAMAGE

Post-mortem studies reveal the presence of demyelination and neurodegeneration within deep GM nuclei (both thalami and basal ganglia), hippocampi, cerebellum and spinal cord *(Geurts et al., 2007; Gilmore et al., 2006; Kutzelnigg et al., 2007; Vercellino et al., 2009)*. Lesions in these structures are less frequent and extensive when compared to neocortical regions. Moreover, they have less inflammatory involvement and neurodegeneration may vary *(Van Munster et al., 2015)*.

Demyelination has been detected in 53 to 79% of postmortem MS hippocampi. Cornu ammonis 1 (CA1) and subiculum seem to be most vulnerable to subpial demyelinating lesions. However, no hippocampal subregion appears to be spared in more advanced stages of the disease. In demyelinated hippocampus sample, extensive synaptic loss with relatively intact neuronal count was reported *(Dutta et al., 2011; Geurts et al., 2007; Papadopoulos et al., 2009)*. Interestingly, two pathological studies report that hippocampal demyelination in MS induced alterations in genic expression profiles, leading to abnormalities in hippocampal axonal traffic, synaptic plasticity and neurotransmitter homeostasis *(Dutta et al., 2013, 2011)*. These molecular changes are not detected in demyelinated MS motor cortex and therefore point out the specialized function of hippocampal myelin *(Dutta et al., 2011)*.

Deep GM demyelination was found in all MS phenotypes, beginning in the earlier stage, contrary to what is generally observed in cortex. GM focal demyelinating lesions were most frequently detected in the hypothalamus and caudate, followed by thalamus *(Haider et al., 2014; Vercellino et al., 2009)*.

Neuronal loss and axonal injury are the dominant elements of MS thalamic pathology, and contribute to the significant volume loss which occurs very early in the disease course *(Eshaghi et al., 2018; Schoonheim et al., 2013)*. The thalamus has extensive reciprocal connections with cortical and subcortical structures and is particularly vulnerable to neuronal damage through trans-synaptic – anterograde and retrograde – neurono-axonal degeneration. Diffuse activation of microglia is also detectable within thalami, albeit at a lower degree than in NAWM, and is involved in thalamic neurodegeneration *(Haider et al., 2016; Vercellino et al., 2009)*.

3. MECHANISMS UNDERLYING MS PATHOLOGY

Different molecular mechanisms are thought to underly MS brain pathological changes. Inflammation, microglial activation, oxidative injury and mitochondrial damage may represent key factors in triggering demyelination and neurodegeneration. Their relative contribution may differ according to the type and location of lesions as well as the disease stage. **Figure 4** highlights the evolution of structural pathology and disease mechanisms during the course of MS.

3.1 INFLAMMATION

Whether inflammation is a primary event in the evolution of lesion formation or just a reaction to tissue injury resulting from non-inflammatory mechanisms has been disputed for many years. Various arguments support the role of inflammatory process as the major driving force of demyelination and neurodegeneration in all stages of MS, at least as long as the disease is active *(Frischer et al., 2009)*.

As described above, in the earliest stage of lesion formation, inflammation starts around small veins and venules. The more active the lesions, the larger the inflammatory infiltrates within CNS tissue: pronounced in active lesions, lower in inactive lesions and NAWM, rare or absent in the cortical parenchyma *(Frischer et al., 2009)*. They are composed of lymphocytes, the vast majority of them being CD8+ T cells, showing clonal expansion within lesions. CD20+ B cells or plasma cells and CD4+ T cells are mainly seen in perivascular spaces and meninges, whereas their infiltration in CNS tissue is sparse *(Frischer et al., 2009; Haider et al., 2016; Lassmann, 2018; Lassmann and Van Horssen, 2011)* **(Figure 3)**. Interestingly, CD8+ T cells involved in MS have recently been identified as tissue resident memory T cells, that invade CNS tissues after ente-

ring in contact with antigen, without recirculating. They reactivate and sustain the inflammatory response when re-exposed to their specific antigen (likely a foreign antigen or a modified self-antigen) *(Machado-Santos et al., 2018)*. The inflammatory processes are associated with the expression of pro-inflammatory/anti-inflammatory cytokines and adhesion molecules which are involved in the recruitment of different lymphocytes subsets and macrophages, and in the profound activation of microglia *(Cannella and Raine, 1995; Lassmann, 2014; Sørensen et al., 1999)*. Studies based on a large set of brain biopsies with acute demyelinating lesions reveal that, despite similarities in the inflammatory reaction, active demyelinating lesions segregate into different patterns of myelin destruction: macrophage-associated demyelination (type I), antibody/complement-mediated demyelination (type II), distal oligodendrogliopathy-associated demyelination (type III) and primary oligodendrocytes damage with secondary demyelination (type IV). A profound heterogeneity in the patterns of demyelination between different patients are observed although active plaques from the same patient are very similar *(Lassmann et al., 2001)*. The pattern of demyelination is more uniform in chronic active lesions, the major subtype in active progressive MS, probably because their slow expansion hinders the identification of specific patterns *(Lassmann and Van Horssen, 2011)*.

Inflammation during early stages of MS is associated with profound blood-brain barrier leakage, indicating the infiltration of the CNS by new waves of inflammatory cells. With progression of the disease, inflammation becomes trapped within the CNS, behind a closed or repaired blood-brain barrier *(Hochmeister et al., 2006)*. Furthermore, in progressive MS, dense aggregates of inflammatory cells, which may organize in structures like secondary lymph follicles, are seen in the meninges and, at a lesser extent, in the large Perivascular Virchow Robin Space *(Popescu et al., 2012)*. This compartmentalized meningeal inflammation is responsible for profound active subpial demyelination and neurode-

generation in the underlying cortex, without parenchymal cellular infiltrations **(Figure 3)** *(Howell et al., 2011; Magliozzi et al., 2007; Popescu et al., 2012)*. Such demyelination is preferentially located in cortical sulci and deep invaginations of the brain surface, which are exposed to relative cerebrospinal fluid stasis. These observations suggest that subpial demyelination might be driven by a soluble factor produced by inflammatory follicles, which diffuses into the cortex and triggers demyelination either directly or through activation of microglia. *(Howell et al., 2011; Magliozzi et al., 2018, 2007)*. The nature of this soluble factor is still unknow despite intensive international efforts to identify it. Beyond potential MS-specific antibodies, ceramides *(Vidaurre et al., 2014)*, semaphorin 4A *(Chiou et al., 2018)*, B-lymphocyte derived factor of 300kD *(Lisak et al., 2017)*,… are also suggested as potential demyelinating or cytotoxic factors.

Histopathological data also suggest that, at the very last stage or "burn-out" stage of MS, the inflammatory process may die out. In that case, inflammation and ongoing neurodegeneration may decline to levels observed in age-matched controls. However, the previously accrued MS lesions, combined with aged-related neurodegeneration and co-morbidities (i.e. vascular diseases) result in further clinical disease progression *(Frischer et al., 2009)*.

The above described observations support the view that inflammation drives demyelination and neurodegeneration in MS. The differences in the nature of inflammatory response between RRMS and PMS emphasize the heterogeneity of the disease between- and within-patient, and help explain the differences in the effectiveness of anti-inflammatory treatments.

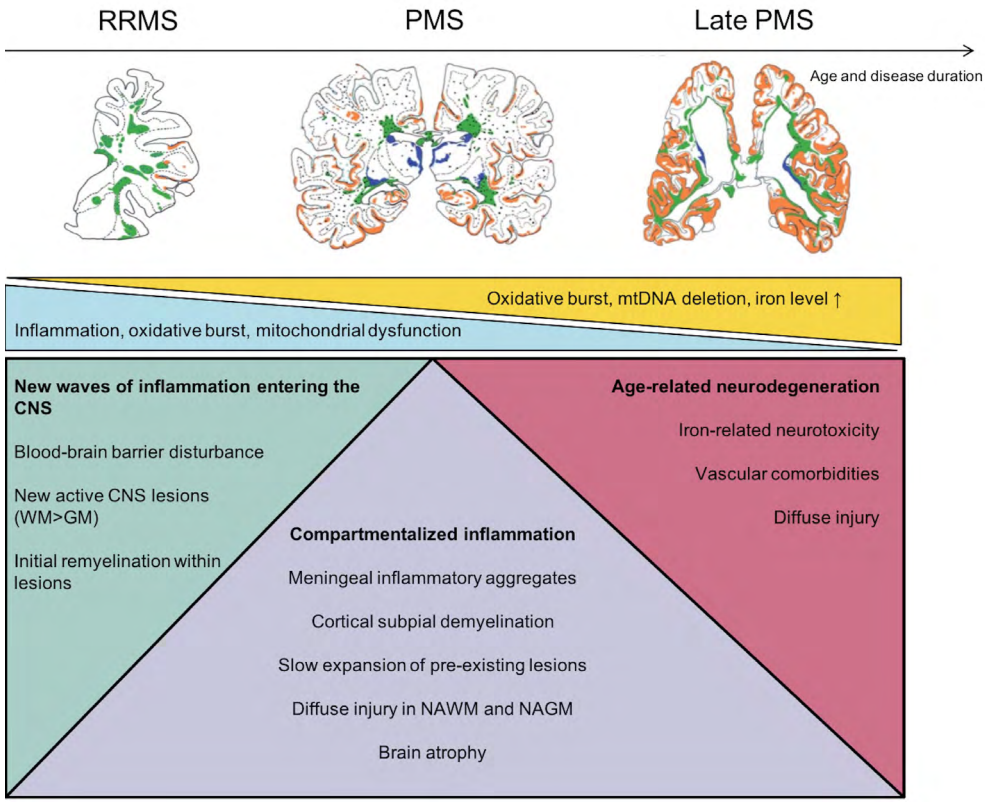

Figure 4: Evolution of structural pathology and disease mechanisms during the course of MS.

In RRMS, WM lesions dominate (green). In PMS, massive cortical demyelination (orange) and diffuse inflammation in NAWM (blue dots) are seen, in addition to focal white matter lesions (green) and deep GM lesions (blue). Atrophy becomes more pronounced. In the late stage of the disease, lesions accumulate at sites of low vascular perfusion and the influence of age-related factors and comorbidities amplify demyelination and neurodegeneration. Specific pathological features associated with RRMS (green box), PMS (purple box) and late PMS (red box), specific disease mechanisms (yellow and blue bars) occurring with time. Adapted from *(Kutzelnigg et al., 2005; Lassmann et al., 2012; Lassmann and Van Horssen, 2011)*.

3.2 MICROGLIAL ACTIVATION AND OXIDATIVE BURST

At all MS stages, microglial activation is observed in relation with the chronic inflammatory reaction induced by the adaptive immune system. However microglial activation is a non-specific response raised in many other neuro-inflammatory or neurodegenerative diseases. Therefore, if microglial activation undoubtedly contributes to MS neurodegeneration, it unlikely triggers initial tissue damage specific to MS *(Correale, 2014)*.

Oxidative bursts by activated microglia and macrophages seem to play a major role in the induction of progressive demyelination and axonal injury in MS *(Correale, 2014)*. These innate immune cells massively produce reactive oxygen and nitrogen species (respectively ROS and RNS), as reflected by the expression of inducible nitric oxide synthase, NADPH oxidase complexes and myeloperoxidase in microglial infiltrates *(Fischer et al., 2012)*. Moreover, in active lesions, oxidized DNA and phospholipids are abundantly detected in cytoplasm of oligodendrocytes and neurons showing signs of degeneration or apoptosis. This process is associated with profound mitochondrial dysfunction *(Haider et al., 2011)*.

Oxidative injury is clearly associated with focal inflammation in active plaques and is considered as an early event. However, it is also pronounced in PMS NAWM and NAGM. This suggests additional mechanisms of radical generation, amplifying neurodegeneration in PMS patients *(Friese et al., 2014)*.

Importantly, iron in ferrous state (Fe2+) is released into the extracellular space by injured oligodendrocytes and amplifies oxidative damage through formation of highly toxic hydroxyl (OH) radicals from H2O2. Iron uptake by macrophages and activated microglia causes partial cellular dystrophy. Eventually

these cells undergo fragmentation and degeneration, leading to a second wave of Fe2+ release, which can reinforce free-radical induced demyelination and neurono-axonal destruction.

3.3 MITOCHONDRIAL DYSFUNCTION

Mitochondrial dysfunction driven by oxidative burst stands as an important component of MS pathogenesis. It results from disruption of mitochondrial enzyme function, degradation of mitochondrial protein, interference with de novo synthesis of respiratory chain components as well as direct mitochondrial DNA (mtDNA) damage *(Campbell et al., 2011; Haider et al., 2011; Mahad et al., 2008)*. In principle, CNS tissue injury secondary to mitochondrial dysfunction can be induced by three different mechanisms: induction of apoptosis, energy failure and enhanced production of ROS *(Lassmann and Van Horssen, 2011)*.

Mitochondrial injury can result in a pro-apoptotic event, by the release of apoptotic-inducing factors (AIF) which translocate into the nuclei and induce irreversible DNA damage. This represents an important pathway for oligodendrocytes destruction *(Lassmann et al., 2012)*.

While axonal transport is highly energy-demanding, energy deficiency may contribute to a "virtual chronic hypoxia" environment, disturbing axonal ion homeostasis. Demyelinating axons show aberrant expression of Na+ channels, increasing the energy demands of nerve conduction. In conditions of energy deficiency, the ATP-dependent Na+ pump does not expel Na+, which accumulates in the axon and is replaced by Ca2+ through reverse operation of Na+/Ca2+ exchanger. Additional Ca2+ enters the axon via receptor for glutamate, which levels are elevated in MS, apparently deriving from dying neurons and secretion by activated microglia. When axoplasmic accumulation of Ca2+ exceeds the mitochondrial

buffering capacity, it precipitates axonal demise *(Friese et al., 2014)*.

Finally, mtDNA deletions over time increase mitochondrial dysfunction and dyscoupling of the respiratory chain, chronically enhancing ROS production through electron leakage *(Mahad et al., 2008; Murphy, 2009)*.

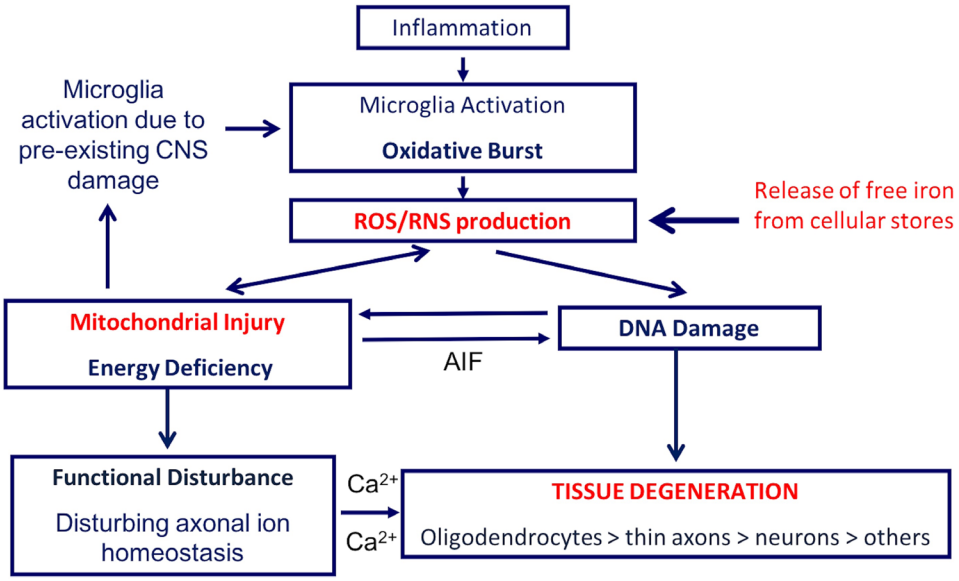

Figure 5: Proposed diagram centering MS pathophysiology on oxidative burst and mitochondrial dysfunction.

See text for further details. Adapted from Prof. Hans Lassmann's slide presented at the second "Journée Liégeoise de la Sclérose en Plaques", University of Liège, March 2019.

Oxidative burst and mitochondrial dysfunction are considered as the main culprit of tissue injury in MS (**Figure 5**). Interestingly, the implication of "virtual hypoxia" can explain the accumulation of MS persistent lesions at sites of low vascular perfusion and the influence of age-related vascular comorbidities in amplifying demyelination and neurodegeneration *(Haider et al., 2016)*.

3.4 THE ROLE OF IRON

Most iron found in the human brain is stored as non-heme iron in oligodendrocytes and its concentration increases with age. The maintenance of proper iron concentration in the CNS is vital to optimal functioning. Iron is involved in many crucial processes including myelin production and repair, oxygen transport, glucose metabolism, synthesis of neurotransmitters and DNA replication. However, as discussed above, free Fe2+ may also generate toxic ROS, enhancing the oxidative burst and related tissue damage *(Stephenson et al., 2014)*.

Histopathological studies provide important information about altered iron homeostasis in MS. In active MS lesions, iron is released by dying oligodendrocytes, resulting in extracellular accumulation of iron and uptake by microglia and macrophages at the rim of lesion *(Hametner et al., 2013)*. Particularly in PMS patients, iron accumulation is also observed in deep GM, at a significantly higher level than that in the cortical GM *(Haider et al., 2014)*. In patients with short disease duration, age-related increase of iron is observed in NAWM. In PMS, however, there is a significant decrease of iron in the NAWM, corresponding with disease duration. This decrease of iron is associated with loss of oligodendrocytes and myelin but also with an upregulation of iron-exporting ferroxidases in relation with chronic inflammation *(Hametner et al., 2013)*.

Other sources of iron dysregulation are also possible but their implication in MS remains hypothetical: perturbation of iron transport and regulatory proteins, vascular damage or interference with the blood-brain barrier *(Stephenson et al., 2014)*.

3.5 REMYELINATION AND REPAIR

Endogenous remyelination is observed in both acute and chronic phases of MS. However, remyelination is often heterogeneous and even when repair occurs, myelin formed after inflammatory injury is qualitatively different, with thinner myelin sheets and short internodes. Remyelinated area are more susceptible to a second inflammatory attack and are more likely to suffer from chronic demyelination and axonal degeneration *(Brück et al., 2003; Cunniffe and Coles, 2019)*.

Key factors are required for successful remyelination. First, functionally healthy axons are needed. Axonal injury diffusely occurs in MS and therefore limits successful myelin repair. Second, remyelination depends upon successful differentiation and maturation of OPCs. OPCs are found throughout the adult CNS and are present in MS plaques. Their maturation relies on highly regulated microenvironment with a careful balance of pro- and anti-inflammatory mediators, which is not easy to reach on a chronic inflammatory demyelinating background. Age, disease duration and anatomical considerations are also contributing factors to insufficient remyelination. As an example, periventricular lesions are less able to remyelinate than subcortical lesions, reflecting the heterogeneity in OPCs location or permissibility for their differentiation.

Together, these observations contribute to the almost total absence of repair in chronic MS. However, there remain many unanswered questions on the complexity of this process *(Brück et al., 2003; Cunniffe and Coles, 2019)*.

Chapter III: MEASURING MULTIPLE SCLEROSIS ACTIVITY IN VIVO: DISEASE BIOMARKERS

A biomarker refers to an objective characteristic that can be evaluated and measured. It may reflect normal biological processes, pathogenic processes or a response to therapy. To be useful, biomarkers should be clinically informative, correlated with a clinical outcome, easily measurable and routinely accessible. While the value of established biomarkers to diagnose and manage human disease is undeniable, the difficulty remains to achieve key optimal features: reproducibility, validation in pathologic studies, high sensitivity and specificity *(Bielekova and Martin, 2004)*.

As previously discussed, multiple sclerosis is a complex disease, involving several diffuse and focal pathophysiological processes: inflammation, demyelination, neurono-axonal loss and repair mechanisms. At the beginning of the disease, most of these processes are clinically silent. Furthermore, they are not uniformly represented across patients, contributing to the heterogeneity of clinical phenotype, prognosis and response to treatment. Using the currently validated biomarkers in the routine practice – conventional MRI and oligo-clonal bands in the CSF – only a little part of the MS iceberg is visible above water *(Housley et al., 2015)*. This analogy requires the development of new valuable biomarkers, to access the immersed part of the disease and allow earlier diagnosis, measurement of distinct damage mechanisms, identification of prognosis as well as evaluation of treatment response.

During the last two decades, there has been an ever-growing number of publications on potential new MS biomarkers: serum and CSF measurements **(see Appendix 1, Table S1.2)** *(Bielekova and Martin, 2004; Housley et al., 2015; Teu-*

nissen et al., 2015), markers of genetic susceptibility *(Housley et al., 2015)*, new electrophysiological *(Giffroy et al., 2019, 2016)* as well as imaging techniques *(Comabella et al., 2016; Enzinger et al., 2015; Filippi and Rocca, 2010)*. This chapter focuses on new potential MR-derived measures to overcome the current limitations of conventional MRI.

1. CONVENTIONAL MRI

Conventional MRI **(Figure 6)** readily depicts focal WM lesions on T2-weighted or fluid-attenuated inversion recovery (FLAIR) sequences. These lesions appear as non-specific focal areas of signal increase, resembling many other types of pathology. Characteristic features become more evident when considering lesion appearance, location and signal evolution with additional MR sequences *(Filippi et al., 2012)*.

WM lesions are typically oval- or elliptic-shaped (because centered on vein) and preferentially located in periventricular regions, corpus callosum, brainstem, juxta-cortical border and spinal cord *(Filippi and Agosta, 2010)*.
Ten to 30% of T2 hyperintensities are also visible on T1-weighted sequence as area of low signal intensity. In the acute phase, it is probably the consequence of edema while chronic foci of T1 hypointensity – the so-called persisting black holes – indicate areas with pathologically confirmed severe tissue destruction *(Waesberghe et al., 1999)*.

Conventional MRI can distinguish between acute and allegedly chronic lesions, primarily on the evidence of blood-brain barrier breakdown, as indicated by contrast enhancement. The enhancement pattern is variable: nodular, ring- or arc-like. It can change over time in the same lesion and generally persists for 2 to 6 weeks. Regrettably, several factors can affect enhancement: gadolinium

dose, delay and characteristics of MR images acquisitions, IV corticosteroids for relapse treatment,… *(Filippi, 2000)*

A small number of cortical lesions can be detected with double inversion recovery (DIR) sequence, which increases contrast between GM and WM *(Geurts et al., 2011)*. Nevertheless, the majority of cortical lesions, especially subpial ones, remain undetected with DIR at 1.5 or 3 Tesla *(Geurts et al., 2005)*. While combination of different MR sequences – FLAIR, DIR, PSIR (phase sensitive inversion recovery) – is able to increase the sensitivity of detection at 3 Tesla *(Favaretto et al., 2015; Tallantyre et al., 2010)*, the best ability to visualize all types of cortical lesions is achieved by much higher resolution acquisitions (T2*/ FLAIR), at 7 Tesla *(Beck et al., 2018; Kilsdonk et al., 2016; Pitt et al., 2010)*.

Conventional MRI plays an established role in diagnosing MS, providing both evidence of dissemination in space and time. It is still the keystone of McDonald diagnostic criteria, which were perfected with time **(see Appendix 1, Table S1.3)** *(Thompson et al., 2017)*. Conventional MRI also makes an important contribution to the monitoring of WM lesion burden and helps predict long-term disability as well as treatment response *(Louapre et al., 2017; Wattjes et al., 2015)*.

However, despite their high sensibility in depicting WM focal inflammatory activity (detected up to 10 times more frequently than with clinical assessment of relapse) *(Barkhof et al., 1992)*, conventional MRI sequences are not able to efficiently assess GM lesions or detect diffuse changes in normal appearing brain tissues (NABT). This shortcoming is particulary apparent in the poor correlation of imaging results with short and long-term clinical outcomes, at least at the individual level *(Barkhof, 2002; Zivadinov and Leist, 2005)*.

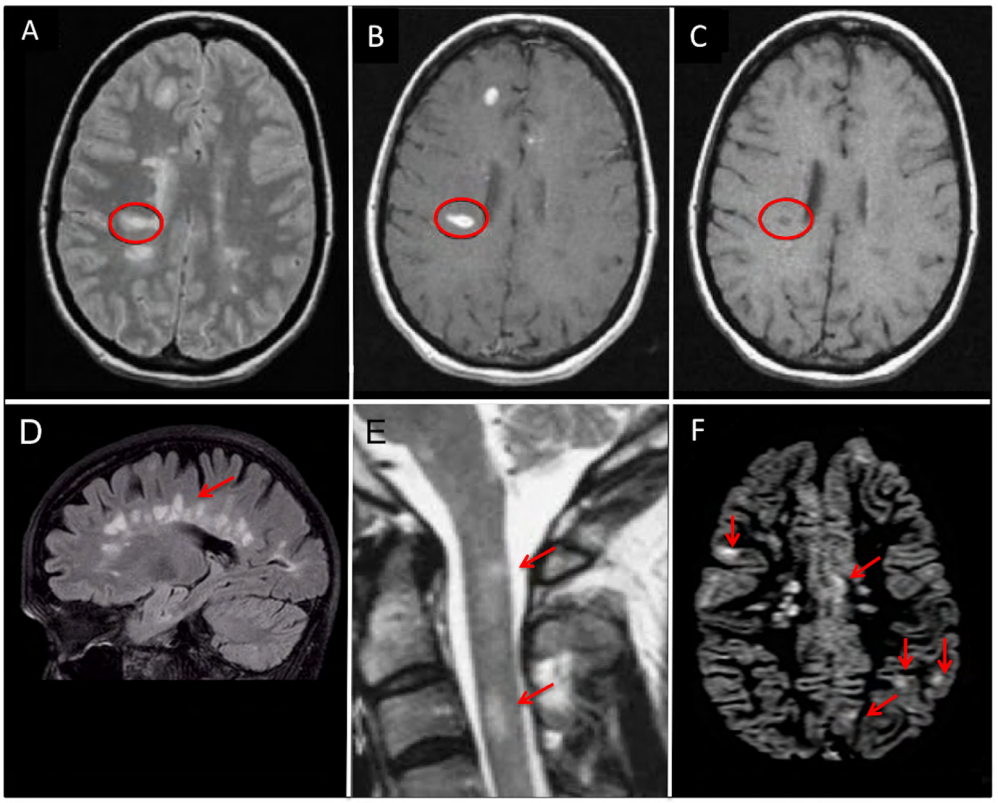

Figure 6: Conventional MRI in MS.

Conventional MRI readily depicts focal inflammatory lesions on (A) T2/FLAIR and (B) T1 post-Gadolinium sequences; (C) Chronic hypointense foci on T1 sequence – black holes – give information about focal axonal damage; (D) Typical Dawson fingers representing periventricular demyelinating plaques distributed along the axis of medullary veins, perpendicular to the body of the lateral ventricles and/or callosal junction; (E) Two spinal cord lesions visualized on short TI recovery (STIR) sequence; (F) 3D DIR sequence allowing the detection of some cortical lesions at 3 Tesla. Adapted from *(Compston and Confavreux, 2006; Umino et al., 2019).*

2. ATROPHY-BASED MEASURES

CNS atrophy occurs in all stages of MS, since the preclinical phase of the disease and progresses throughout its course, at a much higher rate that one reported in normal aging *(De Stefano et al., 2010; Eshaghi et al., 2018)*. The annualized percentage brain volume change of - 0.4% has been suggested as the cutoff to distinguish physiological and pathological atrophy accrual *(De Stefano et al., 2016)*.

Interestingly, a significant higher increase in GM atrophy occurs in more advanced disease stages, while WM atrophy rates remain more constant over time *(Fisher et al., 2008; Shiee et al., 2012)*. In addition, regional GM atrophy measurements allow better correlation with both cognitive and motor impairment *(Damjanovic et al., 2017; Eshaghi et al., 2018; Jacobsen et al., 2014; Steenwijk et al., 2016)*. Especially, atrophy of deep GM nuclei, such as thalami, are strongly associated with disability progression *(Eshaghi et al., 2018)* **(Figure 7)**.

The pathological substrate of brain atrophy mainly relies on neuronal, dendritic and axonal loss *(Klaver et al., 2015; Popescu et al., 2015)*. However, numerous factors can have a confounding effect, leading to over- or under-estimation of brain volume: physiological factors (i.e. circadian rhythm, level of hydration) *(Nakamura et al., 2015)*, lifestyle (i.e. alcohol, smoking, high body mass index), concomitant pathophysiological conditions (cardiovascular risks), age-related risk factors, anti-inflammatory treatments,... Particularly, anti-inflammatory drugs (steroids as well as disease-modifying treatments) significantly decrease brain volume within the first 6 months to 1 year of treatment, which then stabilizes *(De Stefano et al., 2014)*. This phenomenon is called "pseudo-atrophy" and may reflect the resolution of inflammation and edema *(Zivadinov et al., 2008)*.

Besides visualy atrophy estimations provided in routine clinical practice, quantitative three-dimensional measures of brain atrophy are by far the most powerful *(Amiri et al., 2018; De Stefano et al., 2014)*. They typically require 3D T1-weighted MR images. Cross-sectional methods – i.e. brain parenchymal fraction [BPF] *(Rudick et al., 1999)*, SIENAX *(Smith et al., 2002)*, FreeSurfer *(Fischl and Dale, 2000)*, voxel-based morphometry [VBM] *(Ashburner and Friston, 2000)*, MSmetrix *(Jain et al., 2015)* – measure brain volume at single time point, using a single MRI scan. They are usually based on automatic or semi-automatic tissue segmentation and allow the measurement of either global or regional brain volumes; Longitudinal methods (i.e. SIENA, VBM, MSmetrix) measure change in brain volume over time by comparing two sets of MRI scans acquired at different time points, after co-registration. Generally, segmentation-based techniques are well adapted for cross-sectional pathophysiological studies, but are less reliable for longitudinal atrophy quantification than registration-based methods *(Amiri et al., 2018; De Stefano et al., 2014)*. Results obtained between these two methods cannot be directly compared. Furthermore, even when applying a rather similar image processing, large differences in atrophy measurement are observed. This must be related to variation in MRI protocol, MRI signal heterogeneity, lack of normative data, slight differences in segmentation or registration procedures, upgrade of toolboxes and hardware,…*(Popescu et al., 2016; Steenwijk et al., 2017)*

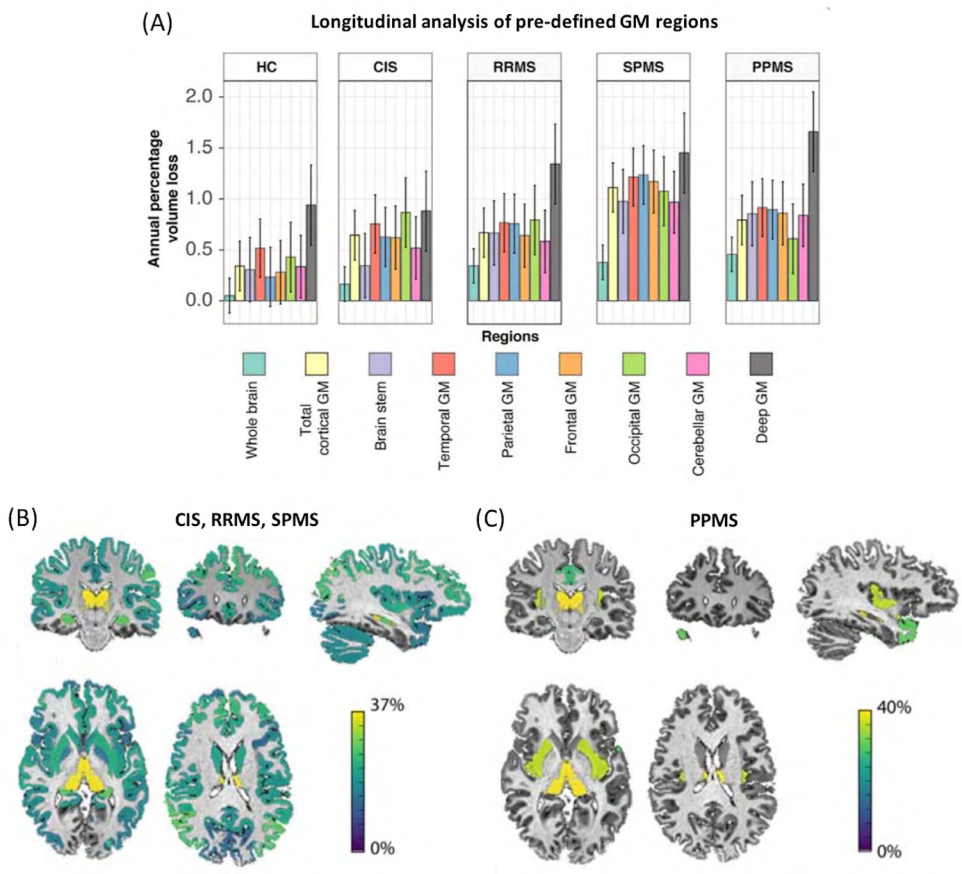

Figure 7: Longitudinal GM atrophy by predefined regions and correlation with EDSS in a large population of patients *(from Eshaghi et al., 2018).*

(A) Bar charts of the adjusted annual percentage of volume loss are shown in predefined GM regions, for each population: healthy controls (HC), clinically isolated syndrome (CIS), RRMS, secondary and primary PMS. The overage follow-up duration is 2.41 years (1.97 SD). Risk of EDSS progression during follow-up in relation with regional brain volume loss at baseline in (B) CIS, RRMS, secondary PMS and (C) primary PMS. For example, for every Z-score loss of the thalamus volume at baseline, the risk of EDSS worsening during follow-up increased by 37% for the CIS, RRMS, and secondary PMS group and 40% for primary PMS. Color maps code the importance of baseline volumes of the regions to predict EDSS worsening during follow-up.

Despite its conceptual appeal, a number of caveats should be considered before using brain volume measurement in clinical practice *(Alroughani et al., 2016)*. First, there is a need to challenge the technical variability between scans and methods. One should also remember that brain volume loss is influenced by several factors, which relate to MS or not, and thus contribute to a relatively weak specificity of atrophy measurements. Moreover, most studies which support the clinical relevance of brain volume changes allow only for inferences at the group level, making them barely applicable at the individual level. Finally, brain atrophy is a measure of the irreversible/destructive or end-stage phenomenon occurring in MS. Earlier markers of disease evolution should be explored, especially in a neuroprotective and repair purpose.

3. ADVANCED IMAGING TECHNIQUES

With overall progress in images acquisition and processing, several novel imaging-derived markers have emerged to probe MS-related cerebral changes, in a more specific and quantitative manner. They include metabolic, functional and structural measures, derived from MR and PET imaging. Although advanced imaging techniques have provided interesting and more specific insights into the pathophysiology of MS, they have still a limited role in clinical practice *(Enzinger et al., 2015)*. **Table S1.4** (see Appendix 1) allows an overview of the imaging techniques investigated during the last two decades. In this section, we will review structural quantitative MRI (qMRI) techniques, which form the basis of our work: magnetization transfer (MT), effective transverse (R2*****) and longitudinal (R1) relaxation rates. They are able to quantify physical properties of cerebral tissues; which changes may provide information about MS-related microstructural alterations.

In the following sections of this manuscript, the term "normal appearing" brain tissues (NABT), including normal appearing white and grey matters (respectively NAWM and NAGM) will be defined on the MRI field strength and its ability to detect cortical lesions. Consequently and without any further mention, MRI-defined NAGM will relate to both focal and diffuse GM damages.

3.1 MAGNETIZATION TRANSFER IMAGING

Magnetization transfer MRI is based on the interaction between protons in free-fluid and those bound to macromolecules. When off-resonance radio-frequency (RF) pulse is applied, the magnetization of bound protons becomes saturated and is transferred to more mobile protons, which causes a reduction of tissue signal. The MT ratio (MTR) is a semi-quantitative measure, obtained by computing the difference in signal intensity between images acquired before (S_0) and after (S_{MT}) the application of the RF pulse: $MTR = [(S_0 - S_{MT})/ S_0]$. It reflects the efficiency of magnetization exchange between the two proton pools. As a consequence, a low MTR reflect a reduced capacity of macromolecules in tissue to exchange magnetization with surroundings water molecules *(Enzinger et al., 2015; Filippi and Agosta, 2007; Henkelman et al., 2001)*.

Post-mortem studies comparing the relative contribution from myelin content and axonal density, indicate that the former has a stronger and more direct influence on the measured MTR. T1-dependent effects such as tissue water content (inflammation, edema,…) also account for MTR variability *(Schmierer et al., 2004)*.

Magnetization transfer imaging have been used extensively for quantifying the extent of damage, in focal WM lesion as well as NABT *(Enzinger et al., 2015; Filippi and Agosta, 2007)*.

Variable degrees of MTR reduction are found within acute and chronic WM lesions. On average, MTR drops substantially when lesions start to enhance but can recover during the subsequent six months, indicating remyelination *(Dousset et al., 1998)*. Established lesions show wide range of MTR values, with the most profound reduction in chronic lesions *(Rocca et al., 1999)*. Interestingly, reduction of MTR can be observed within NAWM, days to weeks before the formation of a new lesion *(Filippi et al., 1998)*. In addition, in RRMS, the average percentage change in lesion MTR after 12 months is able to predict disability worsening over 8 years *(Agosta et al., 2006)*.

Reduced MTR values are also shown in NAWM and NAGM of patients with different MS phenotypes **(Figure 8)** *(Davies et al., 2005; Yulin et al., 2002)*, starting from the earliest stage of the disease (clinically isolated syndrome) *(Fernando et al., 2005; Traboulsee et al., 2002)*. However, such abnormalities tend to be more pronounced in PMS and are associated with severity of locomotor disability and cognitive impairment. This is particularly striking for MTR reduction within NAGM, which shows a predictive value for long-term clinical deterioration *(Agosta et al., 2006; Ramio-Torrenta et al., 2006; Traboulsee et al., 2003)*. In line with histopathological studies, MTR reduction in NABT modestly correlates with the extent of focal WM lesions visible on T2/FLAIR sequences *(Filippi and Agosta, 2007; Tortorella et al., 2000)*.

Magnetization transfer imaging clearly appears as a promising technique to assess demyelination and remyelination in MS, particularly in the context of clinical trials. However, MTR is a semi-quantitative measure which is particularly sensitive to biophysical parameters and field strength. The alternative approach of quantitative MT saturation offers a measure that, unlike MTR, is minimally affected by T1 relaxation and is less sensitive to B1 transmit field inhomogeneities *(Lema et al., 2017)*.

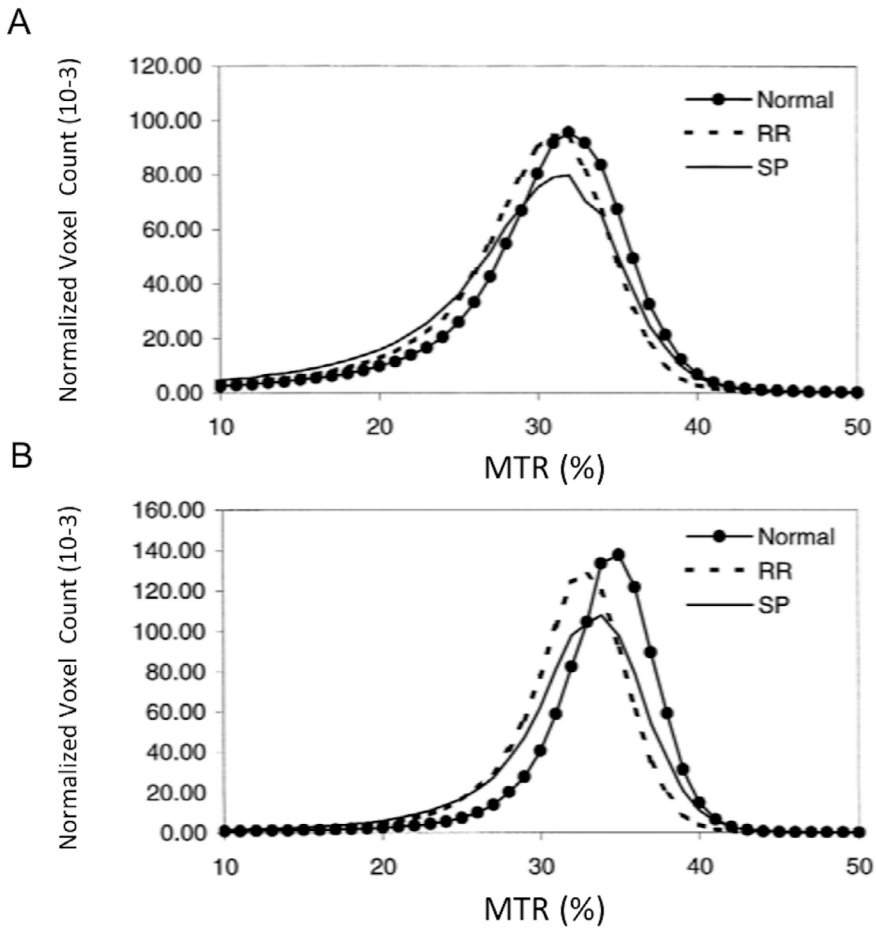

Figure 8: MTR histograms in NABT of MS patients *(from Yulin et al., 2002)*.

Average MTR histograms obtained from three groups (HC, RRMS and secondary PMS) for global (A) NAGM and (B) NAWM tissues. For both NAGM and NAWM, the MTR histograms of the MS patients are significantly shifted toward smaller values from the histograms of HC (smaller mean, median, and first and third quartiles). The histogram peak height of secondary PMS patients, not of RRMS population, is significantly lower compared to HC, for both NAGM and NAWM.

3.2 EFFECTIVE TRANSVERSE RELAXATION RATE: R2*

The transverse relaxation time T2* reflects the effective decay of transverse magnetization T2, when considering intra-voxel magnetic field inhomogeneities. In the CNS, paramagnetic iron and diamagnetic myelin generate microscopic field gradients, thus shortening T2* and increasing the R2* (1/T2*) relaxation rate *(Bagnato et al., 2018; Cohen-Adad, 2014; Paling et al., 2012)*.

In MS and non-MS post-mortem studies, R2* values differ across brain regions and are positively correlated with both myelin and iron contents (mostly ferritin and hemosiderin) **(Figure 9)**. Orientation and density of myelin fibers, which molecular basis is attributable to water content, are also a determining factor of R2* values *(Bagnato et al., 2018; Hametner et al., 2018; Langkammer et al., 2012, 2010; Stüber et al., 2014)*. As a consequence, R2* needs to be cautiously interpreted depending on the relative contribution of iron and myelin contents as well as their interplay, in each CNS tissue class *(Bagnato et al., 2018; Langkammer et al., 2012)*.

A few relaxometry studies in MS indicate that R2* significantly increases in deep GM (essentially basal ganglia), beyond age-related effects *(Elkady et al., 2017; Khalil et al., 2011, 2009; Paling et al., 2012; Ropele et al., 2014)*. These observations are more pronounced in PMS and correlate with brain atrophy *(Khalil et al., 2011, 2009; Ropele et al., 2014)* and disability *(Khalil et al., 2011; Ropele et al., 2014)*. In line with histopathological studies discussed above, increased R2* in deep GM (structures with lower myelin content) is consistent with iron deposition.

Interestingly, several recent publications more specifically focusing on thalami, reveal that thalamic R2* values are lower in MS patients compared to controls

(Elkady et al., 2019; Hametner et al., 2018; Hernández-torres et al., 2015; Khalil et al., 2015; Louapre et al., 2018). Actually, these values are close to those described in NAWM and suggest a decrease in myelin and/or iron content *(Bagnato et al., 2018; Hametner et al., 2018; Hernández-torres et al., 2015; Paling et al., 2012)*. Lower R2*/R2 (or higher T2*/T2) values are also described within lesion and cortical GM *(Gracien et al., 2016a; Neema et al., 2007; Reitz et al., 2016)*. Moreover, ultra-high resolution data acquired at 7 Tesla demonstrate a gradient in the expression of cortical pathology, with higher T2* values observed in the outer cortical layer, closed to the pial surface *(Mainero et al., 2015)*.

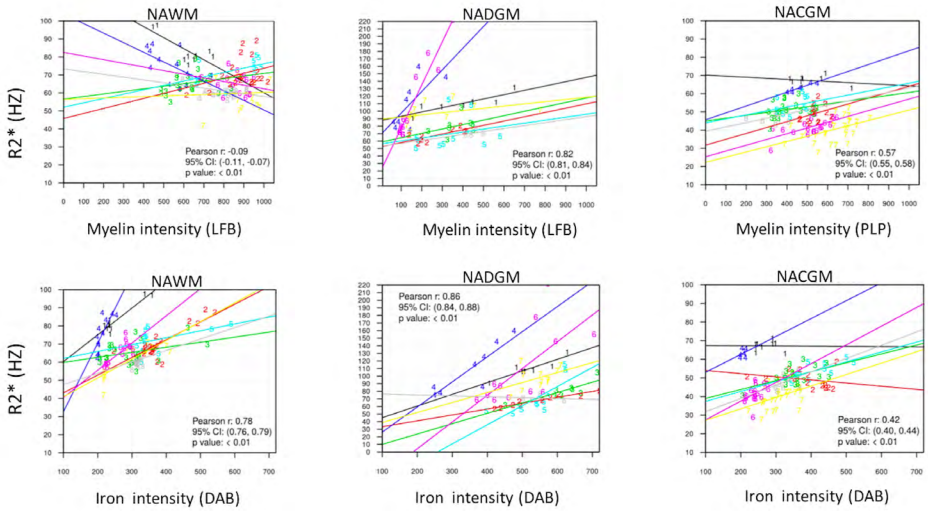

Figure 9: Scatter plots of R2* values in NABT for both myelin and iron intensities *(from Bagnato et al., 2018)*.

Upper row displays R2* values for myelin intensities (Luxol Fast Blue – LFB, Proteolipid Protein – PLP) in regions of interest within NAWM, NADM and NACGM (respectively normal appearing deep and cortical grey matters). Bottom row shows R2* values for iron intensity (3,3'-diaminobenzidine-tetra-hydrochloride – DAD), according to the same regions.

R2* mapping seems to be quite reliable to estimate iron concentration within deep GM, but its sensitivity decreases by confounding effect of myelin content and orientation in WM. As recently suggested, higher field strength might enhance sensitivity for iron as well as combination of R2* and quantitative susceptibility maps (QSM) *(Elkady et al., 2018, 2017; Hametner et al., 2018)*. Limitations can arise from macroscopic susceptibility effects and concomitant signal loss at tissue-air/tissue-bone interfaces. Homogenization of B0 magnetic field (generated by magnetic coils) and shorter echo times help minimizing these artifacts *(Ropele et al., 2011)*.

3.3 LONGITUDINAL RELAXATION RATE: R1

The longitudinal relaxation time T1 is an intrinsic properties of hydrogen protons and describes how fast the longitudinal component of magnetization recovers after excitation by RF pulse. T1 is the time after which ~63% of the longitudinal magnetization has recovered.

In CNS, longitudinal relaxation rate R1 (1/T1) is strongly correlated to tissue myelination and water content *(Stüber et al., 2014)*. R1 is also influenced by iron concentration, though the association is much smaller than what is observed with R2*. Moreover, R1 is largely unaffected by the direction of myelinated fibers, unlike R2* *(Ogg and Steen, 1998; Stüber et al., 2014)*.

Little literature is available on the use of R1 or T1 parameter in MS. However, results of these few studies are quite consistent. Compared to controls, they show global reduction of R1 (or increase of T1) values in NAWM and NAGM **(Figure 10)**, suggesting diffuse demyelination *(Gracien et al., 2016b; Manfredonia et al., 2007; Parry et al., 2002; Vrenken et al., 2006)*. These changes are more pronounced in PMS patients *(Vrenken et al., 2006)* and are able to

predict their clinical evolution over the short term *(Manfredonia et al., 2007)*. Despite the absence of post-mortem validation studies in MS, R1 represent a valuable marker of myelination, especially in cortical GM and NAWM, where iron does not accumulate to the same extent as in deep GM. Even more, combined acquisitions of R1 and R2* maps have the potential to generate in vivo quantitative maps of myelin and iron densities *(Stüber et al., 2014)*. Together, R1 and R2* mappings are robust and comparable across scanners, provided that a standardized protocol is used.

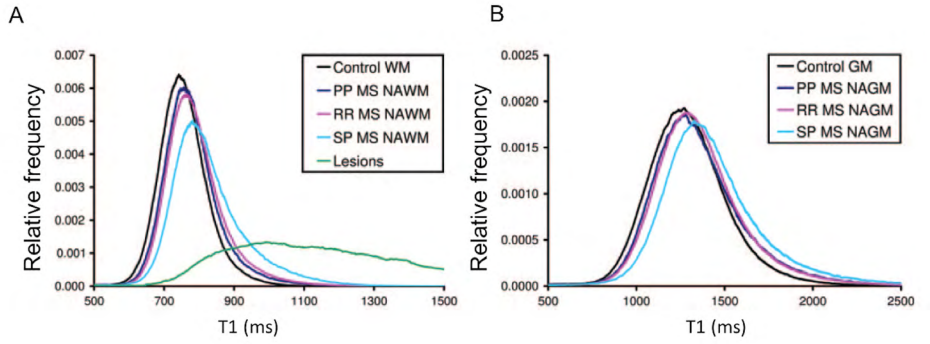

Figure 10: T1 histograms in NABT of MS patients *(from Vrenken et al., 2006).*

Average T1 histograms obtained from four groups (HC, RRMS, primary and secondary PMS) for global (A) WM (NAWM and lesions) and (B) NAGM. In both NAWM and NAGM, there is a shift of T1 histograms toward higher T1 values in patients with MS, wich is most severe for the group with PMS.

PART B

PERSONNAL CONTRIBUTION

Chapter IV: OBJECTIVES

Although conventional MRI is playing a valuable role in the routine clinical practice, it merely captures a very small proportion of MS-related pathological processes. It is particularly not sensitive to detect and track diffuse pathological changes that occur both in normal appearing grey and white matters (NAGM and NAWM, respectively) *(Filippi et al., 2012; Zivadinov and Leist, 2005)*, and to a significant extent in the progressive phenotype of the disease *(Kutzelnigg et al., 2005)*. In addition, conventional MRI has a poor specificity and shows only limited associations with clinical status *(Barkhof, 2002; Zivadinov and Leist, 2005)*. Quantitative MRI (qMRI) potentially overcomes these limitations by a direct noninvasive quantification of NABT physical properties; which changes may provide information about MS-related microstructural alterations.

To assess the superiority and potential usefulness of qMRI in MS, we designed a prospective cross-sectional study to explore NABT of MS patients, by simultaneously quantifying three MRI parameters – MT saturation, R1, R2* – derived from a multiparameter mapping (MPM) protocol. Because each qMRI parameters is differently sensitive to histologically measured iron and myelin contents, we reasoned that a multivariate qMRI approach would allow a more comprehensive measurement of microstructural damage occurring in MS. At the same time, we also aimed at improving clinico-radiological correlations.

Analyses comparing both RRMS and PMS patients to healthy control population were conducted on the basis of two distinct approaches. General analysis looked for differences in qMRI parameters, summarized over three different MRI-defined NABT classes: NAWM, normal appearing cortical grey matter (NACGM) and normal appearing deep grey matter (NADGM). Furthermore, loco-regional analysis assessed

the spatial distribution of qMRI changes within NAGM, using a voxel-based strategy. Chapter V will detail common methodological issues, whereas general and loco-regional analyses will be discussed one at a time, respectively in chapters VI and VII. In light of our results, the general discussion will address some reflections about MS as well as future prospects.

Chapter V: METHODOLOGICAL ISSUES

1. POPULATION DEMOGRAPHY

Seventy-two participants took part in this study, which was approved by the local ethic committee. Written informed consent was obtained from all participants. Thirty-six patients were recruited at the specialized MS outpatient clinic of the CHU Liège, Belgium, with a diagnosis of MS according to McDonald criteria 2010 *(Polman et al., 2011)*. The inclusion criteria were (1) age between 18 and 65 years, (2) Expanded Disability Status Scale (EDSS) inferior or equal to 6.5; (3) absence of relapse within the previous 4 weeks; (4) compatibility with MRI. Patients were classified as relapsing-remitting MS (15 RRMS) or progressive MS (primary and secondary progressive – 21 PMS). Twenty-one patients were receiving disease-modifying treatments (DMTs; 11 first lines, 8 second lines, 2 non-validated therapies). Thirty-six healthy control (HC) participants, matched for age and gender, free from neurological or psychiatric disease, followed the exact same experimental protocol **(Table 1)**.

Patients with MS were scored by a qualified MS specialist (EL) on the EDSS, Time 25-Foot Walk (T25FW), 9-Hole Peg Test (9-HPT) of both hands, oral Symbol Digit Modalities Test (SDMT) and five recalls of California Verbal Learning Test (CVLT). Z-scores for T25FW, 9-HPT, SDMT and CVLT were standardized to HC summary statistics and transformed to make improvement a positive number. Finally, a motor ($[Z_{T25FW} + Z_{9\text{-HPT dominant hand}} + Z_{9\text{-HPTnon dominant hand}}]/3$) and a cognitive ($[Z_{SDMT} + Z_{CVLT}]/2$) composite scores were computed.

Table 1: Demographic data (general analysis)

	All Patients (n=36)	**RRMS** (n=15, 41.6%)	**SPMS** (n=7, 18.4%)	**PPMS** (n=14, 38.8%)	**HC** (n=36)
Age y, mean (SD)	45.69 (11.85)	36.53 (9.32) °	50.14 (6.46)	53.28 (9.78)	45.86 (12.45)
Sex ratio (F/M)	21/15	9/6	7/0	5/9	20/16
Disease duration y, median (range)	13 (0,5 to 35)	6 (0.5 to 28)	21 (9 to 35)	12.5 (2 to 35)	
Baseline EDSS median (range)	4.0 (1.0 to 6.5)	2.0 (1.0 to 5.5) °	4.0 (3.5 to 6.0)	4.75 (3.0 to 6.5)	N/A
Number of relapses median (range)	1.5 (0 to 10)	4 (1 to 6)	10 (2 to 10)	0	

° Difference between RRMS and PMS statistically different (alpha value of 0.05).

Abbreviations: RRMS = relapsing-remitting multiple sclerosis, SPMS = secondary progressive multiple sclerosis, PPMS = primary progressive multiple sclerosis, PMS = progressive multiple sclerosis (SPMS and PPMS), HC = healthy controls.

2. MR IMAGES ACQUISITION

Owing to the replacement of MRI equipment in our research institute, MRI data were acquired either on a 3T head-only MRI-scanner (Magnetom Allegra, Siemens Medical Solutions, Erlangen, Germany) or on a 3T whole-body MRI-scanner (Magnetom Prisma, Siemens Medical Solutions, Erlangen, Germany). The whole-brain MRI acquisitions included a multiparameter mapping (MPM) protocol developed in the framework of an international collaborative effort. This protocol has been gradually optimized and validated for multi-centric acquisitions *(Draganski et al., 2011; Helms and Dechent, 2009; Lutti et al., 2012, 2010; Tabelow et al., 2019; Weiskopf et al., 2013)*.

The MPM protocol consists of three co-localized 3D multi-echo fast low angle shot (FLASH) acquisitions at 1 x 1 x 1 mm3 resolution as well as two calibration sequences. The FLASH data sets were acquired with predominantly proton density (PD), T1 and MT weighting by appropriate choice of the repetition time (TR) and the flip angle. MT-weighting was achieved by applying an off-resonance Gaussian-shaped RF pulse prior to the excitation. Gradient echoes were acquired with alternating readout gradient polarity at 6 or 8 equidistant echo times (TE). PDw, T1w and MTw echoes had high bandwidth to minimize off-resonance and chemical shift artifacts. Volumes were acquired in 176 sagittal slices using a 256 x 224 voxel matrix.

The design of the protocol took into account the following criteria. GRAPPA parallel imaging was combined with partial Fourier acquisition to speed up acquisition time to approximately 20 minutes. The echo train length was limited to 20ms to trade off emerging R2* contrast against susceptibility-induced signal losses *(Helms and Dechent, 2009)*. The flip angles of the acquisitions were optimized using a semi-empirical approach, in order to maximize the signal-to-noise ratio (SNR) while limiting bias due to imperfect RF spoiling *(Helms et al., 2011)*. Two additional sequences allowing to correct for RF transmit field inhomogeneities, were also acquired *(Lutti et al., 2012, 2010)*.

Details of the MPM protocol used in our research work are available in supplementary material **(see Appendix 2, table S2.1)**. An additional FLAIR sequence was recorded with spatial resolution 1 x 1 x 1 mm3 and TR/TE/TI = 5000 ms/516 ms/1800ms.

3. MR IMAGES PROCESSING

All data analyses and processing were performed in Matlab (The MathWorks Inc., Natick, MA, USA) using SPM12 (www.fil.ion.ucl.ac.uk/spm) and three additional dedicated SPM-extension toolboxes:

- LST version 1.2.3 (www.statisticalmodelling.de/lst.html) *(Schmidt et al., 2012)*
- hMRI (http://hmri.info) *(Tabelow et al., 2019)*
- USwithLesion (https://github.com/CyclotronResearchCentre/USwLesion) *(Phillips et al., 2016)*

3.1 ESTIMATION OF PARAMETER MAPS

MT saturation, R1 and R2* quantitative maps were estimated using the hMRI toolbox, which also generates proton density map (PD*). We chose not to use the latter due to a potential residual T2* weighting. Echoes for T1w, PDw and MTw were extrapolated to TE = 0 to increase the SNR and get rid of the otherwise remaining R2* bias *(Balteau et al., 2018; Weiskopf et al., 2014)*. The resulting MTw and T1w (TE=0) images were used to calculate MT saturation and R1 quantitative maps. To maximize the accuracy of the R1 and MT saturation maps, inhomogeneity in the flip angle was corrected by mapping the B1 transmit field according to the procedure detailed in *(Lutti et al., 2012)*. In addition, intrinsically imperfect spoiling characteristics were accounted for and corrected in R1 map, using the approach described by *(Preibisch, C. and Deichmann et al., 2009)*. The MT saturation map differs from the commonly used MT ratio (MTR, percent reduction in steady state signal) by explicitly accounting

for spatially varying T1 relaxation time and flip angles. MT saturation shows a higher brain contrast to noise ratio than the MTR, leading to improved and more robust segmentation in healthy subjects *(Helms et al., 2010)*. The R2* map was estimated from all three multi-echo series using the ESTATICS model *(Weiskopf et al., 2014)*. Example maps are shown in **(figure 11)**. Note that these MR sequences at 3 Tesla are not sensitive to cortical lesions as described in *(Filippi et al., 2013; Hulst and Geurts, 2011)* although a few lesions at the cortico-subcortical border (cortical lesions Type I) were detected. Quantification of cortical parameters is thus confounded by a minority of voxels potentially located within cortical lesions.

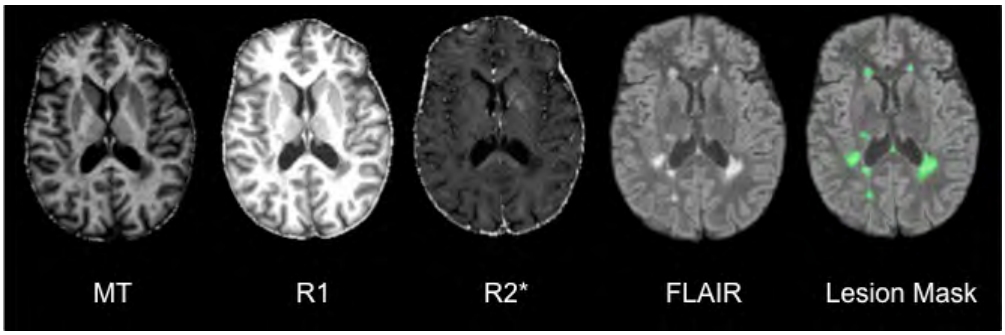

Figure 11: Example of MPM quantitative maps for a specific MS patient.

From left to right: 3 MPM quantitative maps (MT, R1, R2*), standard FLAIR sequence image, and FLAIR image overlaid with the estimated lesion mask. MT = magnetization transfer saturation, R1 = longitudinal relaxation rate (1/T1), R2* = effective transverse relaxation rate (1/T2*). Lesion mask = posterior probability map of lesion tissue thresholded at 90%.

3.2 SEGMENTATION

Quantitative maps of MS patients were segmented with the USwithLesion toolbox, in different cerebral tissue classes: normal appearing cortical grey matter (NACGM), normal appearing deep grey matter (NADGM), normal appearing white matter (NAWM) and lesions. The presence of focal demyelinated lesions required improvement of automated segmentation procedure available in SPM software that uses the tissue contrast in the image(s) and a priori tissue probability maps (TPM) *(Ashburner and Friston, 2005)*. We followed a multi-step procedure for each patient individually *(Phillips et al., 2016)* **(figure 12)**. A preliminary lesion mask was generated from FLAIR and T1 weighted images by the lesion growth algorithm *(Schmidt et al., 2012)* as implemented in the LST toolbox. Optimal initial threshold kappa was determined by visual inspection and manual corrections were performed when necessary. Based on this binary lesion mask, the USwithLesion toolbox generated a patient-specific TPM by adding an extra lesion tissue class to MPM dedicated TPM *(Lorio et al., 2016)* and updating the white matter prior map accordingly *(Moon et al., 2002)*. The individual number of lesions impinging upon the cortical ribbon was so low that we did not update the grey matter TPM. Importantly small inaccuracies in this preliminary mask were smoothed out during the update of the TPM. A multi-channel unified segmentation approach *(Ashburner and Friston, 2005)* using multiple contrast images (FLAIR, MT, R1, R2*) was then applied to MR images with these updated patient-specific TPM. The outputs were the segmented tissue classes (a posteriori tissue probability maps, including lesions) and spatial warping into standard template space (Figure 13). For HC, multi-channel unified segmentation was applied with the same MPM specific TPM *(Lorio et al., 2016)*.

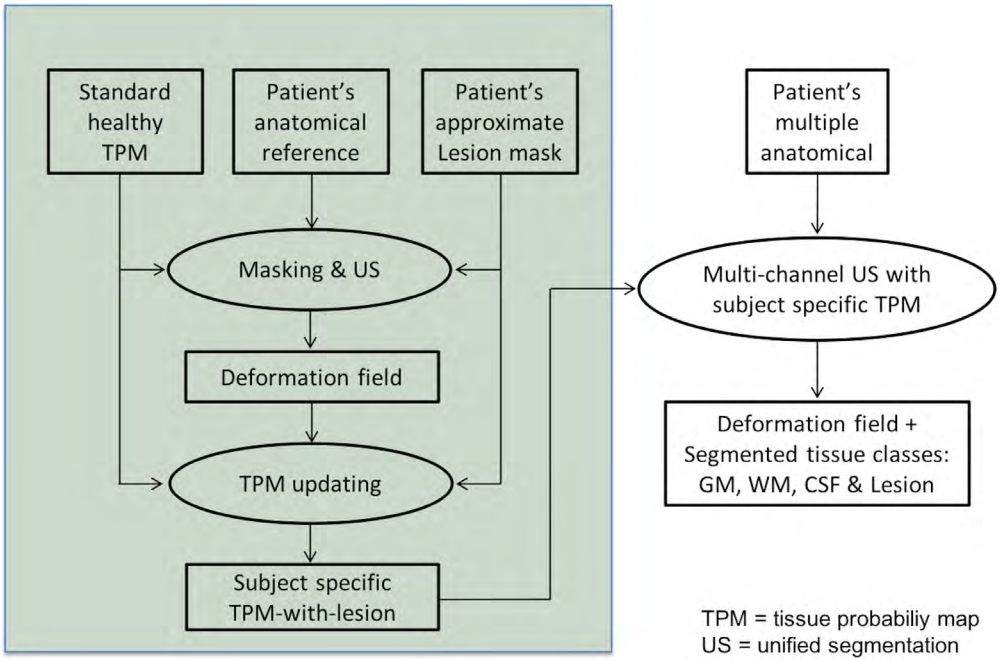

Figure 12: Workflow of the USwithLesion approach.

The green box summarizes the creation of the patient specific TPM with lesions. (A) Production of an approximate map of lesioned area(s) (lesion mask), manually or through some algorithm. (B) Modification of standard TPM by adding a subject-specific lesion probability map in 2 steps: (1) "Masking & US", i.e estimate a preliminary spatial warping from subject to MNI space with the "cost function masking" approach applied on one anatomical MRI and the approximate lesion mask → MNI-warped approximate lesion mask (2) "TPM updating", i.e add a new tissue class for the lesion (defined from the smoothed MNI-warped approximate lesion mask) to the standard TPM and update the tissue class(es) affected by the lesion. (C) Finally new patient-specific TPMs are fed into the US with the patient's anatomical MR image(s). If multiple contrast images (T1, T2, PD, FLAIR, …) are available, then multi-channel segmentation is performed. TPM = Tissue probability map, US = Unified segmentation, MNI = Montreal Neurological Institute.

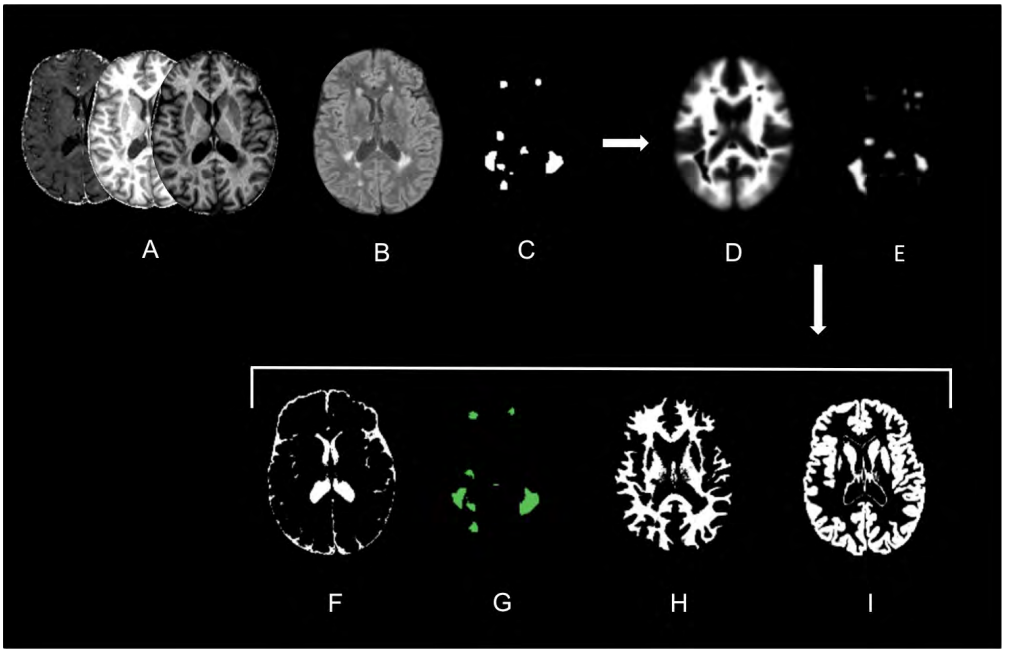

Figure 13: Example of USwithLesion toolbox application on a specific MS patient.

(A) 3 MPM quantitative maps (MT, R1, R2*); (B) FLAIR-weighted MR images; (C) approximate binary lesion mask; (D, E) updated WM and lesion prior probability maps; (F-I) a posteriori probability maps for CSF, lesion, WM and GM tissue classes.

Chapter VI: MULTIVARIATE APPROACH OF MS MICROSTRUCTURAL ALTERATIONS: GENERAL ANALYSIS

Section based upon the following publication:

Lommers, E., Simon, J., Reuter, G., Delrue, G., Dive, D., Degueldre, C., Balteau, E., Phillips, C., Maquet, P., 2019. Multiparameter MRI quantification of microstructural tissue alterations in multiple sclerosis. NeuroImage: Clinical, 23.

1. INTRODUCTION

This prospective cross-sectional study aims at revisiting differences in microstructure within three tissue classes of MRI-defined NABT (normal appearing cortical and deep grey matters – NACGM and NADGM, respectively, and NAWM), between MS patients (both RRMS and PMS) and healthy controls (HC), using a multiparameter mapping (MPM) protocol which simultaneously quantitates MT saturation, R1 and R2* with high resolution and whole brain coverage *(Callaghan et al., 2014; Draganski et al., 2011; Tabelow et al., 2019; Weiskopf et al., 2013)*. We also explore whether these parameters predict motor and cognitive functions in MS patients.

2. MATERIALS AND METHODS

The study population has been described in Chapter V. Demographic data are summarized in **(Table 1)**.

MR images acquisition and processing followed the initial steps detailed in Chapter V. Next, for each participant, a set of three qMRI parameters (MT, R1, R2*) were extracted from all voxels of the three tissue classes (NACGM, NADGM, NAWM), based on a 90% probability to belong to the tissue class. Lesions were considered as an additional tissue class for patients. The brainstem and cerebellum were excluded because of unsatisfactory GM segmentation of some Allegra scans, in relation with MR artifacts within the posterior fossa. Summary measurements were computed for each subject as median values for each tissue class and each qMRI parameter **(Table 2)**. In addition, the following measures of brain volume were generated: total intra-cranial volume (TIV) = volume (NAWM + GM + CSF + lesions), brain parenchymal fraction (BPF) = volume (NAWM + GM + lesions)/TIV, GM fraction (GMF) = volume (GM/TIV), lesion fraction (LF) = volume (lesion/TIV) **(Table 2)**.

Statistical analyses were computed using SAS software, Version 9.4 (SAS Institute Inc., 2013). For demographic data, group differences in brain volume, age and disease duration were assessed using one-way analyses of variance (ANOVA). Between-group differences in gender ratio were estimated by $\chi 2$. RRMS and PMS differences for clinical data were investigated with Wilcoxon rank-sum test (EDSS) and ANOVA (motor and cognitive score). Due to the influence of normal aging on brain microstructure *(Callaghan et al., 2014; Draganski et al., 2011)*, quantitative parameters were all first corrected for age. Residuals of this preliminary analysis were used in subsequent statistical analyses. Three two-way multivariate analyses of variance (MANOVA), one for each

parameter (MT, R1 and R2*), estimated the effects of group (HC, RRMS, PMS) and tissue class (NACGM, NADGM, NAWM), with scanner as independent variable of no interest. Tukey's post-hoc analyses were performed when necessary to explore significant principal effects. We consider an alpha level for statistical significance at 0.05. The relationship of qMRI parameters to volumetric data was evaluated using Bravais-Pearson's correlation coefficient in the two MS groups. Inferences were performed at an alpha level for statistical significance at 0.01. A stepwise regression including age (forced), scan (forced), gender, disease duration, lesion fraction and all qMRI features, looked across all patients for the best predictors of clinical scores (motor score, cognitive score and EDSS).

Table 2: Quantitative MR parameters

	RRMS	PMS	HC
Scanner 1/ Scanner 2	11/4	15/6	11/25
Volumetric Data, %, mean (SD)			
BPF	84.99 (2.02)	83.67 (2.47) *	85.39 (1.75)
GMF	51.06 (2.11)	48.49 (3.16) *	52.76 (1.99)
Lesion F	1.21 (0.98)	2.26 (1.50) °	N/A
Median MPM values, mean (SD)			
MT (p.u)			
NACGM	0.71 (0.09) **	0.68 (0.09) *	0.82 (0.09)
NADGM	0.91 (0.12)	0.83 (0.10) *	0.98 (1.13)
NAWM	1.49 (0.18) **	1.45 (0.16) *	1.68 (0.14)
Lesion	0.96 (0.26)	0.89 (0.24)	N/A
R1 (Hz)			
NACGM	0.62 (0.02) **	0.61 (0.03) *	0.64 (0.02)
NADGM	0.75 (0.05)	0.75 (0.05)	0.77 (0.06)
NAWM	0.99 (0.05) **	0.99 (0.05) *	1.04 (0.03)
Lesion	0.78 (0.12)	0.75 (0.10)	N/A
R2* (Hz)			
NACGM	15.20 (1.19) **	15.35 (1.17) *	16.62 (1.02)
NADGM	20.74 (2.63)	22.46 (2.94)	22.04 (3.10)
NAWM	20.08 (1.34) **	20.24 (1.27) *	21.60 (1.03)
Lesion	15.03 (2.23)	14.51 (2.30)	N/A

° Difference between RRMS and PMS statistically different (alpha value of 0.05)
* Difference between PMS and HC statistically different (alpha value of 0.05)
** Difference between RRMS and HC statistically different (alpha value of 0.05)

Abbreviations: BPF = brain parenchymal fraction, GMF = grey matter fraction, Lesion F = lesion fraction, NACGM = normal appearing cortical grey matter, NADGM = normal appearing deep grey matter, NAWM = normal appearing white matter, N/A = not applicable

3. RESULTS

Patients and HC did not differ by age ($F(1,70) = 0.00$, $p = 0.95$). However, RRMS patients were younger than PMS patients and HC ($F(2,69) = 9.26$ $p < 0.001$). The three groups matched in terms of gender ($\chi^2 = 0.26$, $p = 0.88$). Disease duration was similar in the two patient groups ($F(1,34) = 3.72$ $p = 0.06$) **(Table 1)**. PMS patients were clinically more impaired than RRMS patients with higher EDSS ($S = 174$ $p < 0.001$) and lower motor ($F(1,34) = 13.62$ $p = 0.01$) and cognitive ($F(1,34) = 5.76$ $p = 0.02$) composite scores. We observed a principal group effect on BPF ($F(2,69) = 4.76$, $p = 0.01$) and GMF ($F(2,69) = 20.81$, $p < 0.001$) with lower volumes in PMS patients than HC. No significant differences were observed for RRMS although these two volume fractions tend to be reduced compared to HC, at a lower extend than PMS. Progressive patients had higher LF than relapsing remitting ones ($F(1,34) = 5.64$, $p = 0.02$) **(Table 2)**.

Two-way MANOVAs testing for group differences revealed that vector of means was different across groups for each parameter: MT [Wilks' Lambda $= 0.50$, $F(6,128) = 8.92$, $p < 0.001$, $R^2 = 0.50$], R1 [Wilks' Lambda $= 0.67$, $F(6,128) = 4.77$, $p < 0.001$, $R^2 = 0.33$], R2* [Wilks' Lambda $= 0.64$, $F(6,128) = 5.39$, $p < 0.0001$, $R^2 = 0.36$]. More specifically, MT in NACGM and NAWM was lower in patients than in HC, suggesting a demyelination in these normal appearing tissue classes. Patient groups did not significantly differ from each other, although MT in these two tissue classes tended to be lower in PMS group. In NADGM, MT was lower in PMS patients than in HC. R1 and R2* from NACGM and NAWM were lower in patients than in HC suggesting reduction of myelin and/or iron content. Patient groups did not significantly differ from each other **(Figure 14)**. We did not observe any increase of R2* in NADGM between HC and patients. The group by scan interaction was significant for

R2* [Wilks' Lambda = 0.80, F (6,128) = 3.06, $p < 0.007$, $R^2 = 0.20$], due to a simple, or ordinal, interaction in NACGM and NAWM for R2* **(Figure 15)**.

In the RRMS group, there was no significant correlation between qMRI parameters and LF or BPF. In PMS patients, R1 was negatively correlated to LF in NACGM ($r = -0.7$, $p < 0.001$) and in NAWM ($r = -0.72$, $p < 0.001$). Regarding BPF, we observed positive correlation with MT in NACGM ($r = 0.65$, $p < 0.001$), NADGM ($r = 0.63$, $p = 0.002$) and NAWM ($r = 0.62$, $p = 0.002$). Positive correlations with BPF were also noted for R1 in NADGM ($r = 0.62$, $p = 0.002$), R2* in NACGM ($r = 0.65$, $p = 0.001$) and R2* in NAWM ($r = 0.64$, $p = 0.004$).

Stepwise regression identified that LF and R2* in NADGM are the best predictors of motor score. It also revealed that cognitive score is best predicted by LF and MT parameter within lesions. Finally, R2* in NADGM and R1 in NACGM predict EDSS **(Table 3)**. Simple linear regressions illustrate these relationships **(Figure 16)**. Slopes did not differ between groups of patients except for motor score with lesion load. This simple linear regression was stronger in RRMS ($R^2 = 0.58$, $p = 0.001$) than PMS patients ($R^2 = 0.1$, $p = 0.24$). By contrast, simple regression between EDSS and R^2* in NADGM was significant in the PMS group ($R^2 = 0.23$, $p = 0.03$) but not in the RRMS group ($R^2 = 0.003$, $p = 0.9$).

Table 3: Stepwise regression results

Motor Score	**Model**	F (4,31) = 7.18 (p < 0.001)					
	Step	Predictor	ΔR²	R²	Adj R²	ΔF	p Value
	1	Age/scanner *	0.30	0.30	0.25	6.97	0.003
	2	Lesion F	0.11	0.4	0.35	5.82	0.02
	3	R2* NADGM	0.08	0.48	0.42	4.51	0.04
Cognitive Score	**Model**	F (4,30) = 11.99 (p < 0.001)					
	Step	Predictor	ΔR²	R²	Adj R²	ΔF	p Value
	1	Age/scanner *	0.22	0.22	0.17	4.42	0.02
	2	Lesion F	0.34	0.56	0.52	24.12	< 0.001
	3	MT Lesion	0.06	0.61	0.56	4.32	0.04
EDSS	**Model**	F (4,31) = 8.33 (p < 0.001)					
	Step	Predictor	ΔR²	R²	Adj R²	ΔF	p Value
	1	Age/scanner *	0.35	0.35	0.31	8.70	< 0.001
	2	R2* NADGM	0.09	0.44	0.39	5.27	0.03
	3	R1 NACGM	0.08	0.52	0.46	5.15	0.03

* Forced into the model

Significant level for entry into the model = 0.05.

Abbreviations: NACGM = normal appearing cortical grey matter, NADGM = normal appearing deep grey matter, Lesion F = lesion fraction, EDSS = expanded disability status scale.

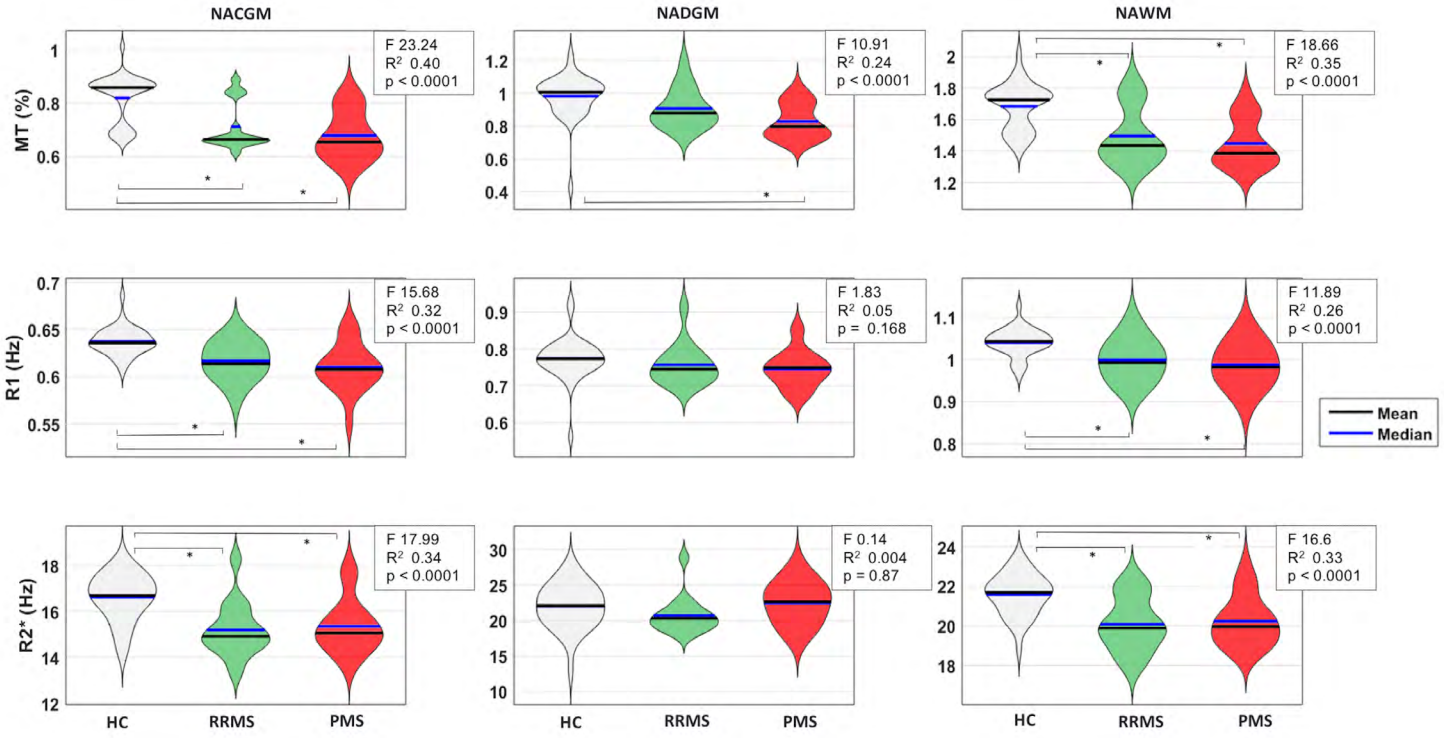

Figure 14: Violin plots and results of post-hoc analysis.

Plots and post-hoc results for each parameter (MT, R1, R2*) in each tissue class (NACGM, NADGM NAWM), across the 3 groups of subjects (HC, RRMS, PMS). Statistical significance (*) set at $p < 0.05$.

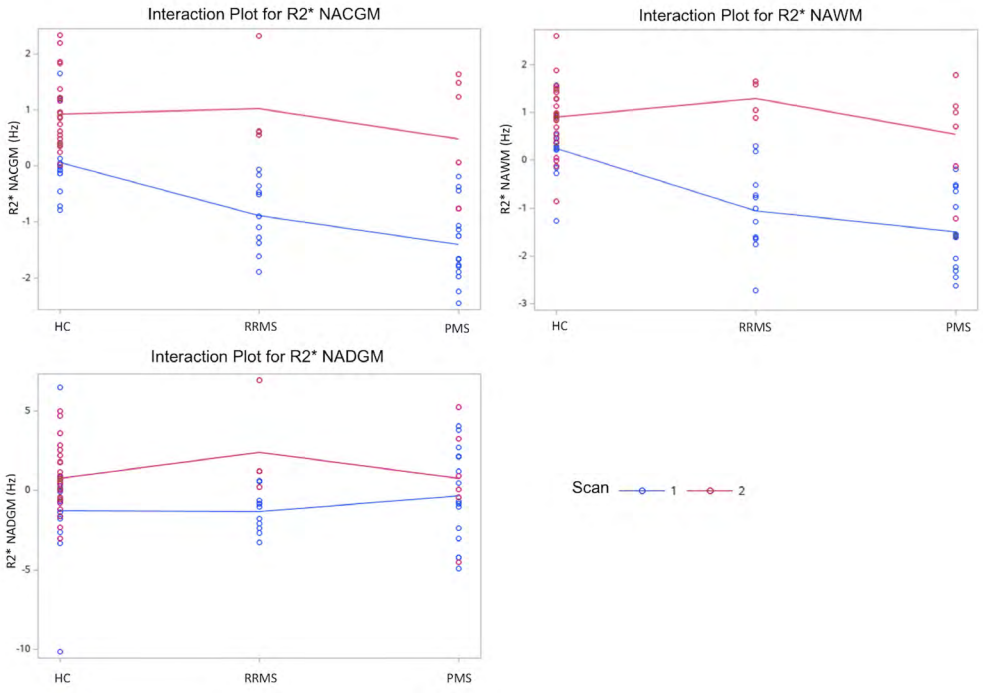

Figure 15: Plots of R2* values for each group on two different scanners.

The scanner effect on qMRI values is undisputable. However, the group by scanner interaction was solely significant for R2* within NACGM and NAWM. These plots show that R2* values acquired on two different scanners are not parallel across group but never cross. This is a simple interaction and the group effect can still reliably be discussed. Scan 1 (blue) = Allegra MR scanner and scan 2 (red) = Prisma MR scanner.

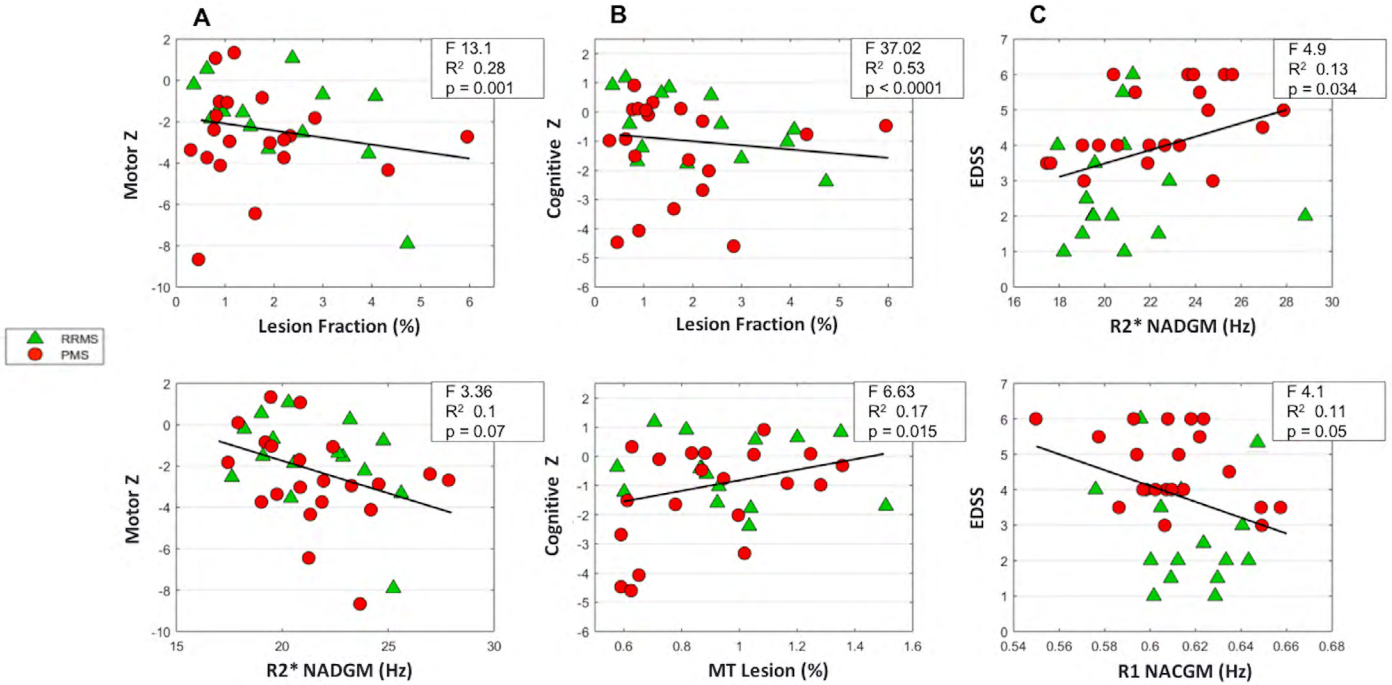

Figure 16: Interconnections between quantitative MR parameters and clinical scores across the entire group of MS patients.

(A) Simple linear regression between motor score and lesion fraction or R2* within NADGM; (B) simple linear regression between cognitive score and lesion fraction or MT within lesions; (C) simple linear regression between EDSS and R2* within NADGM or R1 within NACGM. Statistical significance set at $p < 0.05$.

4. DISCUSSION

In this prospective cross-sectional study, quantitative MRI (qMRI) based on a multiparameter mapping (MPM) protocol derives fully quantitative and reproducible *(Weiskopf et al., 2013)* high-resolution maps of multiple parameters (MT, R1, R2*) from data acquired in a single scanning session of clinically acceptable duration *(Tabelow et al., 2019)*. Dedicated toolboxes for qMRI in the presence of lesions (hMRI and USwithLesion) were successfully applied to the data. Expectedly, median values of all parameters in HC are similar to those reported in other studies evaluating the MPM protocol **(Table 2)** *(Callaghan et al., 2014; Weiskopf et al., 2013)*. By contrast to volumetric analyses, mainly interested in global T2/FLAIR lesion volume and brain atrophy, the multivariate qMRI approach characterizes microstructural features in 4 different tissue classes (NACGM, NADGM, NAWM and lesions), providing informative proxies about diffuse pathogenic changes such as demyelination or iron deposition. On average, MS patients are characterized by a decrease in MT, R1 and R2* within NACGM and NAWM, whereas in NADGM, MT decrease contrasts with normal R2* and R1 values.

Magnetization transfer is usually assessed by MTR, a semi-quantitative estimation of the steady-state MRI signal attenuation by an off-resonance MT pulse *(Helms et al., 2010)*. Here we quantified MT saturation, which differs from MTR by explicitly removing the bias introduced by the spatially varying T1 relaxation time and B1 transmit field *(Helms et al., 2010)*. The reduction of NAWM and NACGM MT in MS concords with similar observations based on MTR, which is reduced in normal appearing brain tissues of MS patients, particularly in PMS patients *(Filippi and Agosta, 2007; Gracien et al., 2016b)*. MT was also selectively decreased in PMS within NADGM. This result tallies with the demyelination reported post-mortem within NADGM *(Haider et al., 2014;*

Kutzelnigg et al., 2005; Schmierer et al., 2007, 2004) which contributes to clinical deficits over and above cerebral cortical and WM lesion burden *(DeLuca et al., 2015; Haider et al., 2014)*.

Effective transverse relaxation rate R2* is primarily affected by iron, local myelin content as well as fiber orientation *(Bagnato et al., 2018; Hametner et al., 2018)*. R2* is decreased in MS NACGM and NAWM, suggesting a reduction in iron and/or myelin content, in keeping with histopathological *(Hametner et al., 2013)* and MR evidence *(Bagnato et al., 2018; Hernández-torres et al., 2015; Neema et al., 2007; Paling et al., 2012; Reitz et al., 2016)*. In contrast to previous reports *(Elkady et al., 2017; Khalil et al., 2011, 2009; Paling et al., 2012; Ropele et al., 2014)*, we did not observe any significant increase in R2* value within NADGM of MS patients. It might arise from a residual effect of age on R2*, RRMS patients being younger than HC. However, age difference was not statistically significant between PMS patients and HC. In more recent publications, the source of R2* increase within NADGM of MS patients has been exclusively attributed to basal ganglia, in relation with iron accumulation. In opposition, lower R2* thalamic values were observed, closed to NAWM ones, suggesting mainly myelin but also iron losses *(Elkady et al., 2019; Hametner et al., 2018; Hernández-torres et al., 2015; Khalil et al., 2015; Louapre et al., 2018)*. These observations help explain the absence of R2* increase in our study, where deep grey matter nuclei were analysed together.

Longitudinal relaxation rate R1 is closely related to tissue myelination, particularly in NACGM and NAWM. It is also influenced by iron concentration, though at a lesser extent than R2* *(Neema et al., 2007; Sereno et al., 2012; Stüber et al., 2014)*. In this study, we observed a reduction of R1 in NACGM and NAWM in both patient groups, indicating a diffuse demyelination in these normal appearing tissues, as previously reported *(Gracien et al., 2016b; Gracien et al.,*

2016c; Neema et al., 2007; Vrenken et al., 2006). No significant change in NADGM R1 was observed either because there was no significant demyelination or iron deposition, or because demyelination (which reduces R1) was compensated by increased iron (which increases R1).

4.1 RELATION TO CLINICAL MEASURES AND LESION FRACTION

This study probes both focal (FLAIR positive lesions) and diffuse microstructural aspects (qMRI parameters) altered by MS, although the latter are to some extent confounded by GM lesions to which MPM protocol is insensitive at 3 Tesla.

Both focal and diffuse processes relate to disability in MS patients. Stepwise regression indicates that qMRI features are independent predictors of clinical status, supporting the role of diffuse microstructural alterations in clinical impairment: EDSS is significantly related to R1 in NACGM and R2* in NADGM; the latter also predicts motor score. By contrast, cognitive score was intriguingly related to MT within lesions. This finding suggests that cognition not only depends on the spatial extension of the lesions *(Giorgio and Stefano, 2010)* but also on the pathogenic mechanisms going on within them, which putatively deteriorate axonal transmission to a variable extent.

By the same token, although cohort sizes did not allow us to consider RRMS and PMS separately in our stepwise regression model, simple regressions showed that the motor score depended significantly more on LF in the RRMS group and EDSS more strongly on DGM R2* in PMS patients. Based on these findings, it is tantalizing to postulate that focal demyelination primarily impacts RRMS clinical status whereas diffuse inflammation and the resulting neurodegeneration mainly cause disability progression in PMS. Specifically, data from

literature highlight the role of NADGM involvement in disability accumulation in MS, that appears even more evident in progressive phenotypes of the disease *(Eshaghi et al., 2018; Haider et al., 2014; Mesaros et al., 2011; Ropele et al., 2014)*.

No association between LF and qMRI parameters was observed in RRMS, suggesting the partial independence of diffuse and focal processes. Conversely, R1 in CGM and NAWM was negatively correlated to LF in PMS, implying that as lesion load increases, the focal and diffuse changes become indistinguishable and jointly impact the clinical status.

Finally, most qMRI parameters in NABT correlated with brain volume loss and might turn out to be useful markers of neurodegeneration. Future studies will assess whether alterations of qMRI parameters precede atrophy. Importantly, quantitative reproducible microstructural parameters might prove more reliable than the estimation of atrophy *(Amiri et al., 2018; Azevedo and Pelletier, 2016)*.

4.2 LIMITATIONS OF THIS STUDY

Of course, these results are not without limitations. Beyond the small sample size, significant differences in age were observed with older PMS than RRMS patients. However, a linear effect of age was included in our statistical models. Moreover, the disease duration was comparable in the 2 groups, minimizing any effect of this factor.

Although the use of 2 scanners might appear as a drawback, we considered it as the opportunity to test the stability of qMRI parameters across devices. Moreover there were minor differences between the two acquisition protocols due to optimization of several parameters on the second scanner. We found a

group by scanner interaction only for R2* in NAGGM and NAWM. These are ordinal, or simple, interactions (MRI data are not parallel across group but never cross) so that the group effect can still reliably be discussed **(Figure 15)**.

The automatic unified segmentation approach, with and without lesions, ensures the systematic and reproducible processing of both patients and controls data. Consequently, it may be affected by noise and artifacts in the data, which would lead to the spurious classification of a few voxels. Nevertheless, since the median over all the voxels having a strong posterior probability (>0.9) of being in a tissue class (NACGM, NADGM or NAWM) is used to build the summary measurements, these should be fairly insensitive to outlier values. At worst this would introduce some between participant variability reducing the sensitivity of the analysis.

5. CONCLUSION

This cross-sectional study demonstrates that simultaneous quantitative estimation of multiple MR parameters can reliably assess NABT microstructure in MS. Results suggest that diffuse pathology, as assessed by this study, might play a significant role in determining irreversible disability and brain volume loss in MS. However, future large-scale studies should evaluate the reproducibility and predictive values of these results and explicitly discriminate the respective effects of diffuse cortical pathology from focal cortical lesions.

Chapter VII: SPATIAL DISTRIBUTION OF MICROSTRUCTURAL DAMAGE IN MS: LOCO-REGIONAL ANALYSIS

Section based upon the following publication:

Lommers, E., Guillemin, C., Reuter, G., Delrue, G., Collette, F., Degueldre, C., Balteau, E., Maquet, P., Phillips, C., 2019. Voxel-based quantitative MRI reveals spatial patterns of grey matter alterations in multiple sclerosis. Submitted to Multiple Sclerosis Journal.

1. INTRODUCTION

As described in the previous chapter and in accordance with other reports, MT saturation, R1 and R2* are altered in MS normal appearing cortical and deep grey matters (respectively NACGM and NADGM), taken as bulk tissue classes *(Filippi and Agosta, 2007; R. Gracien et al., 2016a; R. M. Gracien et al., 2016b; Lommers et al., 2019; Mainero et al., 2015; Ropele et al., 2014; Vrenken et al., 2006)*. In this section, we precisely provide a whole-brain voxel-based quantification (VBQ) of MT, R1 and R2* to assess the spatial distribution of their change in a cross-sectional study contrasting MS patients to healthy controls (HC). Potential grey matter (GM) atrophy was also investigated by a concurrent voxel-based morphometry (VBM) analysis *(Ashburner and Friston, 2000)*.

2. MATERIALS AND METHODS

The study population included 71 (35 MS patients and 36 HC) out of 72 participants described in chapter V. One RRMS patient was excluded because of imperfect normalization of MRI data. Demographic data are reported in **(Table 4)**.

After qMRI maps were estimated and segmented (complete description in chapter V), normalization was performed within the USwithLesion toolbox. For VBM analyses, GM probability map (including NACGM and NADGM) were spatially warped to standard space, modulated by the Jacobian determinants of the deformations, and smoothed with an isotropic Gaussian kernel (6 mm FWHM). For VBQ analyses, the 3 qMRI maps were normalized using the subject-specific deformation field but without modulation. Then we used a tissue weighted smoothing (4 mm FWHM isotropic) procedure as described in *(Draganski et al., 2011)*. This method produces smoothed tissue-specific multi-parameter maps while optimally preserving the quantitative parameter values within each tissue class by reducing any effects of partial volume. Detailed analysis of the influence of spatial deformations onto quantitative parametric values proved this method largely insensitive to volumetric changes (i.e., atrophy) *(Salvoni et al., 2019)*.

Between group differences in demographic and MRI measures of global NAGM damage (obtained from the general analysis) were assessed using analyses of variance (ANOVA). Between-group differences in gender ratio were estimated by $\chi 2$ **(Table 4)**.

Whole-brain voxel-wise VBM and VBQ statistical analyses were carried out using a multiple linear regression model embedded in the general linear model

framework of SPM12. Differences between MS patients and HC in NAGM were estimated by a separate F-test for each quantitative parameter (MT, R1, R2*) and volume. An explicit GM mask was generated as previously proposed *(Callaghan et al., 2014)*: the smooth modulated warped individual GM and WM maps were averaged across all subjects and the GM mask included voxels for which mean GM probability was larger than that of WM and exceeded 20%.

Age, scanner and total intracranial volume were included as regressors of no interest. Post-hoc t-tests explored significant effects. Inferences were conducted at $p < 0.05$ after family-wise error rate (FWER) correction for multiple comparisons at voxel level across the whole brain. Only clusters of at least 10 mm3 were considered. In the patient population, three F tests looked for significant voxel-wise regression between each qMRI parameter and clinical scores (EDSS, motor and cognitive composite scores) as well as lesion fraction. Inferences were conducted at cluster level ($p < 0.05$ FWER corrected, $p < 0.000\ 1$ uncorrected cluster-forming threshold) after small volume correction over the union of the significant main group effects.

Table 4: Demographic data (loco-regional analysis)

	HC (n=36)	**All Patients** (n=35)	**RRMS** (n=14, 40%)	**PMS** (n=21, 60%)
Age, y, mean (SD)	45.86 (12.45)	46.2 (11.62)	37.14 (9.4)	52.23 (8.8)
Sex (F/M)	20/16	21/14	9/5	12/9
Disease duration, y, median (range)	N/A	13 (0.5 to 35)	8 (0.5 to 28)	13 (2 to 35)
Baseline EDSS, median (range)		4.0 (1.0 to 6.5)	2.0 (1.0 to 5.5)	4.5 (3.0 to 6.5)
Scanner 1/Scanner 2	11/25	25/10		
Volumetric Data, %, mean (SD)				
GMF	52.76 (1.99)	49.55 (3.02) *		
Lesion F	N/A	1.82 (1.4)		
Median MPM values summarized over the whole tissue class, mean (SD)				
MT (p.u)				
NACGM	0.82 (0.09)	0.69 (0.27) *		
NADGM	0.98 (1.13)	0.86 (0.11) *		
R1 (Hz)				
NACGM	0.64 (0.02)	0.62 (0.02) *		
NADGM	0.77 (0.06)	0.75 (0.05) **		
R2* (Hz)				
NACGM	16.62 (1.02)	15.29 (1.16) *		
NADGM	22.04 (3.10)	21.74 (2.9) ***		

ANOVA (alpha value of 0.05)
* Differences statistically different at $p < 0.0001$
** Differences not statistically different, $p = 0.06$
*** Differences not statistically different, $p = 0.68$

Abbreviations: RRMS = relapsing-remitting multiple sclerosis, PMS = progressive multiple sclerosis (primary and secondary PMS), HC = healthy controls, TIV= total intracranial volume, GMF = grey matter fraction (GM/TIV volume), LF = lesion fraction (lesion/TIV volume), NACGM = normal appearing cortical grey matter, NADGM = normal appearing deep grey matter.

3. RESULTS

Compared to HC, we identified significant loco-regional reductions of MT and R1 in NAGM of MS patients, bilaterally in superior temporal gyri, Heschl's gyri, insulae, primary sensory-motor cortices and posterior hippocampi. R1 and R2* were significantly reduced in MS patients, compared to HC, respectively in the right cingulate cortex and left sensory-motor cortex (**Figure 17**, C and D).

None of the regressions between GM parameters and clinical scores (EDSS, motor and cognitive composite scores) were significant. R1 and MT negatively regressed with lesion fraction in both thalami.

Extensive GM loss was observed in MS compared with HC in bilateral primary sensory-motor cortices and paracentral lobules as well as bilateral temporal lobes (Heschl's gyri), right posterior hippocampus, right thalamus, hypothalamus, supero-inferior colliculi and the left putamen (**Figure 17**, B) For a complete list of regions showing lower GM volume, lower MT, R1, R2* values and significant regressions, see **Tables S3.1 to S3.5** in supplementary data (see Appendix 3).

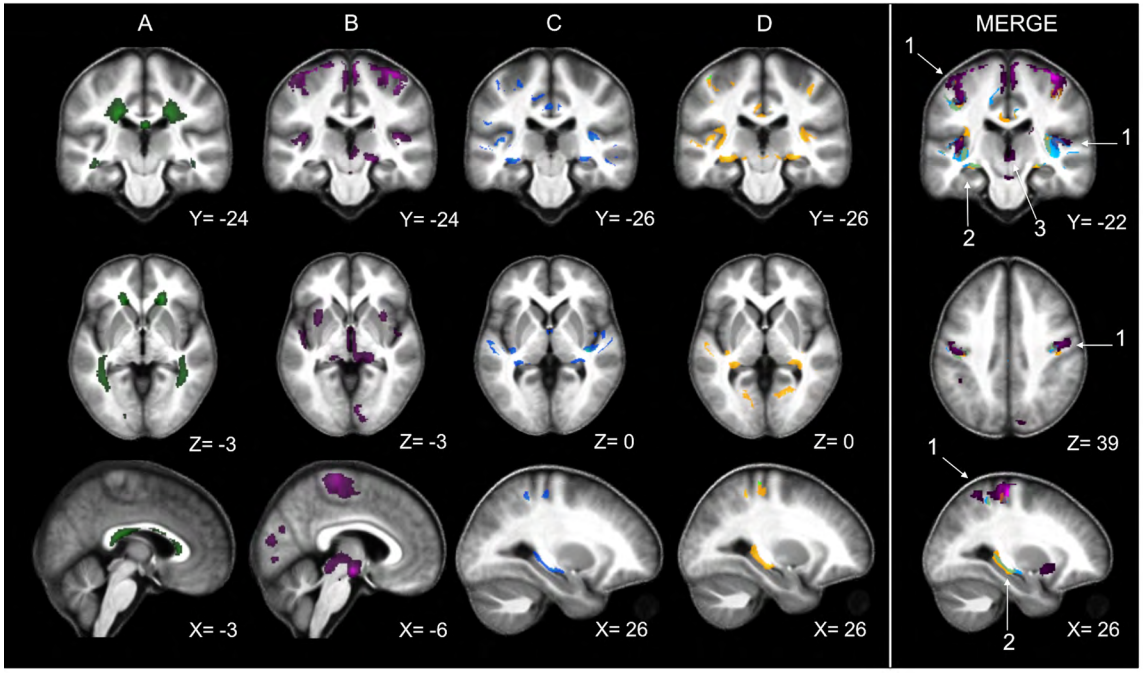

Figure 17: VBM and VBQ results superimposed on the group mean MT map.

(A) Green: Average WM lesion probability map of MS patients, thresholded at 90%; (B, C, D) Significant voxels in MS compared with HC (thresholded at cluster level, $p < 0.05$ FWER-corrected) demonstrating decreased grey matter (GM) volume in violet, MT reduction in blue, R1 reduction in yellow and R2* reduction in bright green (circled). The last column on the right merges B, C and D columns and displays the three different patterns discussed in the main text (1, 2, 3 = pattern 1, 2, 3). Images are shown in neurologic convention and the X/Y/Z coordinates indicate the slice position in millimeter in MNI space.

4. DISCUSSION

In this study, the topography of microstructural and volumetric alterations in NAGM of MS patients was assessed by a multiparametric voxel-based approach, without prior prediction regarding MS damage location. We reasoned that the simultaneous voxel-wise quantification of physical tissue parameters would enrich the understanding of MS pathology by providing a typical microstructural and volumetric pattern over and above the inter-patient variability of disease presentation. Importantly, voxel-based quantification is immune from volumetric changes *(Draganski et al., 2011; Salvoni et al., 2019)* thereby allowing for independently characterizing microstructural and volumetric changes. Quantitative MRI (qMRI) parameters (MT, R1, R2*) are differently sensitive to myelin and iron contents *(Tabelow et al., 2019)* whilst VBM can estimate GM atrophy, secondary to neurono-axonal loss and neuronal shrinkage *(Klaver et al., 2015; Popescu et al., 2015)*. In addition, the voxel-wise lesional probability in the underlying WM was taken into account to interpret GM alterations.

This multiparametric voxel-based strategy has seldom been followed in MS: only a single report on a cohort of 19 patients is available *(Engström et al., 2014)*. In consequence, our results cannot be directly contrasted with the existing literature. A few available voxel-based studies have examined the spatial distribution of MT ratio together with GM atrophy *(Audoin et al., 2007; Crespy et al., 2011; Khaleeli et al., 2007; Mallik et al., 2015)*. Our VBM results are fairly consistent with those reported in other MS cohorts including RRMS and PMS patients, excepted that we did not find any significant atrophy within cerebellum *(Bodini et al., 2009; Ceccarelli et al., 2008; Khaleeli et al., 2007; Mallik et al., 2015)*. This is possibly because we adjusted our processing to optimize supra-tentorial GM segmentation. As for regions of lower MT saturation, they agree with previous reports regarding cortical but not deep GM *(Audoin et al., 2007; Khaleeli et al.,*

2007; Mallik et al., 2015). Again, comparison with literature is difficult because the MT saturation used in the current work represents an advanced estimation of magnetization saturation over MT ratio. Moreover, one should also remember that an absence of significant loco-regional differences between MS patients and HC is not the proof of absence. Indeed, it might result from more sparsely distributed areas of altered qMRI values as well as spatial variability in their location across patients.

Statistical inference identified three microstructural/volumetric patterns **(Figure 17)**: (1) Co-localization of GM atrophy with microstructural changes, usually observed in areas overhanging the most abundant WM lesion load. Compared to HC, MS patients show a significant reduction in MT saturation and R1 (both sensitive to myelin content) co-localized with widespread GM atrophy in bilateral primary sensory-motor cortices, Heschl's gyri, and right hippocampus. Significant R2* reduction is restricted to the left sensory-motor cortex. (2) Microstructural modification without significant GM loss: the left hippocampus and paralimbic cortices (cingulate gyrus and insula) show reduced R1 and MT values, without significant atrophy, suggesting a demyelination of residual neurono-axonal tissue, a regional resilience to atrophy or the antecedence of microstructural alterations over neurodegeneration. (3) Significant atrophy without significant change in microstructure. This pattern was identified in deep GM structures (thalami, hypothalamus, putamen), suggesting the predominance of neurono-axonal loss in these regions. The discrepancy between volumetric and microstructural changes highlights the complementarity of these MRI techniques in assessing GM damage in MS.

4.1 PATTERN 1: PRIMARY NEOCORTICAL REGIONS

Although the distribution and extent of GM damage can vary between individual MS patients, several phenomena likely contribute to the combined demyelination and neurodegeneration observed in primary auditory and sensory-motor cortices. These regions show less anatomical variability than other brain areas (i.e prefrontal cortex), which facilitates the detection of commonalities across patients *(Ono et al., 1990)*. They are connected with long-range, densely myelinated tracts *(Nieuwenhuys and Broere, 2017)* that are vulnerable to trans-synaptic – anterograde and retrograde – neurono-axonal degeneration *(Calabrese et al., 2015; Haider et al., 2016)*, because of their intrinsically heavy metabolic load *(Calabrese et al., 2015)* and their frequent involvement in focal WM inflammation. Finally, they are more exposed to cerebrospinal fluid (CSF) stasis, supporting the hypothesis that soluble factors produced in the CSF by lymphocytes influence subpial demyelination, particularly in patients with progressive MS *(Magliozzi et al., 2018)*.

4.2 PATTERN 2: HIPPOCAMPUS

While structural MRI techniques (atrophy measurement, lesion detection, diffusion MRI) have been widely used to assess hippocampal damage in MS *(Rocca et al., 2018)*, the evidence of substantial demyelination of hippocampi beyond atrophic areas constitutes a key contribution of this study. Indeed, demyelination is detected postmortem in 53 to 79% of MS hippocampi *(Dutta et al., 2013, 2011; Geurts et al., 2007)*, and is selectively associated with alterations in genic expression profiles responsible for abnormalities in hippocampal axonal traffic, synaptic plasticity, neurotransmitter homeostasis and memory *(Dutta et al., 2013, 2011)*. This stresses the need for early and specific MRI biomarkers for demyelination in MS.

The mechanisms underpinning the relative resilience of hippocampus to atrophy in MS are beyond the scope of this study. Nevertheless, a few observations are consistent with our results. First, neuronal loss is inconsistently observed in demyelinated hippocampi while synaptic density is systematically decreased *(Dutta et al., 2011; Geurts et al., 2007, Papadopoulos et al., 2009)*. By the same token, chronic inflammation potentially enhances neurogenesis within dentate gyrus *(Rocca et al., 2015)*. Although the functional significance of these cellular changes is still under debate *(Pluchino et al., 2008; Zhao et al., 2008)*, they may balance neuronal loss, at the structural level *(Rocca et al., 2015)*.

4.3 PATTERN 3: DEEP GREY MATTER NUCLEI

Our results show a significant atrophy of deep GM in MS and concord with previous reports *(Hulst and Geurts, 2011; Louapre et al., 2018)*. Thalamic atrophy relates to significant neuronal and axonal loss. It occurs very early in the disease course and is more pronounced compare to cortical atrophy *(Eshaghi et al., 2018)*. Due to its extensive reciprocal connections with cortical and subcortical structures, the thalamus is particularly vulnerable to anterograde and retrograde degeneration. This interpretation is supported by the significant negative regression between thalamic R1 and MT values with lesion load, which suggests that lesions in connecting WM tracts alter thalamic microstructure. These neurodegenerative processes likely dominate local inflammatory activity and oxidative injury which were also reported *(Haider et al., 2016)*, but were not sensitively assessed in this study.

4.4 LIMITATIONS OF THIS STUDY

Again, this study was run on a small sample size and the two MS phenotypes were considered together to preserve statistical power. We cannot rule out

that results are driven by the larger proportion of PMS than RRMS patients, although exploratory contrasts did not show any significant difference between the two patient groups. Differences in microstructure between RRMS and PMS patients is of paramount importance and will be assessed in future work, based on larger and independent population samples.

The results do not confirm previous reports linking thalamic and hippocampal damage to motor performance and cognitive dysfunction in MS patients *(Eshaghi et al., 2018; Rocca et al., 2018)*. Inferences were conservatively made after correction for multiple comparisons over the whole brain, increasing the risk of Type II error. Spinal cord lesions were not taken into account although they impact motor performance. It might also be the case that the microstructural alterations precede the occurrence of clinical symptom. Longitudinal studies are needed to solve that question.

5. CONCLUSION

This multiparametric voxel-based approach identifies three different spatially-segregated patterns of GM microstructural/volumetric alterations in MS patients, that might be associated with different neuropathology. The results highlight the complementarity of qMRI and volumetric techniques in assessing GM status in MS.

Chapter VIII: GENERAL DISCUSSION

Since its first description by Charcot in the 19th century, MS has generally been considered as a pure white matter (WM) disease. This view has been increasingly challenged by novel scientific findings, primarily from histopathological studies. The latter considerably increased our understanding of MS pathology and emphasized various processes such as inflammation, demyelination, neurono-axonal loss and repair mechanisms, which are, to a variable extent, responsible for the severity of both diffuse and focal CNS alterations. These processes are not uniformly expressed across patients, thus contributing to the heterogeneity of clinical phenotype, prognosis as well as response to treatment.

In vivo evaluation of MS patients remains unsatisfactory, because conventional MRI is insensitive to many pathological mechanisms underpinning MS. We precisely aimed at improving the impact of MRI on the detection and characterization of MS pathological processes, especially those that occur within MRI-defined normal appearing brain tissues (NABT). To this effect, we used quantitative MRI (qMRI) parameters as potential biomarkers of microstructural alterations in a prospective cross-sectional study contrasting MS patients to healthy controls.

1. CONTRIBUTING METHODOLOGICAL DEVELOPMENTS

We had the opportunity to test the multiparameter mapping (MPM) protocol and hMRI toolbox, which were developed in a close collaboration including several centers. Gradually optimized and validated for multi-centric studies, these methodological developments derive high-resolution maps of multiple

qMRI parameters (MT, R1, R2*) from data acquired during a single scanning session of acceptable duration *(Draganski et al., 2011; Helms and Dechent, 2009; Lutti et al., 2012, 2010; Tabelow et al., 2019; Weiskopf et al., 2013)*. Expectedly, median values of all parameters in HC population were similar to those reported in other studies evaluating the MPM protocol.

An essential methodological contribution of this project is the development and implementation of a new segmentation method, which allows to include patient-specific tissue probability maps (TPMs) derived from a preliminary binary lesion mask. Together with a multi-channel (FLAIR, MT, R1, R2*) unified segmentation approach, these new TPMs offer an accurate warping into the standard space as well as a better delineation of WM lesions *(Phillips et al., 2016)*. The unified segmentation algorithm is based on differences in intensity values of the subject's image(s) and thus exposed to any noise and artifacts in the data. Considering differences of qMRI values between tissue classes would potentially enhance this algorithm. Future improvements will also include the segmentation of cortical lesions, when using higher field strength MRI.

2. MULTIVARIATE APPROACH OF MICROSTRUCTURAL ALTERATIONS IN MS

As part of the general analysis of MRI data, our multivariate qMRI approach characterizes microstructural features in different tissue classes (NACGM, NADGM, NAWM and lesions), providing informative proxies about diffuse pathogenic changes such as demyelination or iron deposition. Definitely, it proves superior to any one single-parameter relaxometry by positioning each patient, tissue class or voxel in a multidimensional quantitative space **(Figure 18)**.

Fairly consistent with histopathological findings, our results show decreased

MT, R1 and R2* values within NACGM and NAWM of MS patients, suggesting diffuse reduction in myelin and/or iron contents. In NADGM, differences between MS patients and HC are less obvious, with an isolated decrease of MT value. This contrasts with previous report of R2* increase within NADGM, in relation with iron accumulation. Nevertheless, thalami and basal ganglia appear to behave in opposite ways as regard to R2* parameter. Because all deep GM nuclei were analysed together, this may explain the absence of R2* differences between MS and HC subjects in the present study. In the near future, we will seek a more accurate segmentation of deep GM.

Importantly, observed NABT alterations appear to be more diffuse and pronounced in PMS patients and correlate with brain volume loss. Furthermore, stepwise regression indicates that qMRI measures within NABT are independent predictors of clinical status. This is particularly striking for PMS patients, while RRMS patients seem to be more clinically impacted by focal WM demyelination. Here is a remarkable observation suggesting that, at the individual level, variable proportions of both focal and diffuse damages are probably involved in the emergence and progression of disability.

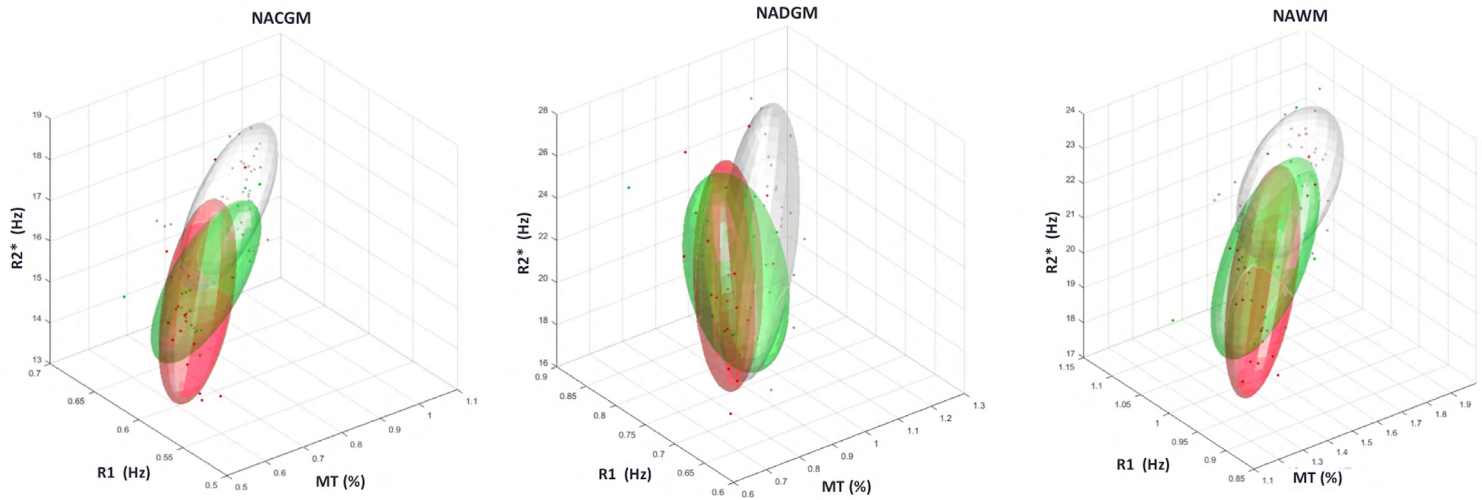

Figure 18: Multivariate Gaussian distribution of MPM quantitative parameters for each tissue class.

Multivariate Gaussian distribution of MPM (MT, R1, R2*) represented as an ellipsoid of the covariance matrix, centered around the mean and for each tissue class. Grey, green and red ellipsoids correspond to HC, RRMS and PMS respectively.

3. IDENTIFICATION OF DIFFERENT PATTERNS OF GREY MATTER DAMAGE IN MS

Loco-regional analyses of MRI data offer the opportunity to assess qMRI parameters at the voxel-level. The simultaneous voxel-wise quantification of microstructural features – reflecting myelin and iron contents – together with atrophy measurement – estimating neurono-axonal loss – enrich the understanding of grey matter (GM) pathology. Without prior prediction regarding GM damage location in MS patients, data unexpectedly identify three different spatially-segregated patterns of GM microstructural/volumetric alterations, potentially associated with different neuropathology. (1) Co-localization of GM atrophy with microstructural changes, usually observed in areas overhanging the most abundant WM lesion load: sensory-motor cortices, auditory cortices, right posterior hippocampus. (2) Microstructural modification without significant volume loss: the left hippocampus and paralimbic cortices. (3) Significant atrophy without significant change in microstructure: deep GM structures.

The discrepancy between volumetric and microstructural changes highlights the complementarity of these MRI techniques in assessing GM pathological changes in MS. Interestingly and despite the absence of significant clinical correlation, this voxel-based analysis allows the detection of GM damage within structures which are decisive for cognitive and motor functions: deep grey matter nuclei and hippocampi. Particularly, the evidence of substantial demyelination of hippocampi beyond atrophic areas constitutes a key contribution of this study.

4. MT, R1 AND R2*: ARE THEY VALUABLE IMAGING BIOMARKERS?

Although still far away from validation studies, the current work provides some evidence that multiple qMRI parameters derived from the MPM protocol might indeed be valuable imaging biomarkers in MS:

- They sensitively detect diffuse alterations within NABT of MS patients, both at the global and loco-regional levels and beyond the ability of atrophy measurements. At the same time, clinico-radiological correlations are largely improved.

- MT, R1 and R2* qMRI parameters differently correlate with histologically measured myelin and/or iron contents and their combination allows a comprehensive characterization of MS microstructural alterations. Although they do not constitute reliable measures of specific pathological processes, new biophysical models are being developed to convert these qMRI data into more specific biological metrics (myelin density, iron density, fiber orientation). Together with high resolution and data quality coming from advanced acquisition methods (ultra-high field MRI, improved gradient strength, motion correction,…), biophysical modelling is getting even closer to in vivo histology *(Weiskopf et al., 2015)*.

- Moreover, important methodological developments ensure reasonable short MRI acquisition time, a nearly fully-automated processing as well as the reproducibility of data in the context of multi-centric studies *(Tabelow et al., 2019; Weiskopf et al., 2013)*.

We recognize, of course, that small sample cross-sectional studies and group-level inferences present some limitations. Future large-scale studies will be needed to evaluate the reproducibility of these results. In addition, longitudinal analyses performed at the individual level will assess the time course of microstructural alterations and their ability to provide predictive information early on in the disease evolution, possibly before the development of significant brain atrophy.

5. FUTURE FOR MS: PERSONNAL VIEW

5.1 BETTER TARGETING OF DISEASE PROGRESSION

No area of neurology has seen greater strides in development of new treatments than MS. However, almost all of the available therapies are effective only for the relapsing-remitting stage, with no or weak impact on progressive evolution. If new therapies are to be developed that can slow or stop worsening disability, it will require a better targeting of manifold and complex processes that are thought to drive progression: slow expanding white matter plaques *(Elliott et al., 2018; Frischer et al., 2015; Luchetti et al., 2018)*, axonal degeneration *(Klaver et al., 2015)*, spinal cord lesions, cortical demyelination *(Haider et al., 2016; Kutzelnigg et al., 2005)*, meningeal inflammation *(Magliozzi et al., 2018, 2007; Wicken et al., 2018)*, failure of full remyelination *(Cunniffe and Coles, 2019)*, deep grey matter alterations,…*(Lassmann, 2019, 2017; Lassmann et al., 2012)* Because it would undoubtedly allow earlier prognostication of clinical evolution and response to treatment, there is still a need for integrating clinical measures and imaging markers which are sensitive to various aspects of MS pathology.

While the results of the present work are promising, we still have a long way to go. Beyond longitudinal qMRI studies at 3 Tesla, which are of course man-

datory, we would like to better seek cortical pathology using both ultra-high field MR and PET imaging. The superior performances of 7 Tesla MRI in detecting cortical lesions *(Kilsdonk et al., 2016; Pitt et al., 2010; Treaba et al., 2019)* resolve problem encountered in the present work and allow us to consider three different types of cortical damages: focal cortical demyelinated lesions (1) microstructural alterations within normal appearing cortical tissue related (2) or unrelated (3) to focal WM lesions. This theoretical parcellation should be made possible through information derived from diffusion MRI (tractography, connectivity). Within these three cortical categories, ultra-high resolution MT, R1, R2*, QSM (quantitative susceptibility mapping) maps as well as derived biological metrics, will provide information about myelin and iron contents. Moreover, we propose to estimate synaptic density with [18F]-UCB-H, a novel PET tracer with a nanomolar affinity for human SV2A protein *(Warnock et al., 2014)*. SV2 is one of the essential integral membrane proteins of synaptic vesicles. SV2A isoform is ubiquitous in the brain *(Bajjalieh et al., 1994)* and expressed in both excitatory and inhibitory synapses *(Bajjalieh et al., 1994)*. SV2A radiotracer constitutes a candidate biomarker to investigate potential for neurodegeneration in MS, possibly before it occurs. Indeed we know from post-mortem and in vitro studies that synaptic activity within MS brain is disturbed, both at the structural *(Jürgens et al., 2016)* and functional *(Centonze et al., 2010; Mandolesi et al., 2015)* levels. Occurring even independently from cortical demyelination or axonal loss *(Jürgens et al., 2016)*, these alterations could drive neuronal loss and clinical progression. We therefore have great expectations for this PET imaging marker.

5.2 TOWARDS PERSONALIZED MEDICINE IN MS

The heterogeneity in phenotypic expression of MS and response to treatment pose major challenges to improve individual patient's care. In this context, the

concept of personalized medicine gains considerable attention from the MS community. Accounting for individual characteristics – environmental and demographic factors, clinical features, imaging and biofluid biomarkers –, this approach aims at improving the precision of diagnosis, capturing the prognosis as early as possible and predicting treatment response.

Necessarily, it implies the validation of candidate biomarkers before they can be properly used in multi-site settings, both in research and clinical practice. It also requires longitudinal collection of datasets in a multimodal perspective (imaging, electrophysiology, genomics, biology, epidemiology...), as well as their encoding within shared international databases. Finally, it involves the development of predictive models integrating those data. To be clinically useful, these models need to be dynamic and able to evolve for more accurate predictions as new data become available. This is what we expect from deep learning algorithms.

Personalized care in MS is certainly not something than can come overnight and the next two decades will be decisive to reach that goal. However, the first steps can be taken immediately, even at a smaller scale.

PART C

APPENDICES

APPENDIX 1: Additional information related to chapter I

Table S1.1: Expanded Disability Status Scale (EDSS)

Score	Criteria
0	Normal neurological examination (all functional scores [FS] = 0)
1	No disability, minimal signs in one FS (one FS = 1)
1.5	No disability, minimal signs in more than one FS (more than one FS = 1)
2.0	Minimal disability in one FS (one FS = 2; others ≤ 1)
2.5	Minimal disability in two FS (two FS = 2; others ≤ 1)
3.0	Moderate disability in one FS (one FS = 3; others ≤ 1) or mild disability in three or four FS (three or four FS = 2; others ≤ 1); though **fully ambulatory**
3.5	Moderate disability in one FS (one FS = 3) with minimal disability in one or two FS (one or two FS = 2; others ≤ 1) or moderate disability in two FS (two FS = 3, others ≤ 1) or minimal disability in five FS (five FS = 2; others ≤ 1); though **fully ambulatory**
4.0	Ambulatory without aid or rest for ≥ **500 m**; severe disability in one FS (one FS = 4; others ≤ 1) or combination of lesser grades exceeding limits of previous steps
4.5	Ambulatory without aid or rest for ≥ **300 m**; severe disability in one FS (one FS = 4) and combination of lesser grades exceeding limits of previous steps
5.0	Ambulatory without aid or rest for ≥ **200 m**; usual FS equivalent include at least one FS = 5, or combination of lesser grades usually exceeding specifications fort step 4.0
5.5	Ambulatory without aid or rest for ≥ **100 m**; usual FS equivalent include at least one FS = 5, or combination of lesser grades usually exceeding specifications fort step 4.0
6.0	Unilateral assistance (cane or crutch) required to walk **at least 100 m** with or without resting
6.5	Constant bilateral assistance required to walk **at least 20 m** without resting
7.0	Unable to walk 5 m even with aid, essentially restricted to wheelchair; wheels self and transfers alone; up and about in wheelchair some 12 h a day
7.5	Unable to take more than a few steps; restricted to wheelchair; may need some hemp in transferring and in wheeling self
8.0	Essentially restricted to bed or chair or perambulated in wheelchair, but out of bed most of day; remains many self-care functions; generally has effective use of arms
8.5	Essentially restricted to bed much of the day; has some effective use of arm(s): retains some self-care functions
9.0	Helpless bed patients; can communicate and eat
9.5	Totally helpless bed patient; unable to communicate effectively or eat/swallow
10.0	Death attributed to MS

Adapted from (Kurtzke, 1983)

Table S1.2: Biofluid biomarkers

	Marker	Source
Clinical Biomarkers	OCBs	CSF
CNS/Neurodegeneration markers	NFL	Serum/CSF
	GFAP	CSF
	MBP	CSF
	S100B	CSF
	Ferritin	CSF
	Tau	CSF
	NCAM	CSF
	NGF	CSF
	CNTF	CSF
Activation/Inflammatory markers	sCD163	Serum/CSF
	YK-40	CSF
	CXCL13	Serum/CSF
	OPN	Serum/CSF
	Myelin-reactive T cells	PBMCs
RNA	miRNA	PBMCs/Serum/CSF
	mRNA transcriptome	PBMCs/Serum/CSF
Antibodies/Autoantibodies	MRZR	CSF
	KIR4.1	Serum
Microbial	Lipid 654	Serum

From (Housley et al., 2015)

OCBs: oligoclonal bands, CSF: cerebrospinal fluid, NFL: neurofilament, GFAP: glial fibrillary acidic protein, MBP: myelin basic protein, S100B: astrocyte proliferation marker, NCAM: neural cell adhesion molecule, NGF: nerve growth factor, CNTF: cytokine ciliary neurotrophic factor, sCD163: specific macrophage/monocytes membrane marker, YKL-40: Chitinase-3-like 1,OPN: osteopontin, PBMCs: peripheral blood mononuclear cells, miRNA: micro RNA, mRNA: messenger RNA, MRZR: antibodies against Measles, Rubella, and Varicella Zoster, KIR4.1: antibodies against potassium channel KIR4., Lipid 654: microbiome associated lipo-peptide.

Table S1.3: 2017 McDonald criteria

Diagnosis of MS requires elimination of fore likely diagnoses and demonstration of dissemination in space and time, within the CNS

Dissemination in Space (DIS)	Dissemination in Time (DIT)
Clinical attack MRI ≥ 1 symptomatic or asymptomatic MS-typical T2 lesions in ≥ 2 areas of CNS: • periventricular • juxta-cortical/cortical • infra-tentorial • spinal cord	Clinical attack MRI • Simultaneous presence of both enhancing and non-enhancing symptomatic or asymptomatic MS-typical MRI lesions • New T2 or enhancing MRI lesions compared to baseline scan (without regard to timing of baseline scan) CSF-specific oligoclonal bands

Clinical presentation	Additional data needed to MS diagnosis
≥ 2 clinical attacks and objective evidence of ≥ 2 lesions	None
≥ 2 clinical attacks and objective evidence of 1 lesion	DIS: an additional attack implicating a different CNS site or by MRI
1 clinical attack and objective evidence of 1 lesion	DIT: an additional clinical attack or by MRI or CSF-specific oligoclonal bands
1 clinical attack and objective evidence of 1 lesion	DIS: an additional clinical attack implicating a different CNS site or by MRI AND DIT: an additional clinical attack or by MRI or CSF-specific oligoclonal bands
Progression from onset	1 year of disability progression (retrospective or prospective) AND two of these criteria: • ≥ 1 symptomatic or asymptomatic MS-typical T2 lesions in ≥ 2 areas of CNS: periventricular, juxtacortical/cortical or infratentorial • ≥ 2 spinal cord lesions • CSF-specific oligoclonal bands

From (Thompson et al., 2017)

Table S1.4: Advanced quantitative imaging techniques proposed to investigate MS pathology (non-exhaustive list)

Imaging technique	Measure relevant to MS pathology	Features and current limitations
	Structural imaging techniques	
Magnetization transfer imaging	Myelin content/axonal density	Not entirely specific to myelin, non-linear relationship to myelin density, calibration required across and within scanners; short acquisition time
R2* and quantitative susceptibility mapping	Iron (mostly ferritin and hemosiderin) Myelin density and orientation Level of blood oxygenation	Orientationally dependent in WM and not able to disentangle the contradictory effect of iron accumulation and demyelination; homogenization of B0 magnetic field and shorter TE minimize artifacts from macroscopic susceptibility effects; short acquisition time
R1 mapping	Myelin density/myelin bound cholesterol Water content Iron	Contradictory effect of iron, at a lesser extent than R2*; optimization of flip angles and correction for RF inhomogeneities help to increase accuracy; short acquisition time
DTI/NODDI	Microstructural organization of brain tissue (neurite density, orientation, free water)	Poor specificity of DTI metrics, higher specificity of NODDI in assessing neurodegeneration, limited spatial resolution, cumbersome data acquisition and analysis
Myelin-water fraction	Myelin integrity	Strong specificity for myelin when correcting for changes in total water content; relatively long acquisition time
Cortical lesion detection and leptomeningeal enhancement	Cortical lesion, cortical myelin integrity, meningeal inflammation	Depend on MRI field strength (better at 7T), lesion type and sequences
Atrophy-based measurement	Neurono-axonal loss	Technical and non-MS related variability, low specificity

Metabolic imaging techniques		
TSPO-PET	Microglial activation	Challenges in quantification, low resolution, high cost, lack of widespread tracer availability, different binding affinity phenotype, radiation exposure
PIB/MMP-PET	Myelin content	
Flumazenil- PET	Neuronal integrity	
NAA from H-MRS	Mitochondrial dysfunction	Not specific enough, low spatial resolution, challenge for quantification, variability across scanners, limited reproducibility
Myo-inositol from H-MRS	Gliotic response	
Na MRI	Axonal function	Moderate specificity, dependence on MRI field strength and sequence, low spatial resolution
GluCEST	Glutamate excitotoxicity	Low SNR, dependence on RF irradiation, difficult to separate Glu signal from overlapping amine signal or other amino-acids
Perfusion imaging	Hypometabolism, ischemia, tissue injury, tissue destruction	Low spatial resolution, low reliability and reproducibility
Beyond brain imaging		
Optical coherence tomography	Retinal neurono-axonal loss	High specificity and sensitivity, inexpensive and reproducible; measurement variability
Spinal cord imaging	Depends on the technique: myelin integrity, axonal loss	Measurement variability, complexity of image analyses

Adapted from (Bakshi et al., 2008; Ciccarelli et al., 2014; Enzinger et al., 2015; Oh et al., 2019)

R2*: effective transverse relaxation rate, R1: longitudinal relaxation rate, DTI: diffusion tensor imaging, NODDI: neurite orientation dispersion and density imaging, PET: positron emission tomography, TSPO: translocator protein, PIB: 2-(-40-methylaminophenyl)-6-hydroxybenzothiazole, MMP: matrix metalloproteinase, NAA: N-acetylaspartate, H-MRS: proton magnetic resonance spectroscopy, CEST: chemical exchange saturation transfer, SNR: signal to noise ratio.

APPENDIX 2: Supplementary material related to chapter V

Table S2.1: Multi-echo 3D FLASH acquisition parameters

	Magnetom ALLEGRA	**Magnetom PRISMA**
PDw		
TR	23.7 [ms]	24.5 [ms]
Flip angle	6°	6°
Bipolar gradient echoes/TE	6/TE 2.2-14.7 [ms]	8/TE 2.34-18.72 [ms]
Bandwidth	425 [Hz/Px]	465 [Hz/Px]
T1W		
TR	18.7 [ms]	24.5 [ms]
Flip angle	20°	21°
Bipolar gradient echoes/TE	6/TE 2.2-14.7 [ms]	8/TE 2.34-18.72 [ms]
Bandwidth	425 [Hz/Px]	465 [Hz/Px]
MTw		
TR	23.7 [ms]	24.5 [ms]
Flip angle	6°	6°
Bipolar gradient echoes/TE	6/TE 2.2-14.7 [ms]	6/TE 2.34-14.04 [ms]
Off-resonance Gaussian MT pulse	FA: 215° Frequency offset: 2 [kHZ]	FA: 220° Frequency offset: 2 [kHZ]
Bandwidth	425 [Hz/Px]	465 [Hz/Px]

APPENDIX 3: Supplementary material related to chapter VII

Table S3.1: Regions with significantly reduced NAGM MT in MS patients compared to HC

Region	Side	MNI coordinates of local maxima			Number of voxels	Local maximum F-value (1, 66)	pFWER (corr)
Heschl's gyrus	R	45	-18	6	875	84.49	< 0.001
Insula	R	35	-24	2		67.57	< 0.001
Insula	R	44	-21	-2		63.84	< 0.001
Insula	R	41	-34	16	19	44.66	0.002
Insula	R	32	-16	15	49	42.78	0.003
Superior temporal gyrus	R	69	-23	3	32	43.84	0.002
Heschl's gyrus	L	-34	-31	11	81	50.52	< 0.001
Heschl's gyrus	L	-44	-24	5		44.24	0.002
Precentral gyrus	R	38	-11	36	29	42.03	0.004
Postcentral gyrus	R	16	-35	67	34	43.92	0.002
Precentral gyrus	L	-42	-14	41	15	43.52	0.003
Postcentral gyrus	L	-42	-23	36	42	49.01	0.001
Frontomarginal gyrus	L	-12	54	-10	10	44.70	0.002
Hippocampus	R	26	-31	-4	23	38.58	0.011
Hippocampus	R	13	-5	-14	22	38.46	0.011
Hippocampus	R	29	-25	-7	13	37.55	0.014
Hippocampus	L	-11	-7	-14	25	43.53	0.003
Hippocampus	L	-31	-26	-7	82	41.62	0.005

Tables S3.2: Regions with significantly reduced NAGM R1 in MS patients compared to HC

Region	Side	MNI coordinates of local maxima			Number of voxels	Local maximum F-value (1, 66)	pFWER (corr)
Transverse temporal gyrus	R	53	-30	8	14	46.37	0.001
Superior temporal gyrus	R	47	-44	10	33	42.11	0.003
Insula	R	32	-25	8	40	44.54	0.002
Transverse temporal gyrus	L	-39	-29	7	132	53.73	< 0.001
Transverse temporal gyrus	L	-38	-37	11		53.18	< 0.001
Superior temporal gyrus	L	-46	2	-25	103	55.84	< 0.001
Superior temporal gyrus	L	-48	-34	8	33	54.91	< 0.001
Superior temporal gyrus	L	-44	-52	19	10	39.18	0.008
Insula	L	-32	-19	17	20	36.02	0.019
Precentral gyrus	R	34	-20	49	18	56.45	< 0.001
Precentral gyrus	R	-47	-5	28	10	45.75	0.001
Precentral gyrus	R	38	-14	37	20	41.07	0.005
Postcentral gyrus	R	41	-21	44	44	60.80	< 0.001
Postcentral gyrus	R	37	-26	46	13	39.18	0.008
Postcentral gyrus	L	-35	-20	36	16	47.12	0.001
Postcentral gyrus	L	-32	-32	51	32	44.14	0.002
Postcentral gyrus	L	-41	-24	37	16	39.07	0.008
Lingual gyrus	R	23	-58	-1	18	43.91	0.002
Cingulate gyrus	R	7	-3	33	10	40.00	0.006
Hippocampus	R	26	-23	-8	68	55.58	< 0.001
Hippocampus	R	30	-30	0	22	36.43	0.017
Hippocampus	L	-30	-29	-5	248	51.67	< 0.001

Tables S3.3: Regions with significantly reduced NAGM R2* in MS patients compared to HC

Region	Side	MNI coordinates of local maxima			Number of voxels	Local maximum F-value (1, 66)	pFWER (corr)
Superior temporal gyrus	L	-41	-35	8	5	37.42	< 0.001
Precentral gyrus	L	-36	-31	60	19	44.01	< 0.001
Postcentral gyrus	L	-44	-22	57	1	32.73	< 0.001

Tables S3.4: Regions with significantly reduced GM volume (VBM) in MS patients compared to HC

Region	Side	MNI coordinates of local maxima			Number of voxels	Local maximum F-value (1, 66)	pFWER (corr)
Heschl's gyrus	R	40	-21	9	132	60.96	< 0.001
Heschl's gyrus	R	46	-14	3		43.99	0.001
Heschl's gyrus	L	-44	-20	3	93	45.74	0.001
Heschl's gyrus	L	-38	-24	10		42.12	0.002
Superior temporal gyrus	L	-50	-14	4		35.57	0.015
Precentral gyrus	R	44	-14	52	1266	85.71	< 0.001
Precentral gyrus	R	30	-21	68		64.73	< 0.001
Precentral gyrus	R	30	-21	68		64.73	< 0.001
Postcentral gyrus	R	28	-45	63	121	40.53	0.004
Postcentral gyrus	R	28	-45	63		40.53	0.004
Precentral gyrus	L	-27	-26	62	1575	110.45	< 0.001
Precentral gyrus	L	-39	-20	48		72.31	< 0.001
Postcentral gyrus	L	-40	-30	58		69.34	< 0.001
Paracentral lobule	R	4	-26	69	179	58.91	< 0.001
Paracentral lobule	L	-4	-30	58	188	59.86	< 0.001
Paracentral lobule	L	-4	-28	72		48.43	< 0.001
Paracentral lobule	L	-3	-18	58		40.28	0.004
Hypothalamus	R	3	-12	-12	350	97.67	< 0.001
Thalamus	R	2	-21	-4		35.82	0.014
Hippocampus	R	18	-26	-9	142	65.28	< 0.001
Superior occipital gyrus	L	-15	-93	-6	26	54.87	< 0.001
Cuneus	R	6	-84	16	28	40.65	0.003

Superior parietal gyrus	R	21	-56	64	11	40.61	0.003
Parietal inferior lobule	L	-33	-50	54	12	36.52	0.011
Superior parietal gyrus	L	-26	-56	60	31	37.74	0.008
Lingual gyrus	R	15	-51	-2	18	47.01	0.001
Lingual gyrus	R	8	-81	-3	19	45.54	0.001
Inferior and superior colliculi	R	4	-33	-9	32	39.88	0.004
Putamen	L	-30	8	-6	27	36.48	0.011

Tables S3.5: Clusters where regional reductions of R1 and MT regress with lesion fraction

qMRI	Region	Side	MNI coordinates of local maxima			Number of voxels	Local maximum F-value (1, 66)	pFWER (corr)
R1	Thalamus	L	-5	-28	4	3119	5.42	< 0.001
R1	Thalamus	R	2	-18	6		5.21	
MT	Thalamus	R	18	-31	4	288	15.54	0.023

PART D

LIST OF PUBLICATIONS

PUBLICATIONS AS FIRST OR CO-AUTHOR

Lommers, E., Guillemin, C., Reuter, G., Delrue, G., Colette, F., Degueldre, C., Balteau, E., Maquet, P., Phillips, C., **2019**. Voxel-based quantitative MRI reveals spatial patterns of grey matter alteration in multiple sclerosis. *Submitted to Multiple Sclerosis Journal.*

Lommers, E., Simon, J., Reuter, G., Delrue, G., Dive, D., Degueldre, C., Balteau, E., Phillips, C., Maquet, P., **2019**. Multiparameter MRI quantification of microstructural tissue alterations in multiple sclerosis. *NeuroImage*: *Clinical*, 23. DOI: 10.1016/j.nicl.2019.101879

Lommers, E., Depierreux, F., Hansen, I., Dive, D., Maquet, P., **2018**. NMOSD with anti-MOG antibodies following anti-TNFα therapy: A case report. *Multiple Sclerosis and Related Disorders,* 26*:* 37-39. DOI: 10.1016/j.msard.2018.08.029

Phillips, C., **Lommers, E**., Pernet, C., **2016**. Unifying lesion masking and tissue probability maps for improved segmentation and normalization. Presented at 23rd Annual Meeting of the Organization for Human Brain Mapping; Vancouver. http://hdl.handle.net/2268/213972

Phan-Ba, R., **Lommers, E**., Tshibanda, L., Calay, P., Dubois, B., Moonen, G., Clifford, D., Belachew, S., **2012**. MRI preclinical detection and asymptomatic course of a progressive multifocal leucoencephalopathy (PML) under natalizumab therapy. *Journal of Neurology, Neurosurgery and Psychiatry,* 83*:* 224-226. DOI: 10.1136/jnnp-2011-300511

Phan-Ba, R., **Lommers, E.**, Moonen, G., Belachew, S., Nath, A., **2012**. Immune Reconstitution Inflammatory Syndrome in Natalizumab-Associated PML. *Neurology*, 78(1): 73. DOI: 10.1212/01.wnl.0000410335.08123.dc

Lommers, E., Lecrompe, L., Moonen, G., Phan-Ba, R., Belachew, S., **2012**. Vitamin D tweets light to genes in multiple sclerosis. *Revue Médicale de Liège*, 67(5-6):359-365.

OTHER PUBLICATIONS

Phan-Ba, R., Calay, P., Grodent, P., Delrue, G., **Lommers, E.**, Delvaux, V., Moonen, G., Nagels, G., Belachew, S., **2012**. A corrected version of the Timed-25 Foot Walk Test with a dynamic start to capture the maximum ambulation speed in multiple sclerosis patients. *NeuroRehabilitation*, 30(4), 261-266. DOI: 10.3233/NRE-2012-0754

Phan-Ba, R., Calay, P., Grodent, P., Delrue, G., **Lommers, E.**, Delvaux, V., Moonen, G., Nagels, G., Belachew, S., **2012**. Motor fatigue measurement by distance-induced slowdown of walking speed in multiple sclerosis. *PLoS ONE*, 7(4), 34744. DOI: 10.3233/NRE-2012-0754

Gillard, F., Andris, C., **Lommers, E.**, **2019**. Extended optic neuropathy with myelin oligodendrocyte glycoprotein antibodies. *Revue Médicale de Liège* 74(4): 179-184.

REFERENCES

Aarli, J.A., Abramsky, O., Browne, P., Chandraratna, D., Angood, C., Tremlett, H., Baker, C., Taylor, B. V, Thompson, A.J., 2014. Atlas of multiple sclerosis **2013**: a growing global problem with widespread inequity. Neurology 83, 1022–1024.

Agosta, F., Rovaris, M., Pagani, E., Sormani, M.P., Comi, G., Filippi, M., **2006**. Magnetization transfer MRI metrics predict the accumulation of disability 8 years later in patients with multiple sclerosis. Brain 129, 2620–2627.

Alroughani, R., Deleu, D., El Salem, K., Al-Hashel, J., Alexander, K.J., Abdelrazek, M.A., Aljishi, A., Alkhaboori, J., Al Azri, F., Al Zadjali, N., Hbahbih, M., Sokrab, T.E., Said, M., Rovira, À., **2016**. A regional consensus recommendation on brain atrophy as an outcome measure in multiple sclerosis. BMC Neurol. 16, 1–9.

Amiri, H., Sitter, A. De, Bendfeldt, K., Battaglini, M., Wheeler-kingshott, C.A.M.G., Calabrese, M., Geurts, J.J.G., Rocca, M.A., Sastre-garriga, J., Enzinger, C., De Stefano, N., Filippi, M., Rovira, Á., Barkhof, F., Vrenken, H., Group, M.S., **2018**. Urgent challenges in quantification and interpretation of brain grey matter atrophy in individual MS patients using MRI. NeuroImage Clin. 19, 466–475.

Ashburner, J., Friston, K.J., **2005**. Unified segmentation. Neuroimage 26, 839–851.

Ashburner, J., Friston, K.J., **2000**. Voxel-Based Morphometry — The Methods. Neuroimage 11, 805–821.

Audoin, B., Davies, G., Rashid, W., Fisniku, L., Thompson, A.J., Miller, D.H., **2007**. Voxel-based analysis of grey matter magnetization transfer ratio maps in early relapsing remitting multiple sclerosis. Mult. Scler. 13, 483–489.

Azevedo, C.J., Pelletier, D., **2016**. Whole-brain atrophy: ready for implementation into clinical decision-making in multiple sclerosis? Curr Opin Neurol 29, 237–242.

Bagnato, F., Hametner, S., Boyd, E., Endmayr, V., Shi, Y., Ikonomidou, V., Chen, G., Pawate, S., Lassmann, H., Smith, S., Brian Welch, E., **2018**. Untangling the R2* contrast in multiple sclerosis: A combined MRI-histology study at 7.0 Tesla. PLoS One 13, 1–19.

Bajjalieh, S.M., Frantz, G.D., Weimann, J.M., McConnell, S.K., Scheller, R.H., **1994**. Differential expression of synaptic vesicle protein 2 (SV2) isoforms. J. Neurosci. 14, 5223–5235.

Bakshi, R., Thompson, A.J., Rocca, M.A., Pelletier, D., Dousset, V., Barkhof, F., Inglese, M., Guttmann, C.R.G., Horsfi, M.A., Filippi, M., **2008**. MRI in multiple sclerosis: current status and future prospects. Lancet Neurol. 7, 615–625.

Balteau, E., Leutritz, T., Weiskopf, N., Reimer, E., Lutti, A., Callaghan, M.F., Mohammadi, S., **2018**. Evaluating T2* bias impact and correction strategies in quantitative proton density mapping. Proceedings of the Joint Annual Meeting ISMRM-ESMRMB, Paris.

Barkhof, F., **2002**. The clinico-radiological paradox in multiple sclerosis revisited. Curr. Opin. Neurol. 15, 239–245.

Barkhof, F., Scheltens, P., Frequin, S., Nauta, J., Tas, M., Valk, J., Hommes, O., **1992**. Relapsing-Remitting Multiple Sclerosis: Sequential Enhanced MR Imaging vs Clinical Findings in Determining Disease Activity. Am. J. Roentgenol. 159, 1041–1047.

Beck, E.S., Sati, P., Sethi, V., Kober, T., Dewey, B., Bhargava, P., Nair, G., Cortese, I.C., Reich, D.S., **2018**. Improved visualization of cortical lesions in multiple sclerosis using 7T MP2RAGE. Am. J. Neuroradiol. 39, 459–466.

Benedict, R.H., Amato, M.P., Boringa, J., Brochet, B., Foley, F., Fredrikson, S., Hamalainen, P., Hartung, H., Krupp, L., Penner, I., Reder, A.T., Langdon, D., **2012**. Brief International Cognitive Assessment for MS (BICAMS): international standards for validation. BMC Neurol. 12, 55.

Bielekova, B., Martin, R., **2004**. Development of biomarkers in multiple sclerosis. Brain 127, 1463–1478.

Bodini, B., Khaleeli, Z., Cercignani, M., Miller, D.H., Thompson, A.J., Ciccarelli, O., **2009**. Exploring the relationship between white matter and gray matter damage in early primary progressive multiple sclerosis: an in vivo study with TBSS and VBM. Hum. Brain Mapp. 30, 2852–2861.

Brownell, B., Hughes, J.T., **1962**. The distribution of plaques in the cerebrum in multiple sclerosis. J. Neurol. Neurosurg. Psychiatr. 25, 315–320.

Brück, W., Kuhlmann, T., Stadelmann, C., **2003**. Remyelination in multiple sclerosis. J. Neurol. Sci. 206, 181–185.

Brück, W., Porada, P., Poser, S., Rieckmann, P., Hanefeld, F., Kretzschmarch, H., Lassmann, H., **1995**. Monocyte/macrophage differentiation in early multiple sclerosis lesions. Ann. Neurol. 38, 788–796.

Calabrese, M., Magliozzi, R., Ciccarelli, O., Geurts, J.J.G., Reynolds, R., Martin, R., **2015**. Exploring the origins of grey matter damage in multiple sclerosis. Nat. Rev. Neurosci. 16, 147–158.

Callaghan, M.F., Freund, P., Draganski, B., Anderson, E., Cappelletti, M., Chowdhury, R., Diedrichsen, J., Fitzgerald, T.H.B., Smittenaar, P., Helms, G., Lutti, A., Weiskopf, N., **2014**. Widespread age-related differences in the human brain microstructure revealed by quantitative magnetic resonance imaging. Neurobiol. Aging 35, 1862–1872.

Campbell, G.R., Ziabreva, I., Reeve, A.K., Krishnan, K.J., Reynolds, R., Howell, O., Lassmann, H., Turnbull, D.M., Mahad, D.J., **2011**. Mitochondrial DNA Deletions and Neurodegeneration in Multiple Sclerosis. Ann. Neurol. 69, 481–492.

Cannella, B., Raine, C.S., **1995**. The adhesion molecule and cytokine profile of multiple sclerosis lesions. Ann. Neurol. 37, 424–435.

Ceccarelli, A., Rocca, M.A., Pagani, E., Colombo, B., Martinelli, V., Comi, G., Filippi, M., **2008**. A voxel-based morphometry study of grey matter loss in MS patients with different clinical phenotypes. Neuroimage 42, 315–322.

Centonze, D., Muzio, L., Rossi, S., Furlan, R., Bernardi, G., Martino, G., **2010**. The link between inflammation, synaptic transmission and neurodegeneration in multiple sclerosis. Cell Death Differ. 17, 1083–1091.

Chiou, B., Lucassen, E., Sather, M., Kallianpur, A., Connor, J., **2018**. Semaphorin4A and H-ferritin utilize Tim-1 on human oligodendrocytes: A novel neuro-immune axis. Glia 66, 1317–1330.

Ciccarelli, O., Barkhof, F., Bodini, B., De Stefano, N., Golay, X., Nicolay, K., Pelletier, D., Pouwels, P.J.W., Smith, S.A., Wheeler-Kingshott, C.A.M., Stankoff, B., Yousry, T., Miller, D.H., **2014**. Pathogenesis of multiple sclerosis: Insights from molecular and metabolic imaging. Lancet Neurol. 13, 807–822.

Cohen-Adad, J., **2014**. What can we learn from T2* maps of the cortex? Neuroimage 93, 189–200.

Comabella, M., Sastre-garriga, J., Montalban, X., **2016**. Precision medicine in multiple sclerosis: biomarkers for diagnosis, prognosis, and treatment response. Curr. Neuropharmacol. 29, 254–262.

Compston, A., Coles, A., **2008**. Seminar Multiple sclerosis. Lancet Neurol. 372, 1502–17.

Compston, A., Confavreux, C., **2006**. McAlpine's Multiple Sclerosis, Fourth Edition, McAlpine's MULTIPLE SCLEROSIS. Elsevier.

Confavreux, C., Vukusic, S., **2006**. Natural history of multiple sclerosis: a unifying concept. Brain, 129, 606–616.

Confavreux, C., Vukusic, S., Moreau, T., Adeleine, P., **2000**. Relapses and progression of disability in multiple sclerosis. N. Engl. J. Med. 343, 1430–1438.

Correale, J., **2014**. The role of microglial activation in disease progression. Mult. Scler. J. 20, 1288–1295.

Crespy, L., Zaaraoui, W., Lemaire, M., Rico, A., Faivre, A., Reuter, F., Malikova, I., Confort-Gouny, S., Cozzone, P.J., Pelletier, J., Ranjeva, J.P., Audoin, B., **2011**. Prevalence of grey matter pathology in early multiple sclerosis assessed by Magnetization transfer ratio imaging. PLoS One 6, 2–7.

Cunniffe, N., Coles, A., **2019**. Promoting remyelination in multiple sclerosis. J. Neurol., [Epub ahead of print].

Damjanovic, D., Valsasina, P., Rocca, M A, Stromillo, M.L., Gallo, A., Enzinger, C., Hulst, H.E., Rovira, A., Muhlert, N., De Stefano, N., Bisecco, A., Fazekas, F., Arevalo, M.., Yousry, T.A., Filippi, M., Yousry, X.T.A., Filippi, X.M., **2017**. Hippocampal and Deep Gray Matter Nuclei Atrophy Is Relevant for Explaining Cognitive Impairment in MS: A Multicenter Study. AJNR. Am. J. Neuroradiol. 38, 18–24.

Davies, G.R., Altmann, D.R., Hadjiprocopis, A., Rashid, W., Chard, D.T., Griffin, C.M., Tofts, P.S., Barker, G.J., Kapoor, R., Thompson, A.J., Miller, D.H., **2005**. Increasing normal-appearing grey and white matter magnetisation transfer ratio abnormality in early relapsing-remitting multiple sclerosis. J. Neurol. 252, 1037–1044.

Dawson, J., **1916**. The histology of multiple sclerosis. Trans R Soc 50, 517–740.

De Stefano, N., Airas, L., Grigoriadis, N., Mattle, H.P., Walczak, A., Wiendl, H., Kieseier, B.C., **2014**. Clinical Relevance of Brain Volume Measures in Multiple Sclerosis M. CNS drugs 28(2), 147–156.

De Stefano, N., Giorgio, a, Battaglini, M., Rovaris, M., Sormani, M.P., Barkhof, F., Korteweg, T., Enzinger, C., Fazekas, F., Calabrese, M., Dinacci, D., Tedeschi, G., Gass, a, Montalban, X., Rovira, a, Thompson, a, Comi, G., Miller, D.H., Filippi, M., **2010**. Assessing brain atrophy rates in a large population of untreated multiple sclerosis subtypes. Neurology 74, 1868–76.

De Stefano, N., Stromillo, M.L., Giorgio, A., Bartolozzi, M.L., Battaglini, M., Baldini, M., Portaccio, E., Amato, M.P., Sormani, M.P., **2016**. Establishing pathological cut-offs of brain atrophy rates in multiple sclerosis. J. Neurol. Neurosurg. Psychiatr. 87, 93–99.

DeLuca, G.C., Williams, K., Evangelou, N., Ebers, G.C., Esiri, M.M., **2006**. The contribution of demyelination to axonal loss in multiple sclerosis. Brain 129, 1507–1516.

DeLuca, G.C., Yates, R.L., Beale, H., Morrow, S.A., **2015**. Cognitive impairment in multiple sclerosis: Clinical, radiologic and pathologic insights. Brain Pathol. 25, 79–98.

Dousset, V., Gayou, A., Brochet, B., Caille, J., **1998**. Early structural changes in acute MS lesions assessed by serial magnetization transfer studies. Neurology 51, 1150–1155.

Draganski, B., Ashburner, J., Hutton, C., Kherif, F., Frackowiak, R.S.J.J., Helms, G., Weiskopf, N., **2011**. Regional specificity of MRI contrast parameter changes in normal ageing revealed by voxel-based quantification (VBQ). Neuroimage 55, 1423–1434.

Dutta, R., Chang, A., Doud, M.K., Kidd, G.J., Ribaudo, M. V., Young, E.A., Fox, R.J., Staugaitis, S.M., Trapp, B.D., **2011**. Demyelination causes synaptic alterations in hippocampi from multiple sclerosis patients. Ann. Neurol. 69, 445–454.

Dutta, R., Chomyk, A.M., Chang, A., Ribaudo, M. V, Deckard, S.A., Doud, M.K., Edberg, D.D., Bai, B., Li, M., Baranzini, S.E., Fox, R.J., Staugaitis, S.M., Macklin, W.B., Trapp, B.D., **2013**. Hippocampal Demyelination and Memory Dysfunction Are Associated with Increased Levels of the Neuronal microRNA miR-124 and Reduced AMPA Receptors. Ann. Neurol. 73, 637–645.

Dutta, R., Trapp, B.D., **2007**. Pathogenesis of axonal and neuronal damage in multiple sclerosis. Neurology 68 (22 SUPPL. 3).

Elkady, A.M., Cobzas, D., Sun, H., Blevins, G., Wilman, A.H., **2018**. Discriminative Analysis of Regional Evolution of Iron and Myelin / Calcium in Deep Gray Matter of Multiple Sclerosis and Healthy Subjects. J Magn Reson Imaging 48, 652–668.

Elkady, A.M., Cobzas, D., Sun, H., Blevins, G., Wilman, A.H., **2017**. Progressive iron accumulation across multiple sclerosis phenotypes revealed by sparse classification of deep gray matter. J. Magn. Reson. Imaging 46, 1464–1473.

Elkady, A.M., Cobzas, D., Sun, H., Seres, P., Blevins, G., Wilman, A.H., **2019**. Five year iron changes in relapsing-remitting multiple sclerosis deep gray matter compared to healthy controls. Mult. Scler. Relat. Disord. 33, 107–115.

Elliott, C., Wolinsky, J.S., Hauser, S.L., Kappos, L., Barkhof, F., Bernasconi, C., Wei, W., Belachew, S., Arnold, D.L., **2018**. Slowly expanding/evolving lesions as a magnetic resonance imaging marker of chronic active multiple sclerosis lesions. Mult. Scler. J., [Epub ahead of print].

Engström, M., Warntjes, J.B.M., Tisell, A., Landtblom, A.-M., Lundberg, P., **2014**. Multi-parametric representation of voxel-based quantitative magnetic resonance imaging. PLoS One 9(11).

Enzinger, C., Barkhof, F., Ciccarelli, O., Filippi, M., Kappos, L., Rocca, M.A., Ropele, S., Rovira, À., Schneider, T., De Stefano, N., Vrenken, H., **2015**. Nonconventional MRI and microstructural cerebral changes in multiple sclerosis. Nat. Rev. Neurol. 11, 676–686.

Eshaghi, A., Brownlee, W.J., Altmann, D.R., Tur, C., Cardoso, M.J., Angelis, F. De, Pavert, S.H. Van De, Cawley, N., De Stefano, N., Stromillo, M.L., Battaglini, M., Ruggieri, S., Gasperini, C., Filippi, M., Rocca, M.A., Rovira, A., Killestein, J., Pirpamer, L., Enzinger, C., Ourselin, S., Wheeler-kingshott, C.A.M.G., Chard, D., Thompson, A.J., Alexander, D.C., **2018**. Deep Gray Matter Volume Loss Drives Disability Worsening in Multiple Sclerosis. Ann. Neurol. 83, 210–222.

Favaretto, A., Poggiali, D., Lazzarotto, A., Rolma, G., Causin, F., Gallo, P., **2015**. The parallel analysis of phase sensitive inversion recovery (PSIR) and double inversion recovery (DIR) images significantly improves the detection of cortical lesions in multiple sclerosis (MS) since clinical onset. PLoS One 10, 1–11.

Fernando, K.T.M., Tozer, D.J., Miszkiel, K., Gordon, R.M., Swanton, J.K., Dalton, C.M., Barker, G.J., Plant, G.T., Thompson, J., Miller, D.H., **2005**. Magnetization transfer histograms in clinically isolated syndromes suggestive of multiple sclerosis. Brain 128, 2911–25.

Filippi, M., **2000**. Enhanced magnetic resonance imaging in multiple sclerosis. Mult. Scler. 6, 320–326.

Filippi, M., Agosta, F., **2010**. Imaging biomarkers in multiple sclerosis. J. Magn. Reson. Imaging 31, 770–788.

Filippi, M., Agosta, F., **2007**. Magnetization transfer MRI in multiple sclerosis. J. Neuroimaging 17 Suppl 1, 22S-26S.

Filippi, M., Rocca, M., **2010**. Novel MRI approaches to assess patients with multiple sclerosis. Curr. Opin. Neurol. 23, 212–7.

Filippi, M., Rocca, M. a, Horsfield, M. a, Hametner, S., Geurts, J.J.G., Comi, G., Lassmann, H., **2013**. Imaging cortical damage and dysfunction in multiple sclerosis. JAMA Neurol. 70, 556–64.

Filippi, M., Rocca, M., Martino, G., **1998**. Magnetization transfer changes in the normal appearing white matter pre-ced the appearance of enhancing lesions in patients with MS. Ann. Neurol. 43, 809–814.

Filippi, M., Rocca, M.A., Barkhof, F., Brück, W., Chen, J.T., Comi, G., Deluca, G., De Stefano, N., Erickson, B.J., Evangelou, N., Fazekas, F., Geurts, J.J.G., Lucchinetti, C., Miller, D.H., Pelletier, D., Popescu, B.F.G., **2012**. Association between pathological and MRI findings in multiple sclerosis. Lancet Neurol. 11, 349–360.

Filippi, M., Tortorella, C., Rovaris, M., Bozzali, M., Possa, F., Sormani, M.P., Iannucci, G., **2000**. Changes in the normal appearing brain tissue and cognitive impairment in multiple sclerosis. J. Neurol. Neurosurg. Psychiatry 68, 157–161.

Fischer, M.T., Sharma, R., Lim, J.L., Haider, L., Frischer, J.M., Drexhage, J., Mahad, D., Bradl, M., Horssen, J. Van, Lassmann, H., **2012**. NADPH oxidase expression in active multiple sclerosis lesions in relation to oxidative tissue damage and mitochondrial injury. Brain 135, 886–899.

Fischl, B., Dale, A.M., **2000**. Measuring the thickness of the human cerebral cortex from magnetic resonance images. PNAS 97, 11050–11055.

Fisher, E., Ph, D., Lee, J., Nakamura, K., Rudick, R.A., **2008**. Gray Matter Atrophy in Multiple Sclerosis: A Longitudinal Study. Ann. Clin. Transl. Neurol. 64, 255–265.

Fisniku, L.K., Brex, P.A., Altmann, D.R., Miszkiel, K.A., Benton, C.E., Lanyon, R., Thompson, A.J., Miller, D.H., **2008**. Disability and T2 MRI lesions: a 20-year follow-up of patients with relapse onset of multiple sclerosis. Brain 131, 808–817.

Fog, T., **1965**. The topography of plaques in multiple sclerosis. Acta Neurol. Scand. suppl. 15, 1–161.

Franklin, R.J.M., ffrench-Constant, C., Edgar, J.M., Smith, K.J., **2012**. Neuroprotection and repair in multiple sclerosis. Nat. Rev. Neurol. 8, 624–34.

Friese, M. a, Schattling, B., Fugger, L., **2014**. Mechanisms of neurodegeneration and axonal dysfunction in multiple sclerosis. Nat. Rev. Neurol. 10, 225–38.

Frischer, J.M., Bramow, S., Dal-Bianco, A., Lucchinetti, C.F., Rauschka, H., Schmidbauer, M., Laursen, H., Sorensen, P.S., Lassmann, H., **2009**. The relation between inflammation and neurodegeneration in multiple sclerosis brains. Brain 132, 1175–89.

Frischer, J.M., Weigand, S.D., Guo, Y., Kale, N., Parisi, J.E., Pirko, I., Mandrekar, J., Bramow, S., Metz, I., Brück, W., Lassmann, H., Lucchinetti, C.F., **2015**. Clinical and pathological insights into the dynamic nature of the white matter multiple sclerosis plaque. Ann. Neurol. 78, 710–721.

Frohman, Elliot M., Racke, Michael K., Raine, Cedric S., 2006. Multiple Sclerosis — The Plaque and Its Pathogenesis. N. Engl. J. Med. 354, 942-955.
Geurts, J.J.G., Bo, L., Pouwels, P.J.W., Castelijns, J.A., Polman, C.H., Barkhof, F., **2005**. Cortical Lesions in Multiple Sclerosis: Combined Postmortem MR Imaging and Histopathology. Am. J. Neuroradiol. 572–577.

Geurts, J.J.G., Bo, L., Roosendaal, S.D., Hazes, T., Barkhof, F., Witter, M.P., Huitinga, I., Valk, P. Van Der, **2007**. Extensive Hippocampal Demyelination in Multiple Sclerosis. J neuropathol Exp Neurol 66, 819–827.

Geurts, J.J.G., Roosendaal, S.., Calabrese, M., Ciccarelli, O., Agosta, F., Chard, D.T., Gass, A., Huerga, E., Moraal, B., Pareto, D., Rocca, M., Wattjes M, Yousry, T.A., Uitdehaag, B.M., Barkhof, F., **2011**. Consensus recommendations for MS cortical lesion scoring using double inversion recovery MRI. Neurology 76, 418–424.

Giffroy, X., Dive, D., Nathalie, J.K., Adelin, M., Catherine, A., Wang, F., **2019**. Is the triple stimulation technique a better quantification tool of motor dysfunction than motor evoked potentials in multiple sclerosis? Acta Neurol. Belg. 119, 47–54.

Giffroy, X., Maes, N., Albert, A., Maquet, P., Crielaard, J., Dive, D., **2016**. Multimodal evoked potentials for functional quantification and prognosis in multiple sclerosis. BMC Neurol. 16, 1–9.

Gilmore, C.P., Bö, L., Owens, T., Lowe, J., Esiri, M.M., **2006**. Spinal Cord Gray Matter Demyelination

in Multiple Sclerosis — A Novel Pattern of Residual Plaque Morphology. Brain Pathol. 16, 202–208.

Giorgio, A., De Stefano, N., **2010**. Cognition in multiple sclerosis: relevance of lesions, brain atrophy and proton MR spectroscopy. Neurol. Sci. 31, 245–248.

Gracien, R.M, Reitz, S.C., Hof, S.M., Fleischer, V., Zimmermann, H., Droby, A., Steinmetz, H., Zipp, F., Deichmann, R., Klein, J.C., **2016a**. Assessment of cortical damage in early multiple sclerosis with quantitative T 2 relaxometry. NMR Biomed. 29, 444–450.

Gracien, R.M., Jurcoane, A., Wagner, M., Reitz, S.C., Mayer, C., Volz, S., Hof, S.M., Fleischer, V., Droby, A., Steinmetz, H., Groppa, S., Hattingen, E., Deichmann, R., Klein, J.C., **2016b**. Multimodal quantitative MRI assessment of cortical damage in relapsing-remitting multiple sclerosis. J. Magn. Reson. Imaging 44, 1600–1607.

Gracien, R.M, Reitz, S.C., Hof, S.M., Fleischer, V., Zimmermann, H., Droby, A., Steinmetz, H., Zipp, F., Deichmann, R., Klein, J.C., **2016c**. Changes and variability of proton density and T1 relaxation times in early multiple sclerosis: MRI markers of neuronal damage in the cerebral cortex. Eur. Radiol. 26, 2578–2586.

Haider, L., Fischer, M.T., Frischer, J.M., Bauer, J., Ho, R., Esterbauer, H., Binder, C.J., Witztum, J.L., **2011**. Oxidative damage in multiple sclerosis lesions. Brain 134, 1914–1924.

Haider, L., Simeonidou, C., Steinberger, G., Hametner, S., Grigoriadis, N., Deretzi, G., Kovacs, G.G., Kutzelnigg, A., Lassmann, H., Frischer, J.M., **2014**. Multiple sclerosis deep grey matter: The relation between demyelination, neurodegeneration, inflammation and iron. J. Neurol. Neurosurg. Psychiatry 85, 1386–1395.

Haider, L., Zrzavy, T., Hametner, S., Ho, R., Trattnig, S., Pfeifenbring, S., Bagnato, F., Bru, W., **2016**. The topograpy of demyelination and neurodegeneration in the multiple sclerosis brain. Brain 139, 807–815.

Hametner, S., Endmayr, V., Deistung, A., Palmrich, P., Prihoda, M., Haimburger, E., Menard, C., Feng, X., Haider, T., Leisser, M., Köck, U., Kaider, A., Höftberger, R., Robinson, S., Reichenbach, J.R., Lassmann, H., Traxler, H., Trattnig, S., Grabner, G., **2018**. The influence of brain iron and myelin on magnetic susceptibility and effective transverse relaxation - A biochemical and histological validation study. Neuroimage 179, 117–133.

Hametner, S., Wimmer, I., Haider, L., Pfeifenbring, S., Brück, W., Lassmann, H., **2013**. Iron and neurodegeneration in the multiple sclerosis brain. Ann. Neurol. 74, 848–861.

Helms, G., Dathe, H., and Dechent, P., **2010**. Modeling the influence of TR and excitation flip angle on the magnetization transfer ratio (MTR) in human brain obtained from 3D spoiled gradient echo MRI. Magn.Reson.Med. 64, 77–185.

Helms, G., Dathe, H., Weiskopf, N., Dechent, P., **2011**. Identification of signal bias in the variable flip angle method by linear display of the algebraic Ernst equation. Magn. Reson. Med. 66, 669–677.

Helms, G., Dechent, P., **2009**. Increased SNR and reduced distortions by averaging multiple gradient echo signals in 3D FLASH imaging of the human brain at 3T. J. Magn. Reson. Imaging 29, 198–204.

Henkelman, R.M., Stanisz, G.J., Graham, S.J., **2001**. Magnetization transfer in MRI: a review. NMR

Biomed. 14, 57–64.

Hernández-torres, E., Wiggermann, V., Hametner, S., **2015**. Orientation Dependent MR Signal Decay Differentiates between People with MS, Their Asymptomatic Siblings and Unrelated Healthy Controls. PLoS One 21, 1–14.

Hochmeister, S., Grundtner, R., Bauer, J., Engelhardt, B., Lyck, R., Gordon, G., Korosec, T., Kutzelnigg, A., Berger, J.J., Bradl, M., Bittner, R.E., Lassmann, H., **2006**. Dysferlin Is a New Marker for Leaky Brain Blood Vessels in Multiple Sclerosis. J Neuropathol Exp Neurol 65, 855–865.

Housley, W.J., Pitt, D., Ha, D.A., **2015**. Biomarkers in multiple sclerosis. Clin. Immunol. 161, 51–58.

Howell, O.W., Reeves, C.A., Nicholas, R., Carassiti, D., Radotra, B., Gentleman, S.M., Serafini, B., Aloisi, F., Roncaroli, F., Magliozzi, R., Reynolds, R., **2011**. Meningeal inflammation is widespread and linked to cortical pathology in multiple sclerosis. Brain 134, 2755–2771.

Hulst, H.E., Geurts, J.J.G., **2011**. Gray matter imaging in multiple sclerosis: what have we learned? BMC Neurol. 11.

IFNB Multiple Sclerosis Study Group, **1993**. Interferon beta-1b is effective in relapsing-remitting multiple sclerosis. I. Clinical results of a multicenter, randomized, double-blind, placebo-controlled trial. Neurology 43, 655–661.

Jacobsen, C., Hagemeier, J., Myhr, K., Nyland, H., Lode, K., Bergsland, N., Ramasamy, D.P., Dalaker, T.O., Larsen, J.P., Farbu, E., Zivadinov, R., **2014**. Brain atrophy and disability progression in multiple sclerosis patients: a 10-year follow-up study. J. Neurol. Neurosurg. Psychiatry 85, 1109–1115.

Jain, S., Sima, D.M., Ribbens, A., Cambron, M., Maertens, A., Van Hecke, W., Mey, J. De, Barkhof, F., Steenwijk, M.D., Daams, M., Maes, F., Huffel, S. Van, Vrenken, H., Smeets, D., **2015**. Automatic segmentation and volumetry of multiple sclerosis brain lesions from MR images. NeuroImage Clin. 8, 367–375.

Johnson, K., Brooks, B., Cohe, J., Ford, C., Goldstein, J., RP, L., Al., E., **1995**. Copolymer 1 reduces relapse rate and improves disability in relapsing- remitting multiple sclerosis: results of a phase III multicenter, double- blind placebo-controlled trial. Neurology 45, 1268–1276.

Jürgens, T., Jafari, M., Kreutzfeldt, M., Bahn, E., Brück, W., Kerschensteiner, M., Merkler, D., **2016**. Reconstruction of single cortical projection neurons reveals primary spine loss in multiple sclerosis. Brain 139, 39–46.

Khaleeli, Z., Cercignani, M., Audoin, B., Ciccarelli, O., Miller, D.H., Thompson, A.J., **2007**. Localized grey matter damage in early primary progressive multiple sclerosis contributes to disability. Neuroimage 37, 253–261.

Khalil, M., Enzinger, C., Langkammer, C., Tscherner, M., Wallner-Blazek, M., Jehna, M., Ropele, S., Fuchs, S., Fazekas, F., **2009**. Quantitative assessment of brain iron by R2* relaxometry in patients with clinically isolated syndrome and relapsing-remitting multiple sclerosis. Mult. Scler. 15, 1048–1054.

Khalil, M., Langkammer, C., Gattringer, T., Bachmaier, G., Ropele, S., Enzinger, C., **2015**. Dynamics of brain iron levels in multiple sclerosis. Neurology 84, 2396-2402.

Khalil, M., Langkammer, C., Ropele, S., Petrovic, K., Wallner-Blazek, M., Loitfelder, M., Jehna, M., Bachmaier, G., Schmidt, R., Enzinger, C., Fuchs, S., Fazekas, F., **2011**. Determinants of brain iron in multiple sclerosis: a quantitative 3T MRI study. Neurology 77, 1691–1697.

Kilsdonk, I.D., Jonkman, L.E., Klaver, R., Van Veluw, S.J., Zwanenburg, J.J.M., Kuijer, J.P.A., Pouwels, P.J.W., Twisk, J.W.R., Wattjes, M.P., Luijten, P.R., Barkhof, F., Geurts, J.J.G., **2016**. Increased cortical grey matter lesion detection in multiple sclerosis with 7 T MRI: A post-mortem verification study. Brain 139, 1472–1481.

Klaver, R., Popescu, V., Voorn, P., Galis-de Graaf, Y., van der Valk, P., de Vries, H.E., Schenk, G.J., Geurts, J.J.G., Graaf, Y.G., Valk, P. Van Der, Vries, H.E. De, Schenk, G.J., Geurts, J.J.G., **2015**. Neuronal and axonal loss in normal-appearing gray matter and subpial lesions in multiple sclerosis. J. Neuropathol. Exp. Neurol. 74, 453–8.

Kos, D., Nagels, G., Hooghe, M., Duquet, W., Delbeke, S., Kerckhofs, E., **2009**. Measuring Activity Patterns Using Actigraphy in Multiple Sclerosis. Chronobiology Int. 24, 345–356.

Kremenchutzky, M., Rice, G.P.A., Baskerville, J., Wingerchuk, D.M., Ebers, G.C., **2006**. The natural history of multiple sclerosis: A geographically based study 9: Observations on the progressive phase of the disease. Brain 129, 584–594.

Kurtzke, J.F., **1983**. Rating neurologic impairment in multiple sclerosis: an expanded disability status scale (EDSS). Neurology 33, 1444–1452.

Kutzelnigg, A., Faber-rod, J.C., Bauer, J., Lucchinetti, C.F., Sorensen, P.S., Laursen, H., Stadelmann, C., Brück, W., **2007**. Widespread Demyelination in the Cerebellar Cortex in Multiple Sclerosis. Brain Pathol. 17, 38–44.

Kutzelnigg, A., Lucchinetti, C.F., Stadelmann, C., Bruck, W., Rauschka, H., Bergmann, M., Schmidbauer, M., Parisi, J.E., Lassmann, H., **2005**. Cortical demyelination and diffuse white matter injury in multiple sclerosis. Brain 128, 2705–2712.

Langdon, D.W., Amato, M.P., Boringa, J., Brochet, B., Foley, F., Fredrikson, S., Hamalainen, P., Hartung, H.P., Krupp, L., Penner, I.K., Reder, A.T., Benedict, R.H., **2012**. Recommendations for a Brief International Cognitive Assessment for Multiple Sclerosis (BICAMS). Mult. Scler. 18, 891–898.

Langkammer, C., Krebs, N., Goessler, W., Scheurer, E., Ebner, F., Yen, K., Fazekas, F., Ropele, S., **2010**. Quantitative MR Imaging of Brain Iron: A Postmortem Validation Study. Radiology 257, 455–462.

Langkammer, C., Krebs, N., Goessler, W., Scheurer, E., Yen, K., Fazekas, F., Ropele, S., **2012**. Susceptibility induced gray – white matter MRI contrast in the human brain. Neuroimage 59, 1413–1419.

Lassmann, H., **2019**. Pathogenic mechanisms associated with different clinical courses of multiple sclerosis. Front. Immunol. 10, 1–14.

Lassmann, H., **2018**. Multiple Sclerosis Pathology. Cold Spring Harb Perspect 8:a028936.

Lassmann, H., **2017**. Targets of therapy in progressive MS. Mult. Scler.J. 23(12), 1593–1599.

Lassmann, H., **2014**. Multiple sclerosis: Lessons from molecular neuropathology. Exp. Neurol. 262, 2–7.

Lassmann, H., **2013**. Pathology and disease mechanisms in different stages of multiple sclerosis . J. Neurol. Sci. 333, 1–4.

Lassmann, H., van Horssen, J., Mahad, D., Horssen, J. Van, Mahad, D., van Horssen, J., Mahad, D., Horssen, J. Van, Mahad, D., **2012**. Progressive multiple sclerosis: pathology and pathogenesis. Nat. Rev. Neurol. 8, 647–56.

Lassmann, H., Van Horssen, J., **2011**. The molecular basis of neurodegeneration in multiple sclerosis. FEBS Lett. 585, 3715–3723.

Lassmann, H., Brück, W., Lucchinetti, C., **2001**. Heterogeneity of multiple sclerosis pathogenesis: Implications for diagnosis and therapy. Trends Mol. Med. 7, 115–121.

Lema, A., Bishop, C., Malik, O., Mattoscio, M., Ali, R., Nicholas, R., Muraro, P.A., Matthews, P.M., Waldman, A.D., Newbould, R. D., **2017**. A Comparison of Magnetization Transfer Methods to Assess Brain and Cervical Cord Microstructure in Multiple Sclerosis. J. Neuroimaging 27 (2): 221–226.

Lisak, R.P., Nedelkoska, L., Benjamins, J.A., Schalk, D., Bealmear, B., Touil, H., Li, R., Muirhead, G., Bar-or, A., **2017**. B cells from patients with multiple sclerosis induce cell death via apoptosis in neurons in vitro. J. Neuroimmunol. 309, 88–99.

Lommers, E., Simon, J., Reuter, G., Delrue, G., Dive, D., Degueldre, C., Balteau, E., Phillips, C., Maquet, P., **2019**. Multiparameter MRI quantification of microstructural tissue alterations in multiple sclerosis. NeuroImage Clin. 23.

Lorio, S., Fresard, S., Adaszewski, S., Kherif, F., Chowdhury, R., Frackowiak, R.S., Ashburner, J., Helms, G., Weiskopf, N., Lutti, A., Draganski, B., **2016**. New tissue priors for improved automated classification of subcortical brain structures on MRI. Neuroimage 130, 157–166.

Louapre, C., Govindarajan, S.T., Giannì, C., Madigan, N., Sloane, J.A., Treaba, C.A., Herranz, E., Kinkel, R.P., Mainero, C., **2018**. Heterogeneous pathological processes account for thalamic degeneration in multiple sclerosis: Insights from 7 T imaging. Mult. Scler. J. 24, 1433–1444.

Louapre, C., Bodini, B., Lubetski, C., Freeman, L., Stankoff, B., **2017**. Imaging markers of multiple sclerosis prognosis. Curr Opin Neurol 30, 231–236.

Lublin, F.D., Reingold, S.C., **1996**. Defining the clinical course of multiple sclerosis: Results of an international survey. Neurology 46, 907–911.

Lublin, F.D., Reingold, S.C., Cohen, J. a, Cutter, G.R., Sørensen, P.S., Thompson, A.J., Wolinsky, J.S., Balcer, L.J., Banwell, B., Barkhof, F., Bebo, B., Calabresi, P. a, Clanet, M., Comi, G., Fox, R.J., Freedman, M.S., Goodman, A.D., Inglese, M., Kappos, L., Kieseier, B.C., Lincoln, J. a, Lubetzki, C., Miller, A.E., Montalban, X., O'Connor, P.W., Petkau, J., Pozzilli, C., Rudick, R. a, Sormani, M.P., Stüve, O., Waubant, E., Polman, C.H., 2014. Defining the clinical course of multiple sclerosis: the **2013** revisions. Neurology 83, 278–86.

Luchetti, S., Fransen, N.L., van Eden, C.G., Ramaglia, V., Mason, M., Huitinga, I., **2018**. Progressive multiple sclerosis patients show substantial lesion activity that correlates with clinical disease severity and

sex: a retrospective autopsy cohort analysis. Acta Neuropathol. 135, 511–528.

Lutti, A., Hutton, C., Finsterbusch, J., Helms, G., Weiskopf, N., **2010**. Optimization and validation of methods for mapping of the radiofrequency transmit field at 3T. Magn. Reson. Med. 64, 229–238.

Lutti, A., Stadler, J., Josephs, O., Windischberger, C., Speck, O., Bernarding, J., Hutton, C., Weiskopf, N., **2012**. Robust and fast whole brain mapping of the RF transmit field B1 at 7T. PLoS One 7, 1–7.

Machado-Santos, J., Saji, E., Tröscher, A.R., Paunovic, M., Liblau, R., Gabriely, G., Bien, C.G., Bauer, J., Lassmann, H., **2018**. The compartmentalized inflammatory response in the multiple sclerosis brain is composed of tissue-resident CD8+ T lymphocytes and B cells. Brain 141, 2066–2082.

Magliozzi, R., Howell, O., Vora, A., Serafini, B., Nicholas, R., Puopolo, M., Reynolds, R., Aloisi, F., **2007**. Meningeal B-cell follicles in secondary progressive multiple sclerosis associate with early onset of disease and severe cortical pathology. Brain 130, 1089–1104.

Magliozzi, R., Howell, O.W., Nicholas, R., Cruciani, C., Castellaro, M., Romualdi, C., Rossi, S., Pitteri, M., Montemezzi, S., Rasia, S., Capra, R., Bertoldo, A., Facchiano, F., Benedetti, M.D., Gajofatto, A., Pizzini, F.B., **2018**. Inflammatory Intrathecal Profiles and Cortical Damage in Multiple Sclerosis. Ann. Neurol. 83, 739–755.

Magliozzi, R., Howell, O.W., Reeves, C., Roncaroli, F., Nicholas, R., Serafini, B., Aloisi, F., Reynolds, R., **2010**. A Gradient of Neuronal Loss and Meningeal Inflammation in Multiple Sclerosis. Ann. Neurol. 68, 477–493.

Mahad, D., Ziabreva, I., Lassmann, H., Douglas, T., **2008**. Mitochondrial defects in acute multiple sclerosis lesions. Brain 131, 1722–1735.

Mainero, C., Louapre, C., Govindarajan, S.T., Gianni, C., Scott Nielsen, A., Cohen-Adad, J., Sloane, J., Kinkel, R.P., Giannı, C., Mainero, C., Nielsen, A.S., Cohen-Adad, J., Sloane, J., Kinkel, R.P., **2015**. A gradient in cortical pathology in multiple sclerosis by in vivo quantitative 7 T imaging. Brain 138, 932–945.

Mallik, S., Muhlert, N., Samson, R.S., Sethi, V., Wheeler-kingshott, C.A.M., Miller, D.H., Chard, D.T., **2015**. Regional patterns of grey matter atrophy and magnetisation transfer ratio abnormalities in multiple sclerosis clinical subgroups: A voxel-based analysis study. Mult. Scler. J. 21, 423–432.

Mandolesi, G., Gentile, A., Musella, A., Fresegna, D., De Vito, F., Bullitta, S., Sepman, H., Marfia, G.A., Centonze, D., Vito, F. De, Bullitta, S., Sepman, H., Marfia, G.A., Centonze, D., **2015**. Synaptopathy connects inflammation and neurodegeneration in multiple sclerosis. Nat. Rev. Neurol. 11, 711–724.

Manfredonia, F., Ciccarelli, O., Khaleeli, Z., Tozer, D.J., Sastre-Garriga, J., Miller, D.H., Thompson, A.J., **2007**. Normal-appearing brain t1 relaxation time predicts disability in early primary progressive multiple sclerosis. Arch. Neurol. 64, 411–5.

Mesaros, S., Rocca, M. a, Pagani, E., Sormani, M.P., Petrolini, M., Comi, G., Filippi, M., **2011**. Thalamic damage predicts the evolution of primary-progressive multiple sclerosis at 5 years. Am. J. Neuroradiol. 32, 1016–20.

Miller, D.H., Leary, S.M., **2007**. Primary-progressive multiple sclerosis. Lancet Neurol. 6, 903–912.

Moon, N., Bullitt, E., Leemput, K. Van, Gerig, G., **2002**. Automatic Brain and Tumor Segmentation in: 5th annuel conference MICCAI. Tokyo.

Murphy, M.P., **2009**. How mitochondria produce reactive oxygen species. Biochem J 417, 1–13.

Nakamura, K., Brown, R.A., Narayanan, S., Collins, D.L., Arnold, D.L., **2015**. Diurnal fluctuations in brain volume: Statistical analyses of MRI from large populations. Neuroimage 118, 126–132.

Neema, M., Stankiewicz, J., Arora, A., Dandamudi, V.S.R., Batt, C.E., Guss, Z.D., Al-Sabbagh, A., Bakshi, R., **2007**. T1- and T2-based MRI measures of diffuse gray matter and white matter damage in patients with multiple sclerosis. J. Neuroimaging 17, 16–21.

Nieuwenhuys, R., Broere, C.A.J., **2017**. A map of the human neocortex showing the estimated overall myelin content of the individual architectonic areas based on the studies of Adolf Hopf. Brain Struct. Funct. 222, 465–480.

Nowinski, C.J., Miller, D.M., Cella, D., **2017**. Evolution of Patient-Reported Outcomes and Their Role in Multiple Sclerosis Clinical Trials. Neurotherapeutics 14, 934–944.

Ogg, R.J., Steen, R.G., **1998**. Age-related changes in brain T1 are correlated with iron concentration. Magn. Reson. Med. 40, 749–753.

Oh, J., Ontaneda, D., Azevedo, C., Klawiter, E.C., Absinta, M., **2019**. Imaging outcome measures of neuroprotection and repair in MS A consensus statement from NAIMS. Neurology 92, 519–533.

Ono, M., Kubik, S., Abernathey, C.D., **1990**. Atlas of the cerebral sulci, 1st ed. New-York.

Paling, D., Tozer, D., Wheeler-Kingshott, C., Kapoor, R., Miller, D.H., Golay, X., **2012**. Reduced R2' in multiple sclerosis normal appearing white matter and lesions may reflect decreased myelin and iron content. J. Neurol. Neurosurg. Psychiatry 83, 785–792.

Papadopoulos, D., Dukes, S., Patel, R., Nicholas, R., Vora, A., Reynolds, R., **2009**. Substantial Archaeocortical Atrophy and Neuronal Loss in Multiple Sclerosis Tissue samples. Brain Pathol. 19, 238–253.

Parry, A., Clare, S., Jenkinson, M., Smith, S., Palace, J., Matthews, P.M., **2002**. White matter and lesion T1 relaxation times increase in parallel and correlate with disability in multiple sclerosis. J. Neurol. 249, 1279–1286.

Phillips, C., Lommers, E., Pernet, C., **2016**. Unifying lesion masking and tissue probability maps for improved segmentation and normalization, in: 23rd Annual Meeting of the Organization for Human Brain Mapping. Vancouver.

Pitt, D., Boster, A., Pei, W., Wohleb, E., Jasne, A., Zachariah, C.R., Rammohan, K., Knopp, M. V., Schmalbrock, P., **2010**. Imaging cortical lesions in multiple sclerosis with ultra-high-field magnetic resonance imaging. Arch. Neurol. 67, 812–818.

Pluchino, S., Muzio, L., Imitola, J., Deleidi, M., Alfaro-cervello, C., Salani, G., Porcheri, C., Brambilla, E., Cavasinni, F., Bergamaschi, A., Garcia-verdugo, J.M., Comi, G., Khoury, S.J., Martino, G., **2008**. Persistent inflammation alters the function of the endogenous brain stem cell compartment 2564–2578.

Polman, C.H., Reingold, S.C., Banwell, B., Clanet, M., Cohen, J.A., Filippi, M., Fujihara, K., Havrdova, E., Hutchinson, M., Kappos, L., Lublin, F.D., Montalban, X., O'Connor, P., Sandberg-Wollheim, M., Thompson, A.J., Waubant, E., Weinshenker, B., Wolinsky, J.S., **2011**. Diagnostic criteria for multiple sclerosis: 2010 revisions to the McDonald criteria. Ann. Neurol. 69, 292–302.

Polman, C.H., Rudick, R., **2010**. The multiple sclerosis functional composite: a clinically meaningful measure of disability. Neurology 74 Suppl 3, S8-15.

Popescu, B.F., Lucchinetti, C.F., Anderson, D., Ellenberg, J., Leventhal, C., Reingold, S., Rodriguez, M., Silberberg, D., Charcot, J., Peterson, J., **2012**. Meningeal and cortical grey matter pathology in multiple sclerosis. BMC Neurol. 12, 11.

Popescu, V., Klaver, R., Voorn, P., Graaf, Y.G., Knol, D.L., Twisk, J.W.R.R., Versteeg, A., Schenk, G.J., Galis-De Graaf, Y., Knol, D.L., Twisk, J.W.R.R., Versteeg, A., Schenk, G.J., Van Der Valk, P., Barkhof, F., De Vries, H.E., Vrenken, H., Geurts, J.J.G., Graaf, Y.G., Knol, D.L., Twisk, J.W.R.R., Versteeg, A., Schenk, G.J., **2015**. What drives MRI-measured cortical atrophy in multiple sclerosis? Mult. Scler. J. 21, 1–11.

Popescu, V., Schoonheim, M.M., Versteeg, A., Chaturvedi, N., Jonker, M., Menezes, R.X. De, Garre, F.G., Bernard, M., Uitdehaag, J., Barkhof, F., Vrenken, H., **2016**. Grey Matter Atrophy in Multiple Sclerosis: Clinical Interpretation Depends on Choice of Analysis Method. PLoS One 11, 1–17.

Preibisch, C., and Deichmann, R., Preibisch, C., Deichmann, R., **2009**. Influence of RF spoiling on the stability and accuracy of T1 mapping based on spoiled FLASH with varying flip angles. Magn. Reson. Med. 61, 25–135.

PRISMS Study Group, **1998**. Randomised double-blind placebo-controlled study of interferon β-1a in relapsing/remitting multiple sclerosis. Lancet 352, 1498–1504.

Ramio-Torrenta, L., Sastre-Garriga, J., Ingle, G.T., Davies, G.R., Ameen, V., Miller, D.H., Thompson, A.J., **2006**. Abnormalities in normal appearing tissues in early primary progressive multiple sclerosis and their relation to disability: a tissue specific magnetisation transfer study. J. Neurol. Neurosurg. Psychiatry 77, 40–45.

Reich, D.S., Lucchinetti, C.F., Calabresi, P.A., **2018**. Multiple Sclerosis. N. Engl. J. Med. 378, 169–180.

Reitz, S.C., Hof, S., Fleischer, V., Brodski, A., Gröger, A., Gracien, R., Droby, A., Steinmetz, H., **2016**. Multi-parametric quantitative MRI of normal appearing white matter in multiple sclerosis, and the effect of disease activity on T2. Brain Imaging Behav. 11, 744–753.

Rocca, M., Mastronardo, G., Rodegher, M., Comi, G., Filippi, M., **1999**. Long-term changes of magnetization transfer-derived measures from patients with relapsing-remitting and secondary progressive multiple sclerosis. AJNR. Am. J. Neuroradiol. 20, 821–827.

Rocca, M.A., Barkhof, F., De Luca, J., Frisén, J., Geurts, J.J.G.G., Hulst, H.E., Sastre-Garriga, J., Filippi, M., Barkhof, F., Ciccarelli, O., De Stefano, N., Enzinger, C., Filippi, M., **2018**. The hippocampus in multiple sclerosis. Lancet Neurol 17, 918–926.

Rocca, M.A., Longoni, G., Pagani, E., Boffa, G., Colombo, B., Rodegher, M., Martino, G., Falini, A.,

Comi, G., Filippi, M., **2015**. In Vivo Evidence of Hippocampal Dentate Gyrus Expansion in Multiple Sclerosis. Hum.Brain Mapp. 36, 4702–4713.

Ropele, S., de Graaf, W., Khalil, M., Wattjes, M.P., Langkammer, C., Rocca, M. a, Rovira, A., Palace, J., Barkhof, F., Filippi, M., Fazekas, F., **2011**. MRI assessment of iron deposition in multiple sclerosis. J. Magn. Reson. Imaging 34, 13–21.

Ropele, S., Kilsdonk, I.D., Wattjes, M.P., Langkammer, C., De Graaf, W.L., Frederiksen, J.L., Larsson, H.B., Yiannakas, M., Wheeler-Kingshott, C.A.M., Enzinger, C., Khalil, M., Rocca, M.A., Sprenger, T., Amann, M., Kappos, L., Filippi, M., Rovira, A., Ciccarelli, O., Barkhof, F., Fazekas, F., **2014**. Determinants of iron accumulation in deep grey matter of multiple sclerosis patients. Mult. Scler. J. 20, 1692–1698.

Rudick, R.A., Fisher, E., Lee, J.-C., Simon, J., Jacobs, L., **1999**. Use of the brain parenchymal fraction to measure whole brain atrophy in relapsing-remitting MS. Neurology 53, 1698–1698.

Rudick, R.A., Trapp, B.D., Ph, D., **2009**. Gray-Matter Injury in Multiple Sclerosis. N. Engl. J. Med. 361, 1505–1506.

Salvoni, G., Mohammadi, S., Corbin, N., Ashburner, J., Callaghan, M.F., Phillips, C., **2019**. Impact of Smoothing Weights on Voxel-Based Quantification (VBQ) analysis, in: 25rd Annual Meeting of the Organization for Human Brain Mapping. Rome.

Scalfari, A., Neuhaus, A., Daumer, M., Muraro, P.A., Ebers, G.C., **2014**. Onset of secondary progressive phase and long-term evolution of multiple sclerosis. J. Neurol. Neurosurg. Psychiatry 85, 67–75.

Scalfari, A., Neuhaus, A., Degenhardt, A., Rice, G.P., Muraro, P.A., Daumer, M., Ebers, G.C., **2010**. a geographically based study 10: relapses and long-term disability. Brain 133, 1914–1929.

Schmidt, P., Gaser, C., Arsic, M., Buck, D., Förschler, A., Berthele, A., Hoshi, M., Ilg, R., Schmid, V.J., Zimmer, C., Hemmer, B., Mühlau, M., **2012**. An automated tool for detection of FLAIR-hyperintense white-matter lesions in Multiple Sclerosis. Neuroimage 59, 3774–83.

Schmierer, K., Scaravilli, F., Altmann, D.R., Barker, G.J., Miller, D.H., **2004**. Magnetization transfer ratio and myelin in postmortem multiple sclerosis brain. Ann. Neurol. 56, 407–415.

Schmierer, K., Tozer, D.J., Scaravilli, F., Altmann Daniel, R., Barker, G.J., Tofts, P.S., Miller, D.H., **2007**. Europe PMC Funders Group Quantitative Magnetization Transfer Imaging in Postmortem Multiple Sclerosis Brain. J. Magn. Reson. Imaging 26, 41–51.

Schoonheim, M.M., Brandt, R.B., Barkhof, F., Geurts, J.J.G., Pagani, E., Sormani, M.P., Minagar, A., Barnett, M.H., Benedict, R.H.B., **2013**. The thalamus and multiple sclerosis: modern views on pathologic, imaging, and clinical aspects. Neurology 80, 210–9.

Schwid, S.R., Goodman, A.D., McDermott, M.P., Bever, C.F., Cook, S.D., **2002**. functional measures in MS: What is a reliable change? Neurology 58, 1294–1296.

Sereno, M.I., Lutti, A., Weiskopf, N., Dick, F., **2012**. Mapping the Human Cortical Surface by Combining Quantitative T1 with Retinotopy. Cereb. Cortex 23, 2261–2268.

Shiee, N., Bazin, P., Zackowski, K.M., Farrell, S.K., Harrison, D.M., Newsome, S.D., Ratchford, J.N., Caffo, B.S., Calabresi, P.A., Pham, D.L., Reich, D.S., **2012**. Revisiting Brain Atrophy and Its Relationship to Disability in Multiple Sclerosis. PLoS One l, 1–9.

Shirani, A., Zhao, Y., Karim, M.E., Evans, C., Kingwell, E., van der Kop, M.L., Oger, J., Gustafson, P., Petkau, J., Tremlett, H., **2012**. Association Between Use of Interferon Beta and Progression of Disability in Patients with Relapsing-Remitting Multiple Sclerosis. J. Amarian Med. Assoc. 308, 247–256.

Smith, S., Zhang, Y., Jenkinson, M., Chen, J., Matthews, P., Federico, A., De Stefano, N., **2002**. Accurate, Robust, and Automated Longitudinal and Cross-Sectional Brain Change Analysis. Neuroimage 17, 479–489.

Sørensen, T.L., Frederiksen, J.L., Richard, M., Invest, J.C., Sørensen, T.L., Tani, M., Jensen, J., Pierce, V., Lucchinetti, C., Folcik, V.A., Qin, S., Rottman, J., Sellebjerg, F., Strieter, R.M., Frederiksen, J.L., Ransohoff, R.M., **1999**. Expression of specific chemokines and chemokine receptors in the central nervous system of multiple sclerosis patients Find the latest version: in the central nervous system of multiple sclerosis patients. J Clin Invest 103, 807–815.

Steenwijk, M.D., Amiri, H., Schoonheim, M.M., Sitter, A. De, Barkhof, F., Pouwels, P.J.W., Vrenken, H., **2017**. Agreement of MSmetrix with established methods for measuring cross- sectional and longitudinal brain atrophy. NeuroImage Clin. 15, 843–853.

Steenwijk, M.D., Geurts, J.J.G., Daams, M., Tijms, B.M., Wink, A.M., Balk, L.J., Tewarie, P.K., Uitdehaag, B.M.J., Barkhof, F., Vrenken, H., Pouwels, P.J.W., **2016**. Cortical atrophy patterns in multiple sclerosis are non-random and clinically relevant. Brain 139, 115–126.

Stephenson, E., Nathoo, N., Mahjoub, Y., Dunn, J.F., Yong, V.W., **2014**. Iron in multiple sclerosis: roles in neurodegeneration and repair. Nat Rev Neurol 10, 459–68.

Stüber, C., Morawski, M., Schäfer, A., Labadie, C., Wähnert, M., Leuze, C., Streicher, M., Barapatre, N., Reimann, K., Geyer, S., Spemann, D., Turner, R., **2014**. Myelin and iron concentration in the human brain: A quantitative study of MRI contrast. Neuroimage 93, 95–106.

Tabelow, K., Balteau, E., Ashburner, J., Callaghan, M.F., Draganski, B., Helms, G., Kherif, F., Leutritz, T., Lutti, A., Phillips, C., Reimer, E., Ruthotto, L., Seif, M., Weiskopf, N., Ziegler, G., Mohammadi, S., **2019**. hMRI – A toolbox for quantitative MRI in neuroscience and clinical research. Neuroimage 194, 191–210.

Tallantyre, E.C., Morgan, P.S., Dixon, J.E., Al-Radaideh, A., Brookes, M.J., Morris, P.G., Evangelou, N., **2010**. 3 Tesla and 7 Tesla MRI of multiple sclerosis cortical lesions. J. Magn. Reson. Imaging 32, 971–977.

Teunissen, C.E., Malekzadeh, A., Leurs, C., Bridel, C., Killestein, J., **2015**. Body fluid biomarkers for multiple sclerosis — the long road to clinical application. Nat. Rev. Neurol. 11, 585–596.

Thompson, A.J., Banwell, B.L., Barkhof, F., Carroll, W.M., Coetzee, T., Comi, G., Correale, J., Fazekas, F., Filippi, M., Freedman, M.S., Fujihara, K., Galetta, S.L., Hartung, H.P., Kappos, L., Lublin, F.D., Marrie, R.A., Miller, A.E., Miller, D.H., Montalban, X., Mowry, E.M., Sorensen, P.S., Tintoré, M., Traboulsee, A.L., Trojano, M., Uitdehaag, B.M.J., Vukusic, S., Waubant, E., Weinshenker, B.G., Reingold, S.C., Cohen, J.A., **2017**. Diagnosis of multiple sclerosis: 2017 revisions of the McDonald criteria. Lancet

Neurol. 17.

Tortorella, C., Viti, B., Bozzali, M., Sormani, M.P., Rizzo, G., Gilardi, M.F., Comi, G., Filippi, M., **2000**. A magnetization transfer histogram study of normal-appearing brain tissue in MS. Neurology 54, 186–193.

Traboulsee, A., Dehmeshki, J., Brex, P.A., Dalton, C.M., Chard, D., Barker, G.J., Plant, G.T., Miller, D.H., **2002**. Normal-appearing brain tissue MTR histograms in clinically isolated syndromes suggestive of MS. Neurology 59, 126–128.

Traboulsee, A., Dehmeshki, J., Peters, K.R., Griffin, C.M., Brex, P.A., Silver, N., Ciccarrelli, O., Chard, D.T., Barker, G.J., Thompson, A.J., Miller, D.H., **2003**. Disability in multiple sclero sis is related to normal appearing brain tissue MTR histo gram abno rmalities. Mult. Scler. 9, 566–573.

Trapp, B.D., Peterson, B.., Ransohoff, R.M., Rudick, R., Mörk, S., Bö, L., Transectionthe, A., Of, L., Sclerosis, M., **1998**. Axonal transection in the lesions of multiple sclerosis. N. Engl. J. Med. 338, 278–285.

Treaba, C.A., Granberg, T.E., Sormani, M.P., Herranz, E., Ouellette, R.A., Louapre, C., Sloane, J.A., Kinkel, R.P., Mainero, C., **2019**. Longitudinal characterization of cortical lesion development and evolution in multiple sclerosis with 7.0-T MRI. Radiology 291, 710–749.

Umino, M., Maeda, M., Ii, Y., Tomimoto, H., Sakuma, H., **2019**. 3D double inversion recovery MR imaging: Clinical applications and usefulness in a wide spectrum of central nervous system diseases. J. Neuroradiol. 46, 107–116.

Van Munster, C.E.P., Jonkman, L.E., Henry, W., Uitdehaag, B.M.J., Geurts, J.J.G., **2015**. Grey Matter Damage in Multiple Sclerosis: Impact on Clinical Symptoms. Neuroscience 303, 446–461.

Vercellino, M., Masera, S., Lorenzatti, M., Condello, C., Merola, A., Mattioda, A., Tribolo, A., Capello, E., Mancardi, G.L., Mutani, R., Giordana, M.T., Cavalla, P., Cifelli, A., Arridge, M., **2009**. Demyelination, Inflammation, and Neurodegeneration in Multiple Sclerosis Deep Gray Matter. J Neuropathol Exp Neurol 68, 489–502.

Vidaurre, O.G., Haines, J.D., Sand, I.K., Adula, K.P., Huynh, J.L., Mcgraw, C.A., Zhang, F., Varghese, M., Sotirchos, E., Bhargava, P., Venkata, V., Bandaru, R., Pasinetti, G., Zhang, W., Inglese, M., Calabresi, P.A., Wu, G., Miller, A.E., Haughey, N.J., Lublin, F.D., Casaccia, P., **2014**. Cerebrospinal fluid ceramides from patients with multiple sclerosis impair neuronal bioenergetics. Brain 137, 2271–2286.

Vrenken, H., Geurts, J.J., Knol, D.L., van Dijk, L.N., Dattola, V., Jasperse, B., van Schijndel, R.A., Polman, C.H., Castelijns, J.A., Barkhof, F., Pouwels, P.J., **2006**. Whole-brain T1 mapping in multiple sclerosis: global changes of normal-appearing gray and white matter. Radiology 240, 811–820.

Waesberghe, J.H.T.M. Van, Kamphorst, W., Groot, C.J.A. De, Van Waesberghe, J.H.T.M., Kamphorst, W., De Groot, C.J. a., Van Walderveen, M. a. a., Castelijns, J. a., Ravid, R., Lycklama Nijeholt, G.J., Van Der Valk, P., Polman, C.H., Thompson, J., Barkhof, F., **1999**. Axonal Loss in Multiple Sclerosis Lesions: Magnetic Resonance Imaging Insights into Substrates of Disability. Ann. Neurol. 46, 747–754.

Warnock, G.I., Aerts, J., Bahri, M.A., Bretin, F., Lemaire, C., Giacomelli, F., Mievis, F., Mestdagh, N., Buchanan, T., Valade, A., Mercier, J., Wood, M., Gillard, M., Seret, A., Luxen, A., Salmon, E., Plenevaux, A., **2014**. Evaluation of 18F-UCB-H as a novel PET tracer for Synaptic vesicle protein 2A in the

Brain. J. Nucl. Med. 55, 1336–1341.

Wattjes, M., Rovira, A., Miller, D., Yoursy, T.A., Sormani, M.P., de Stefano, N., Tintore, M., Auger, C., Filippi, M., Rocca, M.A., Fazekas, F., Kappos, L., Polman, C., Barkhof, F., Montalban, X., **2015**. Magnims consensus guidelines on the use of MRI in multiple sclerosis – establishing disease prognosis and monitoring patients. Nat. Rev. Neurol. 11, 597–606.

Weiskopf, N., Callaghan, M.F., Josephs, O., Lutti, A., Mohammadi, S., **2014**. Estimating the apparent transverse relaxation time (R2*) from images with different contrasts (ESTATICS) reduces motion artifacts. Front. Neurosci. 8, 1–10.

Weiskopf, N., Mohammadi, S., Lutti, A., Callaghan, M.F., **2015**. Advances in MRI-based computational neuroanatomy. Curr. Opin. Neurol. 28, 313–322.

Weiskopf, N., Suckling, J., Williams, G., Correia M., M.M., Inkster, B., Tait, R., Ooi, C., Bullmore T., E.T., Lutti, A., **2013**. Quantitative multi-parameter mapping of R1, PD*, MT, and R2* at 3T: A multi-center validation. Front. Neurosci. 7, 1–11.

Wicken, C., Nguyen, J., Karna, R., Bhargava, P., **2018**. Leptomeningeal inflammation in multiple sclerosis: Insights from animal and human studies. Mult. Scler. Relat. Disord. 26, 173–182.

Yulin, G., Grossman, R.I., Udupa, J.K., Babb, J.S., Mannon, L.J., Mcgowan, J.C., **2002**. Magnetization Transfer Ratio Histogram Analysis of Normal-Appearing Gray Matter and Normal-Appearing White Matter in Multiple Sclerosis. J. Comput. Assist. Tomogr. 26, 62–68.

Zhao, C., Deng, W., Gage, F.H., **2008**. Review Mechanisms and Functional Implications of Adult Neurogenesis. Cell 132, 645–660.

Zivadinov, R., Leist, T.P., **2005**. Clinical-magnetic resonance imaging correlations in multiple sclerosis. J. Neuroimaging 15, 10S-21S.

Zivadinov, R., Reder, A.T., Fillippi, M., Minagar, A., Stüve, O., Lassmann, H., Racke, M.K., Dwyer, M.G., Frohman, E.M., Khan, O., **2008**. Mechanisms of action of disease-modifying agents and brain volume changes in multiple sclerosis. Neurology 71, 136–144.